Development of Portable Undrained Ring Shear Apparatus and Its Application(Dissertation_全文)

AUTHOR(S):

Maja Ostric

Development of Portable Undrained Ring Shear Apparatus and Its Application

Maja Ostric

2013

Development of Portable Undrained Ring Shear Apparatus and Its Application

(ポータブル非排水リングせん断試験機の開発とその応用)

by

Maja Ostric

A dissertation
Submitted in partial fulfillment of the requirements for the
Degree of Doctor of Engineering

Department of Civil and Earth Resources Engineering
Kyoto University, Japan

September 2013

Acknowledgements

The completion of my doctoral work has been an exceedingly challenging endeavor, one that I could not have accomplished without valuable assistance provided by many.

First and foremost, I would like to thank my advisor, Professor Kaoru Takara who accepted me as his student and without him this time in Japan would not be possible. Prof. Takara provided me with continuous support, trust and many opportunities for international experiences and further learning. I also extend my gratitude to Professor Makoto Kimura, Associate Professor Yosuke Yamashiki and Associate Professor Yasuto Tachikawa.

Special thanks are also owed to Professor Emeritus Kyoji Sassa, Director of ICL, for his patience and guidance throughout these years. He gave me many suggestions during the course of this research and my laboratory work. My thanks also go to Associate Professor Hiroshi Fukuoka for valuable discussion and many practical advices during the final period of my research.

For help and assistance in many administrative and technical tasks I want to acknowledge the support of technical staff of DPRI and GCOE-ARS staff members, namely Ms. Sono Inoue, Mr. Shigeo Fujiki, Ms. Florence Lahournat, Ms. Takii Yuko, Ms Yoko Yonekawa and Ms. Mayumi Nishimura. Inoue- san, Fujiki- san and Florence made my “hospital” experience in Japan a positive one and I feel forever indebted for that. Thanks to Ms. Florence Lahournat, I didn’t have the “pleasure” of finding out how to cope with the paperwork for my Internship activities. Also, her friendly support and encouragement during these three years were invaluable.

I am grateful to Associate Professor of GCOE-ARS Educational Unit Dr. Bin He for his help with laboratory work as well as encouragement, and continuous support during my research. Special mention to Dr. Apip for the stimulating discussions about the research and Dr. PingPing Luo for help in everyday life during my stay in Japan.

I express my thanks to the former laboratory members: Dr. Pedro Chaffe, Dr. Roberto Valmir Da Silva, Dr. Netranada Sahu, Dr. Remy Rozainy, Dr. Tsutao Oizumi, Mr. Taku Matsumoto, Mr. Yan Liu, Mr. Wenqiang Cao, Mr. Shin Mizuoka, Mr. Masato Kato, Ms. Young-A Shin, Ms. Eunbi Kang, Ms. Maya Kusajima, Mr. Nobuhiko Sawai; and to my laboratory colleagues: Ms. Tomoko Teramoto, Mrs. Nor Eliza binti Alias, Mr. Weili Duan, Mr. Josko Troselj, Mr. Dang Quang Khang, Mr. Bounhieng Vilaysane, Mr. Han Xue, Mr. Hendy Setiawan, Mr. Masaki Azuma, Mr. Toshiharu Sasaki, Mr. Shota Kurokawa, Mr. Pham Van Tien, Mr. Doan Hui Loi and Mr. Adnan Arutyunov.

I also appreciate the help of Mr. Takaaki Hirano and other engineers of Marui & Co., Ltd., Osaka, Japan for numerous improvement and modification for the practical use of the ICL-1 apparatus. The help of master student Mr. Hendy Setiawan and Mr. Dang Quang Khang in the laboratory work is also highly appreciated.

My deepest thanks to Prof. Oldrich Hungr for receiving me as an internship student in his lab and to Prof. Geoffrey Schladow for sharing good stories in Kyoto and the good time in Japan and overseas.

I gratefully acknowledge Croatian Waters that allowed me unpaid leave thus enabling my research in Japan. I would also like to thank to numerous people from both Rijeka and Zagreb Universities. Among them some should be especially mentioned. My deep appreciation and gratitude goes to Mr. Josip Rubinic and Mr. Igor Ruzic from Rijeka University for their help and support with hydrological part of the research. I also extend my gratitude to Associate Professor Zeljko Arbanas from Rijeka University, Associate Professor Snjezana Mihalic-Arbanas from Zagreb University and Dr. Bojana Horvat from Croatian Waters.

I would like to express my gratitude to the agencies of which financial support allowed me to conduct this research. The Ministry of Education, Culture, Sports, Science and Technology of Japan (MEXT) for providing the scholarship for my studies and accommodation in Japan. The Japanese Society for the Promotion of Science (JSPS) for the travel grant to visit British Columbia, Canada.

Finally, I wish to thank to my family and friends, who have supported me during my stay in Japan, followed me in their thoughts, emailed me frequently, and help me go through all the challenges.

Dragi moji roditelji, neizmjerno vam hvala na vašoj bezuvjentnoj podršci i ljubavi!

Abstract

A new Croatia-Japan Joint Project "Risk identification and land-use planning for disaster mitigation of landslides and floods in Croatia" was initiated in 2009. Grohovo landslide in Rijeka was selected as one of the study areas within the research activities of Working Group on Landslides of Croatia-Japan Project. New, transportable undrained ring shear apparatus, ICL-1, was designed to support research activities. The concept, design and construction of the **Transportable Undrained Ring Shear Apparatus, ICL-1** are explained and described. Stress and pore pressure control tests were conducted on silica sand. The results of the tests on silica sand, as well as the experimental procedure, are described in detail. In order to simulate natural landslide conditions we conducted two types of tests: undrained cyclic stress control tests and naturally drained monotonic pore pressure control tests. Typical test results are presented to show the efficiency of this ring shear apparatus and the dynamic shear behavior of sand.

Then, ICL-1 was applied for the **Assessment of Triggers in Grohovo Landslide**. We described the study area and landslide Grohovo in Croatia and gave overview of preparatory factors of the landslide by describing geomorphological setting and landslide itself. Furthermore, a detail overview of the river characteristics is given with the emphasis on its torrential behavior and flood occurrences that are related to mass movement occurrences in the past. In order to investigate the impact of rainfall as a trigger in reactivation of Grohovo landslide in 1996, we performed rainfall data analysis. Rainfall analysis is performed for both long and short-term rainfall data and estimation of both on the reactivation of landslide is given. We found that the antecedent conditions (60 days before the reactivation) that control groundwater level and soil moisture had a major role in landslide reactivation. For the assessment of seismic trigger we employed new ring shear apparatus, ICL-1 to simulate dynamic loading. By conducting ring shear test on specimen from Grohovo landslide, basic soil parameters are obtained as well. Based on the analysis performed and conducted tests, we concluded that cumulative rainfall is the most probable trigger of this landslide.

Then ICL-1 was applied for the investigation of the **Negative rate effect in sand - bentonite mixtures**. A significant drop in strength was reported in soils showing

transitional shear behavior (between sand and clay), at fast rates of displacement. There is a considerable number on residual strength measurement and only few addressing this issue. Although negative rate effect was reported in these studies, due to the technical difficulties, it was not possible to measure pore pressure during shearing. We conducted a series of ring shear tests in silica sand and sand-bentonite mixtures in order to investigate this effect. Both single- stage and multi-stage tests in the mixtures resulted in drop of residual strength between 0.1 and 1 mm/sec. The results of multi-stage tests in SB 20 and SB 30 specimens showed that the residual friction angle increases linearly with the logarithm of the rate of displacement. The significance of these finding on the practical level is discussed.

Table of Contents

List of Tables

List of Figures

Chapter 1 Introduction

1.1 BACKGROUND

A new Croatia-Japan joint project, “Risk identification and land-use planning for disaster mitigation of landslides and floods in Croatia” was initiated in 2009. The Grohovo landslide in Rijeka was selected as one of the study areas within the research activities of The Working Group on Landslides. Research activities include real time monitoring of landslides, laboratory soil testing, as well as modelling of landslide behaviour and early warning systems (Mihalic and Arbanas 2011). During 2011, monitoring equipment was installed in the Grohovo landslide and two boreholes were drilled in order to install monitoring equipment and obtain soil samples for laboratory tests (Arbanas and Mihalic 2012). A new, transportable, undrained ring shear apparatus, ICL-1, was designed by Professor Kyoji Sassa for laboratory soil testing. This apparatus was developed through 2011 with numerous modifications and corrections during that period. It was necessary to establish experimental procedures and to apply the apparatus in order to verify its use.

The ring shear apparatus was designed specifically for the purpose of determining residual strength. The primary purpose of the ring shear tests is to study the post-peak interval of the stress-displacement curve (Bishop et al. 1971) with emphasis on residual strength. Although initially used for determining residual strength developed in cohesive soils (Hvorslev 1939, Bishop et al. 1971, Skempton 1985), the apparatus has been widely used for better understanding of the undrained shear behaviour of granular soils as well, particularly sands, because of its importance in liquefaction analysis where undrained steady-state shear strength is required (Poulos et al. 1985, Alarcon-Guzman et al. 1988). These conditions are normally reached only at larger shear displacements.

The measurement of residual strength is poorly understood in geotechnical engineering community especially compared to the measurement of peak shear strength (Bromhead 1992). Measurement of residual strength is important for soil stability problems where the existence of shear zones is known or suspected, as in the case with reactivated

landslides. The lack of the interest in the investigation of residual strength compared to the peak strength was attributed to practical difficulties in testing to large displacements and to underassessment of the importance of residual strength in slope stability (Bosdet 1980). Although residual strength is mostly associated with reactivated landslides, some investigations showed that residual conditions may also be present on part of the slip surface of first-time natural or excavated slope failures in stiff clays and clay shales (Mesri and Shahien 2003).

Although many types have been designed and constructed, none of the devices had the capability of measuring pore pressure until 1992. Starting from DPRI-3, all the following apparatus of the series had the capability of shear stress-controlled tests, which enables simulation of both monotonic and dynamic loadings (real seismic waves or sine wave form) under undrained conditions (Sassa et al. 2003, 2004).

The latest apparatus of the DPRI series are used as a simulation test in addition to their basic use for a soil properties measurement. The general purpose of the DPRI ring shear testing program is its use as a simulation test of the entire natural landslide phenomenon. However, because of all the capabilities of the DPRI series of apparatus, they were difficult and expensive to produce. The purpose of the latest apparatus, ICL-1, was to design and develop an inexpensive and transportable apparatus to be used in different locations.

1.2 OBJECTIVES OF THE STUDY

The overall goal of this study is the development and application of a new ring shear apparatus, ICL-1. The specific objectives are:

1. Development of ICL-1 with all related testing procedures by conducting basic tests on materials of known behaviour.
2. Application of ICL-1 on a real landslide by conducting tests to simulate natural conditions. ICL-1 was used for the testing of specimens from the Grohovo landslide.
3. Application of ICL-1 for the investigation of basic spoil behaviour in sand-clay mixtures.

1.3 ORGANIZATION OF THE DISSERTATION

This dissertation consists of five chapters. A brief explanation of each chapter is outlined as follows:

Chapter 1 Introduction. This chapter presents the background, the study objectives, scope of the research, and the organization of the dissertation.

Chapter 2 Stress- and Pore-Pressure Control-Ring Shear Testing for Measurement of the Dynamic Shear Behaviour of Sands. This chapter presents the concept, design, and construction of the portable undrained ring shear apparatus, ICL-1. The overview of the history and the use of ring shear apparatus from the drained ring shear devices by speed-controlled shearing to the undrained ring shear tests with speed and stress-control shearing, is given. Stress and pore pressure control tests were conducted on silica sand. The results of the tests on silica sand, as well as the experimental procedure, are described in detail. To simulate natural landslide conditions, we conducted two types of tests: undrained cyclic-stress control tests and naturally drained monotonic pore-pressure control tests. Typical test results are presented to show the efficiency of this ring shear apparatus and the dynamic shear behaviour of sand.

Chapter 3 Grohovo Landslide- Assessment of Triggers. This chapter describes the study area and the Grohovo landslide in Croatia. It gives overview of the preparatory factors of the landslide by describing the geomorphological setting and the landslide itself. Furthermore, a detailed overview of the river's characteristics is given with emphasis on its torrential behaviour and flood occurrences that are related to mass movement occurrences in the past. To investigate the impact of rainfall as a trigger in the reactivation of the Grohovo landslide in 1996, rainfall data analysis was performed. Rainfall analysis is performed for both long- and short-term rainfall data and an estimation of both on the reactivation of the landslide is given. The antecedent conditions (60 days before the reactivation) that control groundwater level and soil moisture had a major role in landslide reactivation. For the assessment of seismic trigger the new ring shear apparatus, ICL-1, was used to simulate dynamic loading. By conducting a ring shear test on a specimen from the Grohovo landslide, basic soil parameters were obtained as well. Based on the analysis performed, and conducted tests, it was concluded that cumulative rainfall is the most probable trigger of this landslide.

Chapter 4 Negative Rate Effect in Sand-Bentonite Mixtures. The ICL-1 ring shear apparatus was used for the investigation of negative rate effect in cohesive soils. A significant drop in strength was reported in soils showing transitional shear behaviour (between sand and clay), at fast rates of displacement. However, because of technical difficulties, it was not possible to measure pore pressure during shearing. Therefore, a series of ring shear tests in silica sand and sand-bentonite mixtures were conducted to investigate this effect. Both single-stage and multi-stage tests in the mixtures resulted in a drop of residual strength between 0.1 and 1 mm/sec. Comparison of the multi-stage tests with gradual change of the rate of displacement, showed the following: in the case of an increase in the rate of displacement, there is a significant decrease of shear resistance and the effective friction angle in SB20 and SB30 specimens. The results showed that the residual friction angle increases linearly with the logarithm of the rate of displacement. The significance of these finding on a practical level is discussed.

Chapter 5 Conclusion. This dissertation is concluded based on the overall research results and findings presented and discussed in the previous chapters, and future research is suggested. The assessment of the triggers for the Grohovo landslide showed that the groundwater level change is the most important in landslide reactivation. Rainfall analysis indicated that the groundwater level is mainly influenced by a cumulative, long rainy period. However, additional parameters and a physically based rainfall threshold should be determined. The negative rate effect was investigated by conducting a series of ring shear tests on silica sand and sand-bentonite mixtures. Results of both single- and multi-stage tests in SB20 and SB30 specimens confirmed earlier findings; namely, a decrease in strength with an increase of the rate of displacement.

REFERENCES

Alarcon-Guzman, A., Leonards, G.A., and Chameau, J.L., 1988, "Undrained Monotonic and Cyclic Strength of Sands," *Journal of Geotechnical Engineering*, American Society of Civil Engineers, Vol. 114, No. 10, pp. 1089–1109.

Arbanas, Z. and Mihalic, S., 2012, "Progress in the Croatian–Japanese Joint Research Project On Landslides," *Proc. of the IPL Symposium*, Sassa, K., Takara, K. and Bin, He (Eds.), Kyoto, January 2012.

Bishop, A.W., Green, G.E., Garga, V.K., Andersen, A., and Brown, J.D., 1971, "A New Ring Shear Apparatus and its Application to the Measurement of Residual Strength," *Géotechnique*, Vol. 21, No. 1, pp. 273–328.

Bromhead, E.N., 1992, "The stability of slopes", Blackie Academic.

Bosdet, B.W., 1980, "The UBC Ring Shear Device," Master Thesis, University of British Columbia, Canada, 110 p.

Hvorslev, M.J., 1939, "Torsion Shear Tests and Their Place in the Determination of Shearing Resistance of Soils, "*Proceedings of the American Society of Testing and Materials*, Vol. 39, pp. 999–1022.

Mesri, G. and Shahien, M., 2003, "Residual Shear Strength Mobilized in First-Time Slope Failures," *J. Geotech. Geoenviron. Eng*., Vol. 129, No. 1, pp. 12-31.

Mihalic S. and Arbanas Z, 2012, "The Croatian–Japanese joint research project on landslides: activities and public benefits," *Landslides: Global Risk Preparedness*. Sassa, K. (Ed), Springer-Verlag, Berlin- Heidelberg, pp. 345-361.

Poulos, S.J., Castro, G. and France, J.W., 1985, "Liquefaction Evaluation Procedure," *Journal of Geotechnical Engineering Division*, American Society of Civil Engineers, Vol. 111, No. 6, pp. 772–792.

Sassa, K., Wang, G. and Fukuoka, H., 2003, "Performing Undrained Shear Tests on Saturated Sands in a New Intelligent Type of Ring Shear Apparatus," *Geotech. Test. J.*, Vol. 26, No. 3, pp. 257–265.

Sassa, K., Fukuoka, H., Wang, G.H. and Ishikawa, N., 2004, "Undrained Dynamic Loading Ring Shear Apparatus and its Application to Landslide Dynamics," *Landslides*, Vol. 1, No. 1, pp. 7–19.

Skempton. A.W., 1985, "Residual Strength of Clays in Landslides. Folded Strata and the Laboratory," *Géotechnique*, Vol. 35. No. 1, pp. 3-18.

Chapter 2 Stress- and Pore-Pressure Control-Ring Shear Testing for the Measurement of the Dynamic Shear Behaviour of Sands

This chapter presents the concept, design and construction of the portable undrained ring shear apparatus, ICL-1. The apparatus was designed to be inexpensive and transportable, so it could be used in different locations. Although reduced in dimensions, it can keep undrained conditions up to 1 MPa of pore water pressure (up to two times greater than in previous versions of apparatus) and load normal stress up to 1 MPa. Stress- and pore-pressure control tests were conducted on silica sand. The results of the tests on silica sand, as well as the experimental procedure, are described in detail. In order to simulate natural landslide conditions, we conducted two types of tests: undrained cyclic stress control tests and naturally drained monotonic pore pressure control tests. Typical test results are presented to show the efficiency of this ring shear apparatus and the dynamic shear behavior of sands.

2.1 INTRODUCTION: HISTORY AND USE OF RING SHEAR APPARATUS

The drained ring shear apparatus was designed specifically for the purpose of determining residual strength and to study the shear strength at failure and after failure. There are two advantages of the ring shear test: it shears the specimen continuously in one direction for an unlimited displacement and the cross section area of the shear plane is constant during shearing (Bishop et al. 1971). Due to this, a complete shear stress-shear displacement relationship (from peak to residual) can be measured.

The laboratory shear apparatuses most widely used to measure the peak strength for stability analyses are triaxial, direct shear and simple shear apparatuses. However, because

they produce a limited shear displacement, they are not suitable for determination of the residual shear strength. As a result, the ring shear apparatus was designed and developed and then widely used in the analysis of slope stability.

Although the ring shear was initially designed for the measurement of residual shear strength that governs the stability of previously failed structures (reactivated landslides), later, it was used in the investigation of natural phenomena that include large displacement, such as long run-out landslides.

2.1.1 Drained Ring Shear Test without Pore-Pressure Measurement

Today, there are several ring shear apparatuses available but the two most widely used are the apparatus based upon the Imperial College and Norwegian Geotechnical Institute concept (Bishop et al. 1971) and the Bromhead ring shear apparatus (Bromhead 1979). The main difference between these two types is in the configuration of the rings and accordingly, the location of the shear plane. In a split-ring device (Bishop type), the shear zone is at the mid-height, while in the solid-ring device (Bromhead type), the shear zone is at the top of the specimen and is often categorizied as a "smear-type" ring shear device (Meehan et al. 2008). Both types of ring shear apparatus have been modified and improved from their original design (Bromhead type - modified by Savage and Sayed 1984, Stark and Eid 1993, Stark and Poeppel 1994, Stark and Contreras 1996, Garga and Sedano 2002, Sedano et al. 2007, Meehan et al. 2007, 2008, Merchan et al. 2011, and Bishop type by Sassa 1984, Hungr and Morgenstern 1984, Tika 1989, Tika et al. 1996). The Sadrekarimi device is similar to the Bromhead type, except that the shear zone is not at the top, but in the bottom of the specimen (Sadrekarimi and Olson 2009).

All previously described devices were not able to perform undrained shearing tests because it was not possible to prevent water flow through the rotating gap (Table 2.1). Also, they have speed-controlled shearing. The exception is Sadrekarimi's device that can perform both speed and stress-controlled tests.

2.1.2 Undrained Triaxial Tests with Pore-Pressure Measurement

The undrained shear behaviour of sands is an important design issue, especially in liquefaction analysis where undrained steady state shear strength is required (Poulos et al. 1985, Alarcon-Guzman et al. 1988).

Based on the results of triaxial tests, Castro and Poulos (1977) and Poulos (1981) proposed the steady state concept and defined it as the state of deformation in which a soil mass is continuously deforming at constant volume, constant normal effective stress and constant shear stress. It is achieved after all particle breakage and all particle orientation has reached a steady state condition (Poulos et al. 1985).

The study of the steady state condition is very limited in triaxial test. The steady state study by triaxial compression tests has both advantages and limitations. Beside the fact that it has established procedures, triaxial tests can be stress or strain-controlled and they have drainage control, and both drained and undrained tests can be conducted. However, due to the limited displacement of the device, triaxial testing may not reach a true steady state. The steady state conditions are normally reached only at a larger shear displacement, well beyond those which can be attained in a triaxial test.

There are a few papers that give direct comparison of the steady state obtained in triaxial compression tests and ring shear tests. Okada et al. (2000) compared the steady state obtained in triaxial compression tests with the undrained ring shear tests while Garga and Sedano (2002) compared triaxial consolidated-undrained compression with constant volume ring shear tests.

2.1.3 Undrained Ring Shear Tests with Pore-Pressure Measurement

Based on the experimental results of undrained cyclic ring shear tests on soil samples from earthquake-induced catastrophic landslides, the concept of sliding surface liquefaction was introduced by Sassa (Sassa 1996, Sassa et al. 1996). Sliding surface liquefaction has been defined as the liquefaction that takes place only within the shear zone. it occurs due to grain crushing and resulting volume reduction as the shear displacement progress, which is

particularly important for landslides with high mobility and long travel distances (like flow slides or liquefaction failures of slopes).

Sassa and his colleagues have developed seven designs of ring shear apparatus since 1984 (Sassa et al. 2004). The later five apparatus of the series (DPRI-3, 4, 5, 6 and 7) have the capability of shear stress-controlled tests, which enable simulation of both monotonic and dynamic loadings (real seismic waves or sine wave form) under undrained conditions. Some of the apparatuses in the series also have pore-pressure control tests to simulate the ground water rise in the slope and/or displacement-control. Due to all these capabilities, these undrained dynamic loading ring shear apparatus are not used only as a basic soil test, to measure shear resistance as a parameter, but also as a landslide simulation test that can reproduce the stress and pore pressure acting on a potential sliding surface and the resulting sliding surface formation and the post-failure motion which will occur in the natural slopes during rainfalls, earthquakes and other stress changes. Compared to previous apparatus (DPRI-1 to 7), the new apparatus, ICL-1, has much smaller dimensions, but higher performance in undrain capability (Table 2.1). It can keep undrained conditions up to 1 MPa of pore water pressure and load normal stress up to 1 MPa. This makes it suitable for investigation of large-scale and deep-seated landslides.

2.2 UNDRAINED PORTABLE RING SHEAR APPARATUS

The prevention of the leakage of water and soil through the gap between the upper and lower rings and the measurement of pore water pressure are the most difficult in the undrained ring shear apparatus.

As stated by Sadrekarimi and Olson (2009), although the undrained ring shear apparatus is effective and powerful, this device is complex and very expensive to manufacture. The Undrained Portable Ring Shear Apparatus, ICL-1 (Figure 2.1), was designed by Professor Sassa in 2011, as part of a project of SATREPS (Science and Technology Research Partnership for Sustainable Development) and the JICA/JST project "Risk identification and land-use planning for disaster mitigation of landslides and floods in Croatia" (IPL-161). The goal was to develop a much more inexpensive and transportable

Table 2.1 Characteristics of the Portable Undrained Ring Shear Apparatus ICL-1, compared with other ring shear apparatus (modified from Sassa et al. 2004).

	Bishop (1971)	LaGatta (1970)	Hungr & Morgenstern (1984)	Sassa (1992) DPRI-3	Sassa (1996) DPRI-4	Sassa (1997) DPRI-5	Sassa (1997) DPRI-6	Garga & Sendano (2002)	Sassa (2004) DPRI-7	Sadrekarmi & Olson (2009)	Sassa (2011) ICL-1
D_i [a]	10.16	5.08	22.0	21.0	21.0	12.0	25.0	9.2	27.0	20.3	10.0
D_o [b]	15.24	7.11	30.0	31.0	29.0	18.0	35.0	13.3	35.0	26.9	14.0
H_{max} [c]	1.9	2.5	2.0	9.0	9.5	11.5	15.0	2.0	11.5	2.6	5.0
σ_{max} [d]	980	800	200	500	3.000	2.000	2.000	660	500	700	1000
v_{max} [e]	-	0.001	100.0	30.0	18.0	10.0	224.0	-	300.0	788	5.4
UT[f]	No	No	No	Yes	Yes	Yes	Yes	No	Yes	No	Yes
u_{max} [g]					400-600	400-600	400-600		600		1000

[a] D_i-Inner diameter (cm), [b] D_o- Outer diameter (cm), [c] H_{max} -Maximal height of specimen (cm), [d] σ_{max}- Maximal normal stress (kPa), [e] v_{max}-Maximal shear speed (cm/s), [f] UT-Undrained testing, [g] u_{max}-Maximal pore pressure (kPa)

undrained ring shear apparatus for use in different organizations with standard electricity available anywhere (single phase electricity of 220 and 110 V).

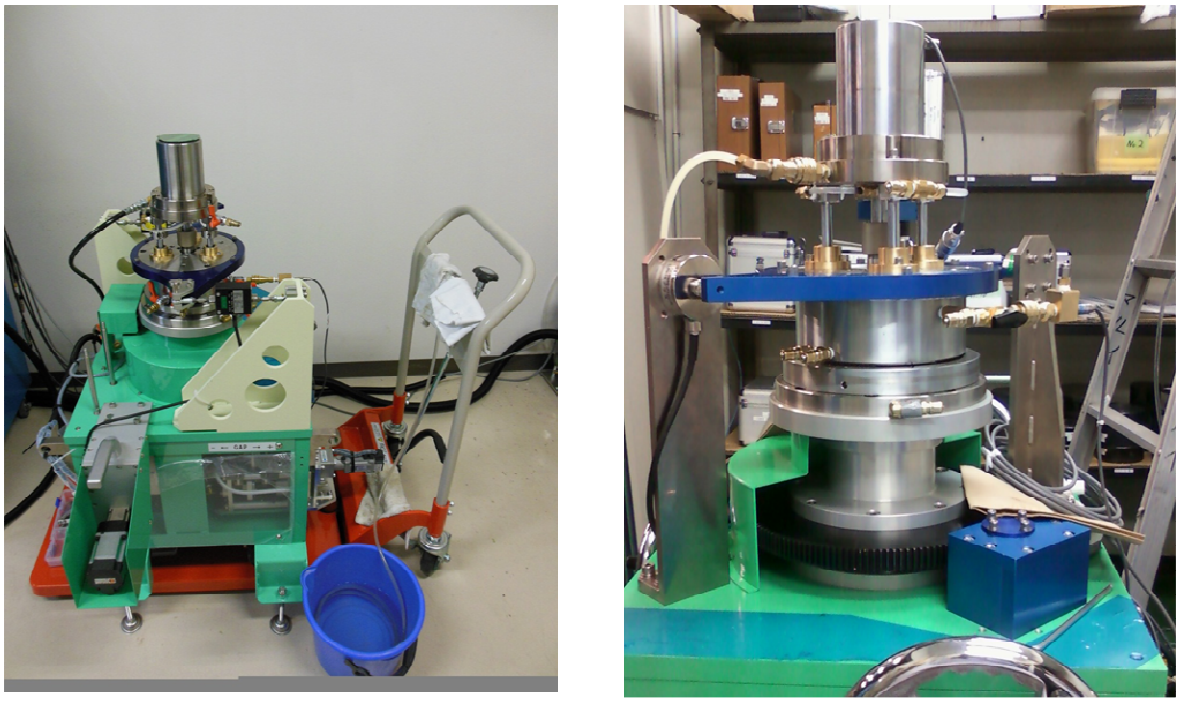

Figure 2.1 Transportable ring shear apparatus (ICL-1): right- ICL-1 on a cart, left- larger view.

In order to be easily transportable, its dimensions were significantly reduced compared to previous apparatus of the DPRI series. ICL-1 has the weight of approximately 100 kg, a maximum height of 95 cm, the dimensions 50x50 cm, and is set on a handcart (Figure 2.1). The reduction in dimensions of the latest apparatus was possible because of smaller shear velocity (5.4 cm/s) and a new loading system in which normal stress is applied by pulling the central axis instead of the high loading frame to push the vertical force onto the sample.

2.2.1 General Structure

An annular ring-shaped specimen (S) is confined laterally between the outer and inner rings and is sheared at its mid-height. During the test, the specimen is subjected to a constant normal stress, and loaded through an annular loading platen connected to an oil

piston (Figure 2.2). The lower half of the shear box (SB) rotates in both directions (marked in Figure 2.2 as the rotating part), while the upper half (marked as a movable part in Figure 2.2) of the shear box is restrained with two shear resistance cells (S1 and S2 in Figure 2.2) that measure shear resistance. When failure occurs, the specimen is sheared by a relative rotary motion and the lower part rotates along with the rotating table.

The inner diameter of the shear box is 10 cm, the outer is 14 cm, and the shear area is 75.36 cm^2. The maximum height of the specimen is 5 cm. By adding porous metals to the lower ring, the lower height of the shear box can be adjusted from 0.7 to 1.3 cm, which is very useful for a limited amount of specimens, as well as for low permeable specimens.

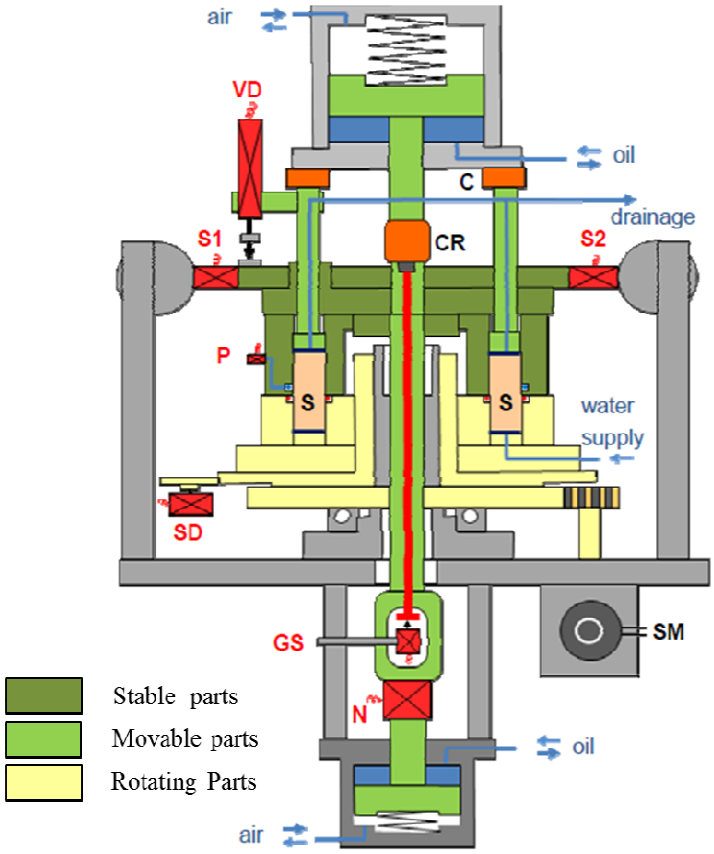

Figure 2.2 Mechanical structure of the apparatus (S- Specimen; CR- Connection ring; C- Connection; N- Load cell for normal stress; S1, S2- Load cell for shear resistance; P- Pore-pressure transducer; GS- Gap sensor; VD- Vertical displacement transducer; SD- Shear displacement transducer).

2.2.2 Loading System and Gap Control System

Static and cyclic normal stress is generated by an oil piston controlled by a servo-motor (200 W) (Figure 2.3). Normal stress is applied by pulling the central axis.

The shear stress is given by the second servo control motor (400 W) either by shear stress-control, speed-control, or displacement-control. Shear stress in stress-control mode can be applied in different ways: as static (monotonic) or dynamic (cyclic or seismic).

During the test, the gap value is maintained constant automatically by the oil piston controlled by the third servo- motor (Figure 2.3). The gap servo-motor uses a feed-back signal obtained from a gap sensor (GS) with the precision of 1/1000 mm. The gap control system (oil piston and gap sensor) enables the prevention of the leakage of water and specimen during high-speed shearing.

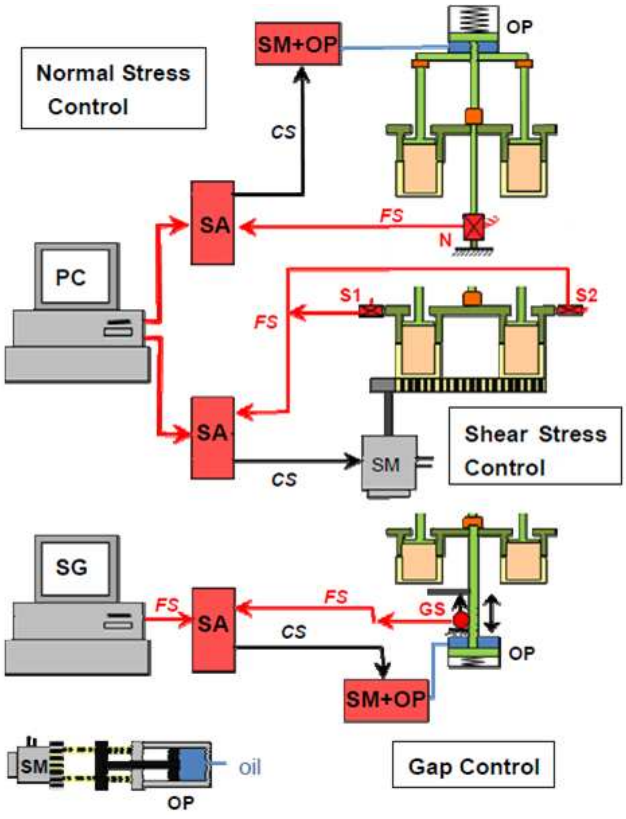

Figure 2.3 Electronic control system (N- Load cell for normal stress; S1, S2- Load cell for shear resistance; GS- Gap sensor; FS- Feedback signal CS- Control signal; PC- Computer; SG- Signal generator; SM- Servo-motor; OP- Oil Piston; SA- Servo amplifier).

2.2.3 Monitoring System

The vertical load is monitored by a normal load cell (N in Figure 2.2) with the capacity of 10 kN. The measured vertical load is the sum of the loads on the rubber edge (contact pressure), the friction between the sample and the sides of the upper shear box (SB) and the weight of the upper part of SB.

The shear load acting on the shear surface is monitored by a pair of the shear load cells (S1 and S2 on Figure 2.2), each of 1 kN capacity. The resistance acting on the shear plane is calculated from the measured value in the load cells (S1 and S2) retaining the upper half from the rotation against the loaded shear stress on the shear plane. The real shear resistance of the soil is the measured value in the load cell minus the rubber-edge friction.

The horizontal shear displacement is monitored by a rotary transducer (SD) at the center of the shear area. The vertical displacement is measured by a linear transducer (VD) that measures the displacement of the loading plate (LP).

The data concerning normal stress σ, shear stress τ, pore pressure u, variation of sample height and shear displacement as well as gap value and control signal given by the servo-motor (for both vertical or shear stress) are stored by a personal computer. A software application developed by Marui & Co., Ltd. Osaka, is used for control and data recording.

2.2.4 Undrained Shear Box and Pore-Pressure Measurement

The most essential part of the ring shear apparatus is the construction of the undrained shear box. Design of the shear box (SB) is illustrated in Figure 2.4 with an enlarged diagram of the left half of the cross section of the SB and its surroundings, including the water pressure measurement system.

Pore pressure is monitored by two pore-pressure transducers (P), connected to the valves placed on the gutter in the shear zone. The pore-pressure transducer has a diaphragm that is deformed by water pressure which provides electrical output. The gutter (7×7 mm) extends along the entire circumference of the inner wall of the outer - upper ring

of the SB (Figure 2.4). The gutter is located 2 mm above the shear surface and is filled with felt cloth sandwiched between two metal filters (with pore sizes of 100 μm and 40 μm). Although the monitoring point is not at the center of the shear zone, this system is sensitive to pore-pressure monitoring.

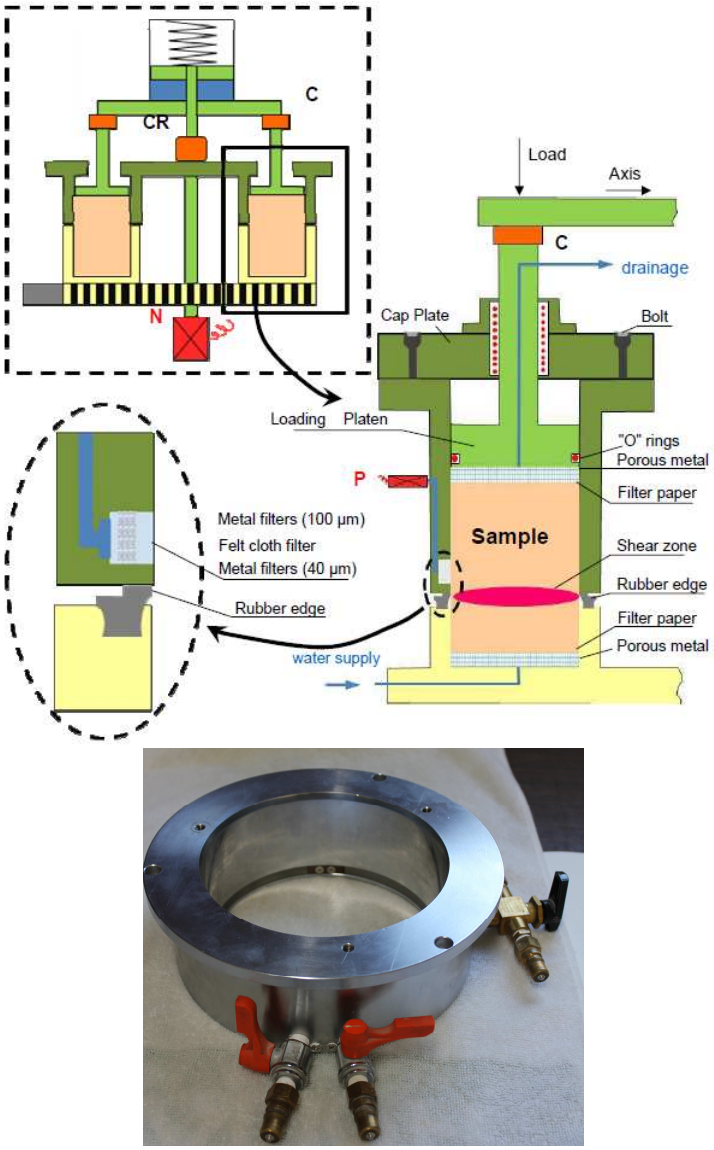

Figure 2.4 A half-section of the shear box and a close-up diagram of the edges plus a photo of the shear box with a metal filter and gutter detail below (CR- Connection ring; C- Connection; N- Load cell for normal stress; P- Pore-pressure transducer).

In the DPRI apparatus, rubber edges are fixed with glue to the lower pair of rings, but in ICL-1 they are pressed by Teflon rings and stainless steel rings without glue. When rubber edges are used or damaged they can be easily replaced with a new pair by

unscrewing the Teflon rings and stainless steel rings. Rubber edges used in ICL-1 have 2 mm width and 90˚ of the rubber-hardness index. Water leakage tightness is provided by O-rings on the upper loading plate and rubber edges on two confining rings of the lower rotary pair.

2.3 SPECIMEN CHARACTERISTICS

In this study Silica Sand No8 is used because it is a material commercially available in Japan and the results can be easily compared to previous studies made on ring shear apparatuses (Okada et al. 2000, 2004, 2005; Sassa et al. 2003). Silica Sand No. 8 is sand made by grinding silica sandstone, mainly consisting of quartz and smaller amounts of feldspar. Silica Sand No 8 is a silty sand (particles ranging from fine sand to silt), with a mean diameter of D_{50} = 0.07 mm, and a specific gravity G_s = 2.59. Figure 2.5 shows the grain-size distribution of used Silica Sand No 8. The range of values of dry densities (minimal 1.29 g/cm^3 and maximal 1.31 g/cm^3) and void ratios are given in Table 2.2.

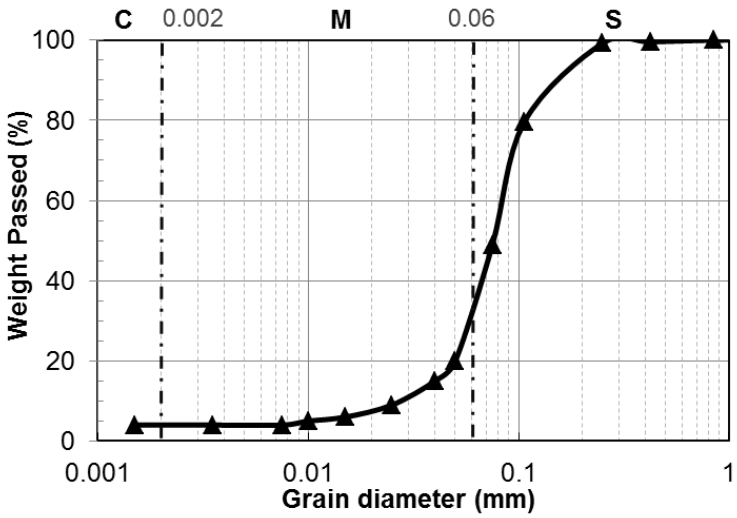

Figure 2.5 Grain-size distribution of Silica Sand No 8.

2.4 PREPARATION TESTS

Before testing the specimen, preparation tests, consisting of water leakage and rubber edge friction tests should be made. Preparation tests are made only with water inside the shear box. To reduce friction and prevent leakage, rubber edges are sprayed with Teflon spray and coated with silicon grease. Then, the shear box is assembled and the gap value is adjusted by applying an initial contact force of 0.8 kN, in order to make contact pressure between the upper pair of rings and the rubber edges on the lower part of the SB. The contact force is maintained constantly during the test through the gap control system. After gap value is adjusted, a water leakage test is conducted to proof that water leakage will not occur under certain normal stress and shear speeds.

Next, the friction between the rubber edge and the upper part of ring is measured. The measured friction corresponds to the applied contact force of 0.8 kN. The results of the rubber edge friction measurement are shown in the Figure 2.6. An initial increase in shear resistance is reached at 0.1 mm of shear displacement and represents elastic deformation of the rubber edge. After this initial peak, the shear resistance has almost the constant value of approximately 15 kPa for all shear speeds.

2.5 SPECIMEN PREPARATION

After preparation tests, tests on a saturated specimen were performed and consisted of the following steps: CO_2 saturation of SB; specimen setting; de-aired water circulation; saturation checking by B_D measurement; specimen consolidation and shearing (by cyclic stress control and pore pressure control).

After the gap was adjusted, SB without specimen was filled with CO_2. The CO_2 was very slowly introduced into the SB through the lower drainage line and discharged from all valves in the SB. This was necessary in order to expel the air entrapped in the gutter, the line to the pore pressure sensor, and porous metal filters of the lower ring.

Dry silica sand was poured by funnel into the SB using a free-fall deposition method. Filter papers were placed on the top and bottom of the specimen to prevent particle entering. The specimen height was 37 mm from the top. Before water circulation

and checking BD, the specimen was initially consolidated under the normal stress of 25-30 kPa in the drained condition, to make contact between the specimen (i.e. filter paper) and porous metal of LP.

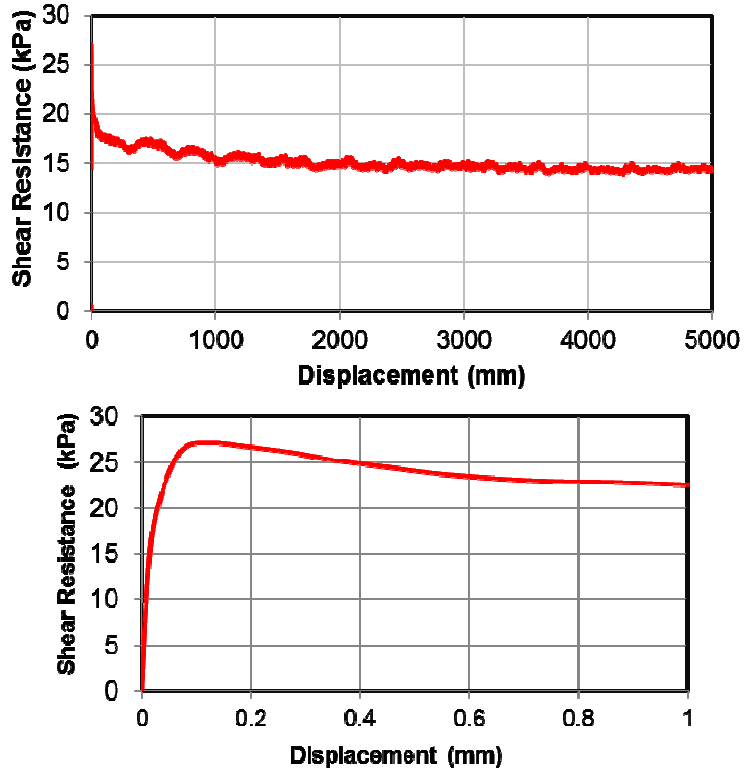

Figure 2.6 Rubber edge friction: **a)** Shear displacement of 5 m and **b)** Shear displacement 1 mm.

After the contact was obtained, water circulation could start to enable full water saturation of the specimen. De-aired water was supplied through the lower drainage line, and discharged from the upper drainage line until all air bubbles were expelled. The water circulation process was kept at a very slow rate.

After the specimen was fully saturated, the degree of saturation was checked by using B_D value. As proposed by Sassa (1988), B_D is a pore-pressure parameter that is related to the degree of saturation in the direct-shear state, formulated as:

$$B_D = \frac{\Delta u}{\Delta \sigma} \qquad \text{(Eq. 2.1)}$$

where Δu is the increment of pore-water pressure and $\Delta\sigma$ is a change in total normal stress- , measured in undrained conditions. Specimens with B_D greater than 0.95 are considered to be fully saturated. For specimens prepared for undrained cyclic stress control tests, we obtained B_D>0.95 (Table 2.2). For pore-pressure controlled tests, it is not necessary to obtain a high B_D value since shearing takes place in the naturally drained state.

After checking the B_D value, normal stress is decreased to a value where the excess pore pressure is close to zero so the upper valve can be open. Then, normal stress was applied to the pre-decided value of 400 kPa. After normal stress, a different shear stress was applied (150, 200, 250 kPa) in a drained condition to simulate the stress state in the slope.

The initial dry density as well as the initial void ratio was calculated after initial normal and shear stress was applied in drained condition, based on vertical displacement monitoring (Table 2.2).

Table 2.2 Ring shear test conditions.

Test	Type	Initial Stress σ_0, τ_0, (kPa)	B_D	Drainage	Initial Dry Density ρ_d (g/cm^3)	Initial Void Ratio e
1	CSSCT [a]	400, 250	0.97	Undrained	1.30	0.99
2	CSSCT [a]	400, 200	0.97	Undrained	1.29	1.01
3	CSSCT [a]	400, 150	0.95	Undrained	1.29	1.01
4	PPCT [b]	400, 250	/	Drained	1.31	0.98
5	PPCT [b]	400, 200	/	Drained	1.30	1.0
6	PPCT [b]	400, 150	/	Drained	1.30	1.0

[a] CSSCT= Cyclic Shear Stress Control test, [b] PPCT= Pore Pressure Control test.

2.6 TESTING AND RESULTS

After initial stresses on the sliding surface were reproduced, undrained cyclic shear stress control tests and naturally drained pore-pressure control tests were performed. Test conditions are summarized in Table 2.2 and test results described later in section.

To simulate natural landslide conditions two types of tests were conducted: undrained cyclic stress control tests and naturally drained pore-pressure control tests. Undrained cyclic stress control tests were made to simulate dynamic loading and earthquake-induced landslides, while pore-pressure control tests were made to simulate the rise of the groundwater level during rainfall.

2.6.1 Undrained Cyclic Stress Test

Undrained cyclic loading tests were performed on saturated silica sand specimens. After initial stresses were created by applying pre-decided normal and shear stress in a drained condition, dynamic, cyclic loading was applied in an undrained condition. For all undrained cyclic tests, 100 cycles of sine wave shear stress were loaded at 0.2 Hz. We used the constant increment of 100 kPa of shear stress. Three tests were conducted, under different initial shear stresses (250, 200 and 150 kPa) that correspond to different slope inclinations (32°, 27° and 21°). Monitored data were recorded with a sampling of 50 Hz.

The results of undrained cyclic tests are presented in Figures 2.7-2.9, where each figure consists of the stress path, time series, and shear displacement data. Stress path graphs (Figures 2.7a, 2.8a and 2.9a) showing the peak failure line and the failure line during motion, and also the apparent friction angle. The blue line is the total stress path (TSP) and the red line is the effective stress path (ESP). Values of the shear resistance shown on Figures 2.7 – 2.9 are the corrected values obtained by subtracting rubber edge friction of 15 kPa (Figure 2.6) from the monitored shear stress value.

Figure 2.7 shows the undrained cyclic test for the specimen consolidated under an initial normal stress of 400 kPa and a shear stress of 250 kPa. In this case, soon after initial increment of 100 kPa of cyclic loading was applied, an effective stress path reached the failure line and moved down along the failure line during motion. Peak shear resistance

was reached at 282.3 kPa at shear displacement of 3.9 mm. The peak friction angle of 35.0° (Figure 2.7a) was calculated. From the failure line during motion, the friction angle during motion was calculated to be 31.0°. The test gave an apparent friction angle of 10.5°. Shearing stopped after 250 seconds at the displacement of 6 meters before 100 cycles were applied (Figure 2.7 b and c).

Figure 2.8 shows the undrained cyclic test for the specimen consolidated under an initial normal stress of 400 kPa and a shear stress of 200 kPa. Similarly to the previous case, soon after cyclic stress was applied, an effective stress path reached the failure line and moved down along the failure line during motion. Peak shear resistance was reached at 260.65 kPa and a peak friction angle of 34.7°, the friction angle during motion (30.5°), as well as the apparent friction angle of 11.5° were calculated (Figure 2.8a). Shearing was stopped when shear displacement reached 3 m (Figure 2.8 b and c).

For the case when the specimen was consolidated under the initial normal stress of 400 kPa and a shear stress of 150 kPa, similar results were obtained. Results of these tests are shown in Figure 2.9. Peak shear resistance was reached at 223.5 kPa and peak and apparent and friction angle during motion were calculated (35.9°, 10.7° and 30.5° respectively).

2.6.2 Pore-Pressure Control Test

Pore-pressure control tests were conducted to simulate the failure and post-failure behaviour corresponding to rainfall in a naturally drained condition. Pore pressure is supplied to the shear box through the upper drainage valve and then gradually increased. Since the upper valve is open, the water is free to move and this is considered to be a naturally drained condition. The pore pressure is controlled by the computer and the water tank connected to the nearby air tank with a servo-controlled air regulator.

Three pore pressure control tests were performed in this study, under the same initial normal stress (400 kPa) and different initial shear stress (150, 200, 250), corresponding to different slope inclinations (21°, 27°, 32°). Then, pore pressure was increased until failure, while keeping normal (400 kPa) and shear stress (150, 200, 250 kPa) constant. The same pore-pressure increase rate (0.5 kPa/s) was used in all tests.

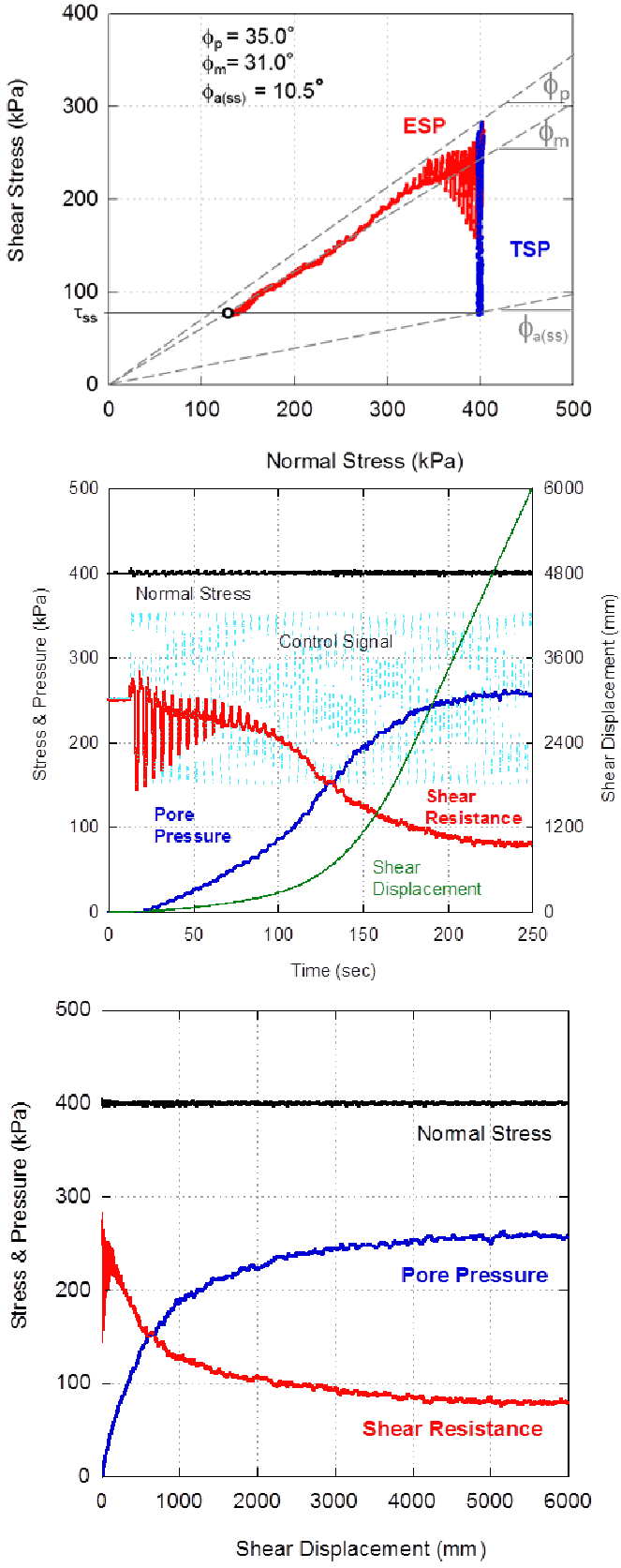

Figure 2.7 Undrained cyclic loading test 1 for initial shear stress of 250 kPa (B_D=0.97, ρ_d =1.30 g/cm^3): **a)** Stress path, **b)** Time series data for normal stress, pore-water pressure, shear resistance, control signal and shear displacement, and **c)** Shear displacement series data for normal stress, pore-water pressure and shear resistance.

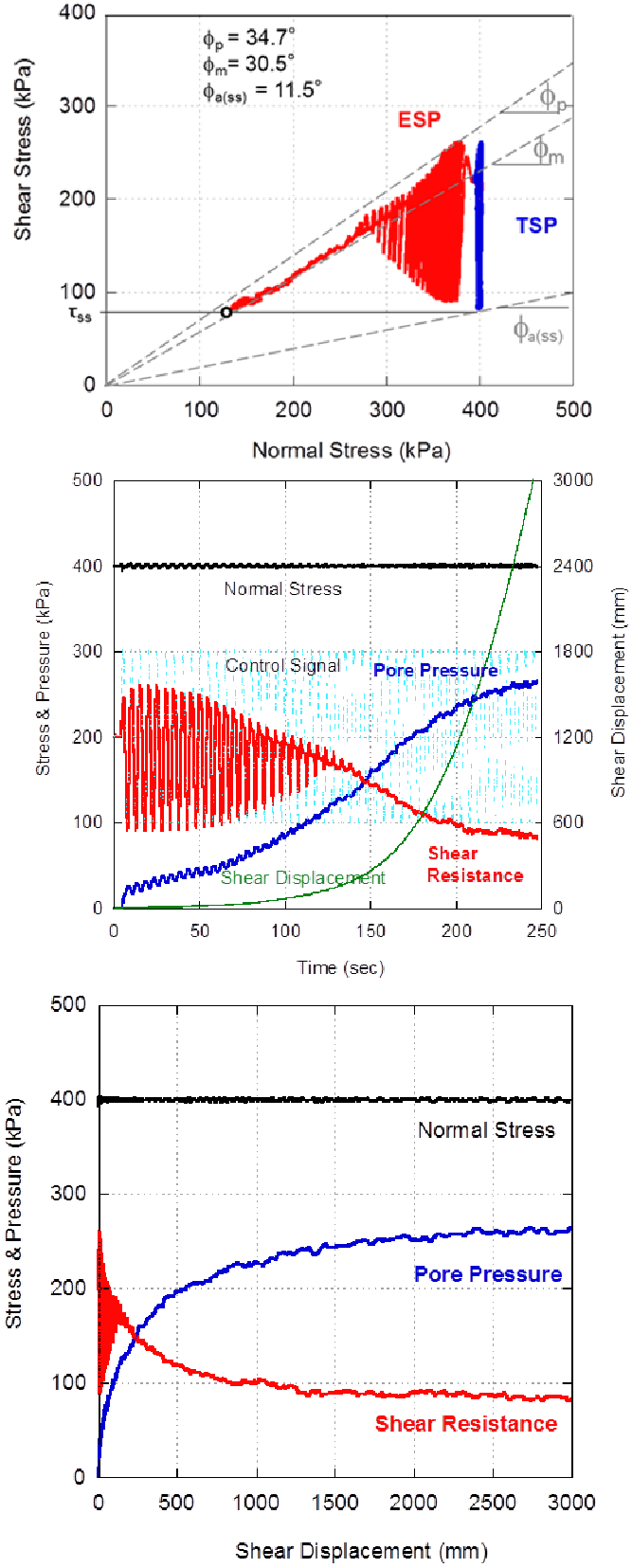

Figure 2.8 Undrained cyclic loading test 2 for initial shear stress of 200 kPa (B_D=0.97, ρ_d=1.29 g/cm^3): **a)** Stress path, **b)** Time series data for normal stress, pore-water pressure, shear resistance, control signal and shear displacement, and **c)** Shear displacement series data for normal stress, pore-water pressure and shear resistance.

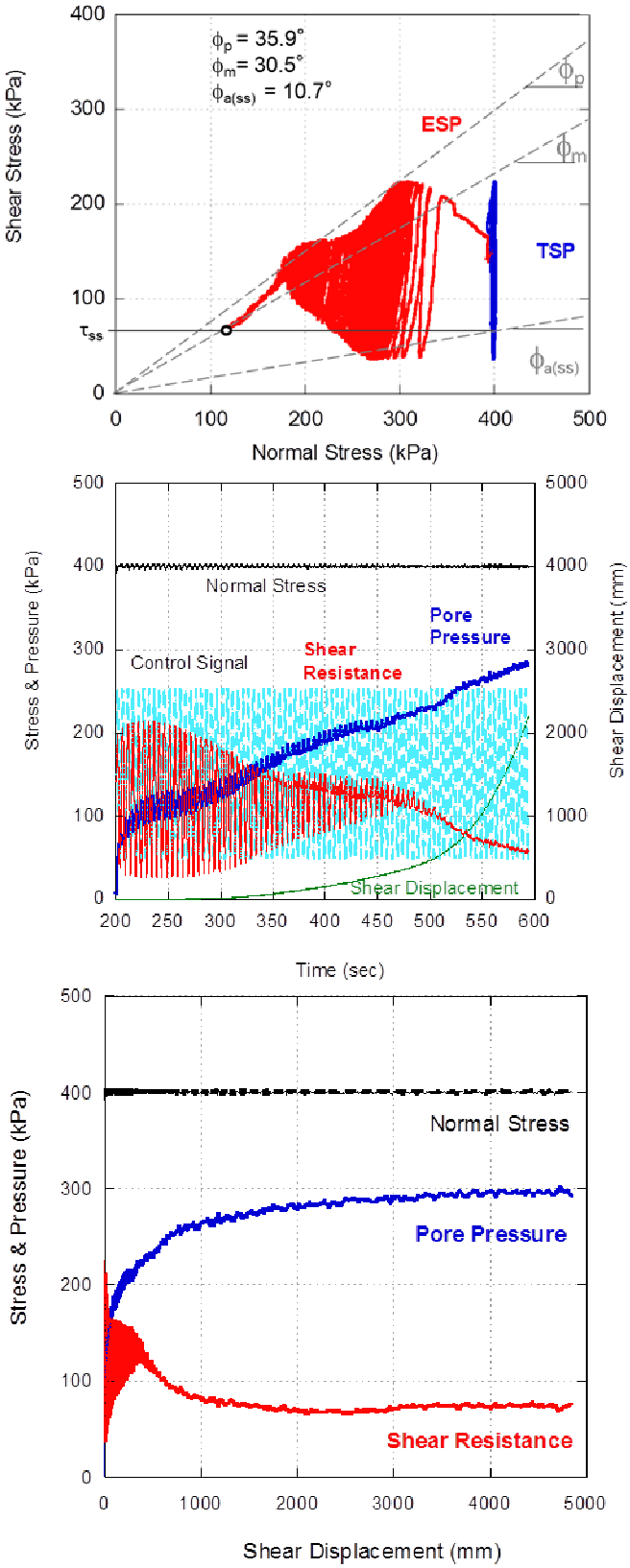

Figure 2.9 Undrained cyclic loading test 3 for initial shear stress of 150 kPa (B_D=0.95, ρ_d=1.29 g/cm^3): **a)** Stress path, **b)** Time series data for normal stress, pore-water pressure, shear resistance, control signal and shear displacement, and **c)** Shear displacement series data for normal stress, pore-water pressure and shear resistance.

Stress paths of all pore pressure control tests are shown in the Figure 2.10 and time series and shear displacement data separately for each test in Figures 2.11-2.13. Shear resistance was corrected by subtracting the rubber edge friction of 15 kPa. Figure 2.10 shows that depending on the initial stress (I_1, I_2 and I_3), specimens reached the failure line at different points (F_1, F_2 and F_3) and different peak friction angles accordingly. Failure occurred when the effective stress path reached the failure line, and it moved down along the failure line during motion.

As can be seen, the failure line during motion is 31.5°. The calculated peak as well as the friction angle during motion obtained in the pore-pressure control tests (Figure 2.10) are in accordance with the values obtained in cyclic stress control tests (Figures 2.7-2.9).

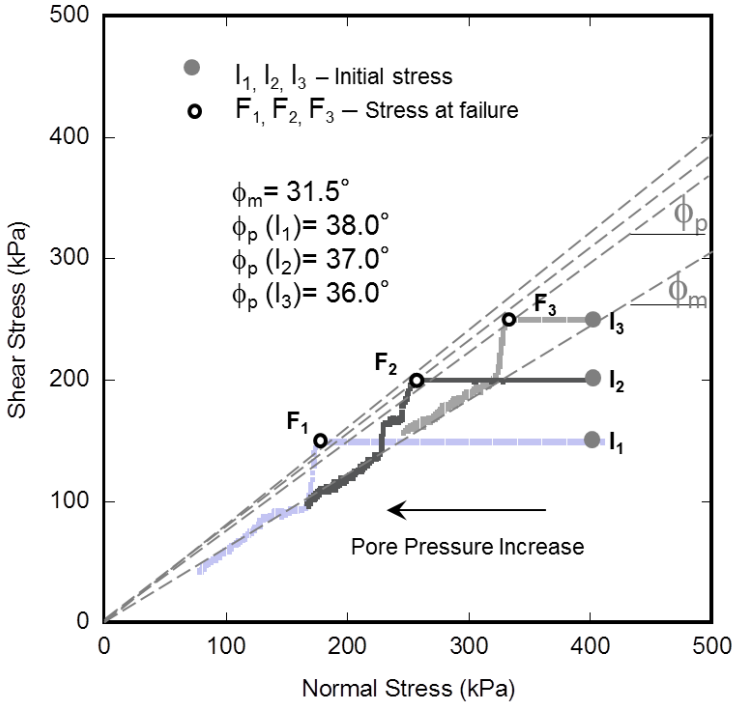

Figure 2.10 Stress paths of pore pressure control tests (I_1-I_3).

The results obtained by cyclic stress control and pore-pressure control tests are in accordance with the results obtained for the same specimen by Okada (Okada et al. 2000, 2005) and Sassa (Sassa et al. 2003) using DPRI-5 and DPRI-6 apparatus.

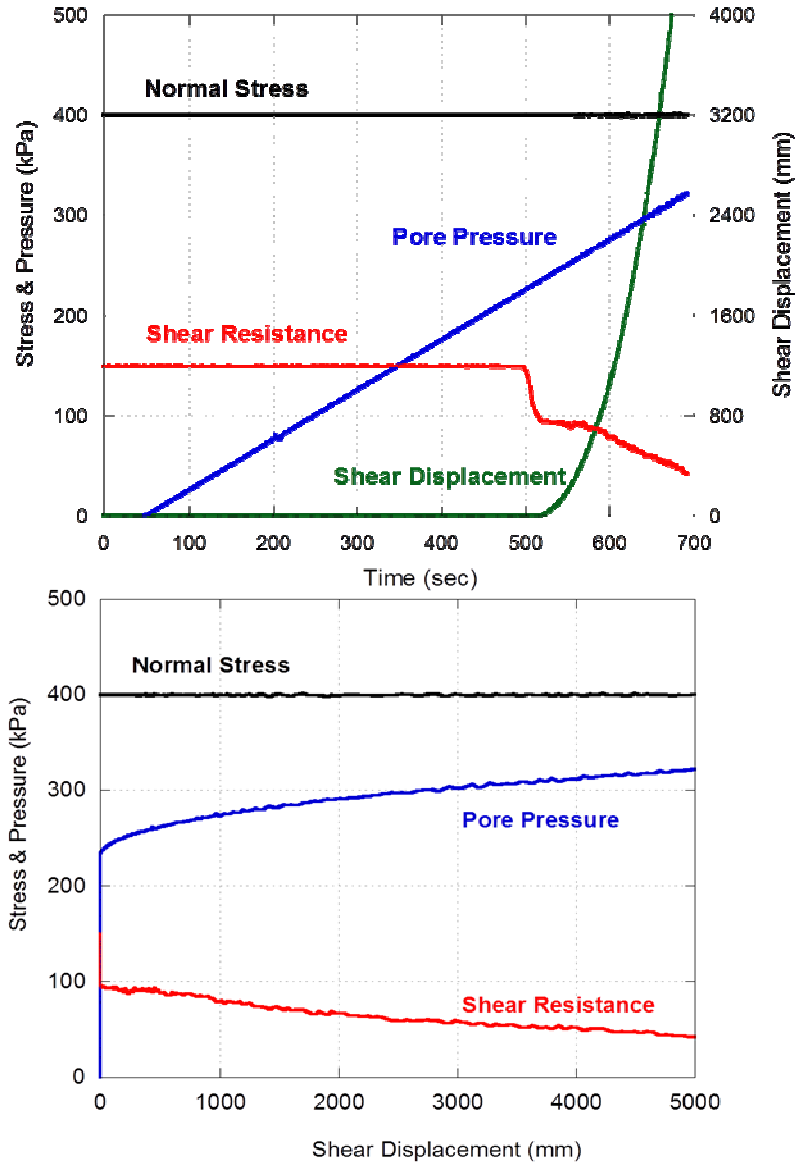

Figure 2.11 Time series and shear displacement data for initial stress I_1 (400 kPa, 150 kPa).

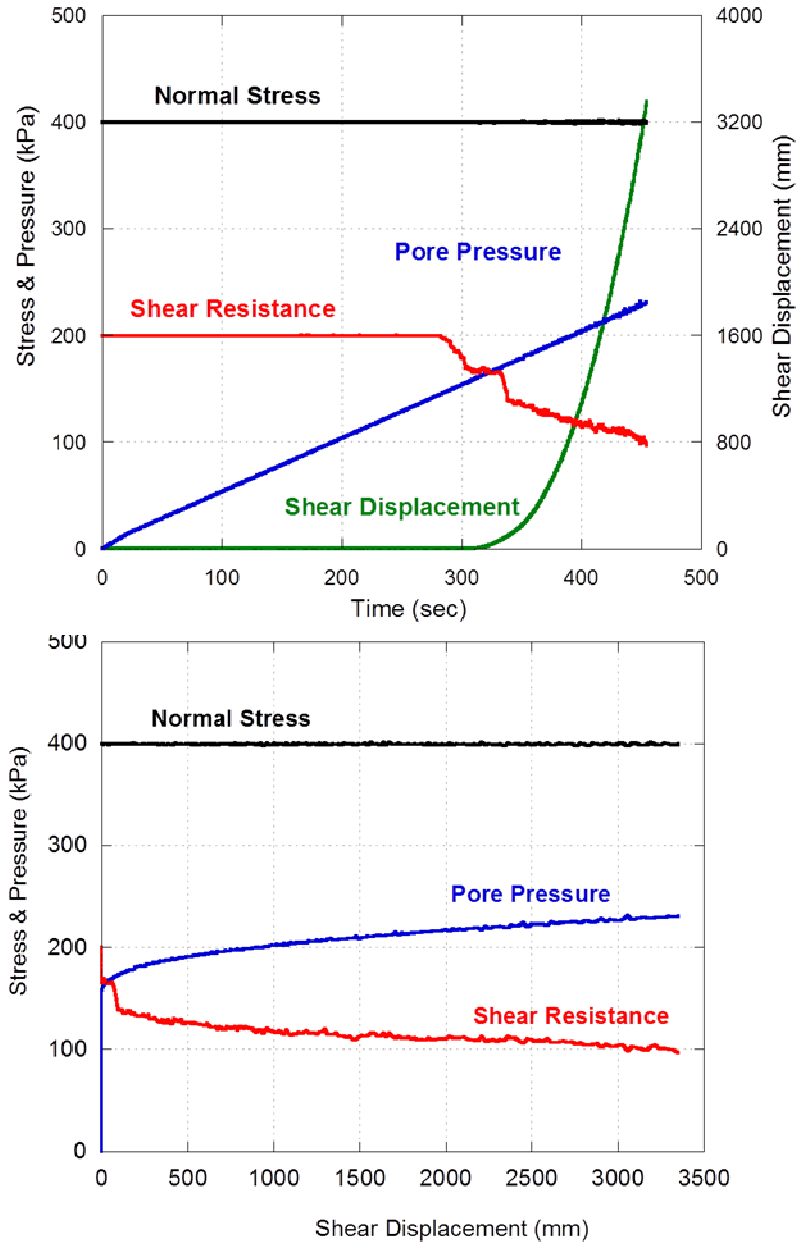

Figure 2.12 Time series and shear displacement data for initial stress I_2 (400 kPa, 200 kPa).

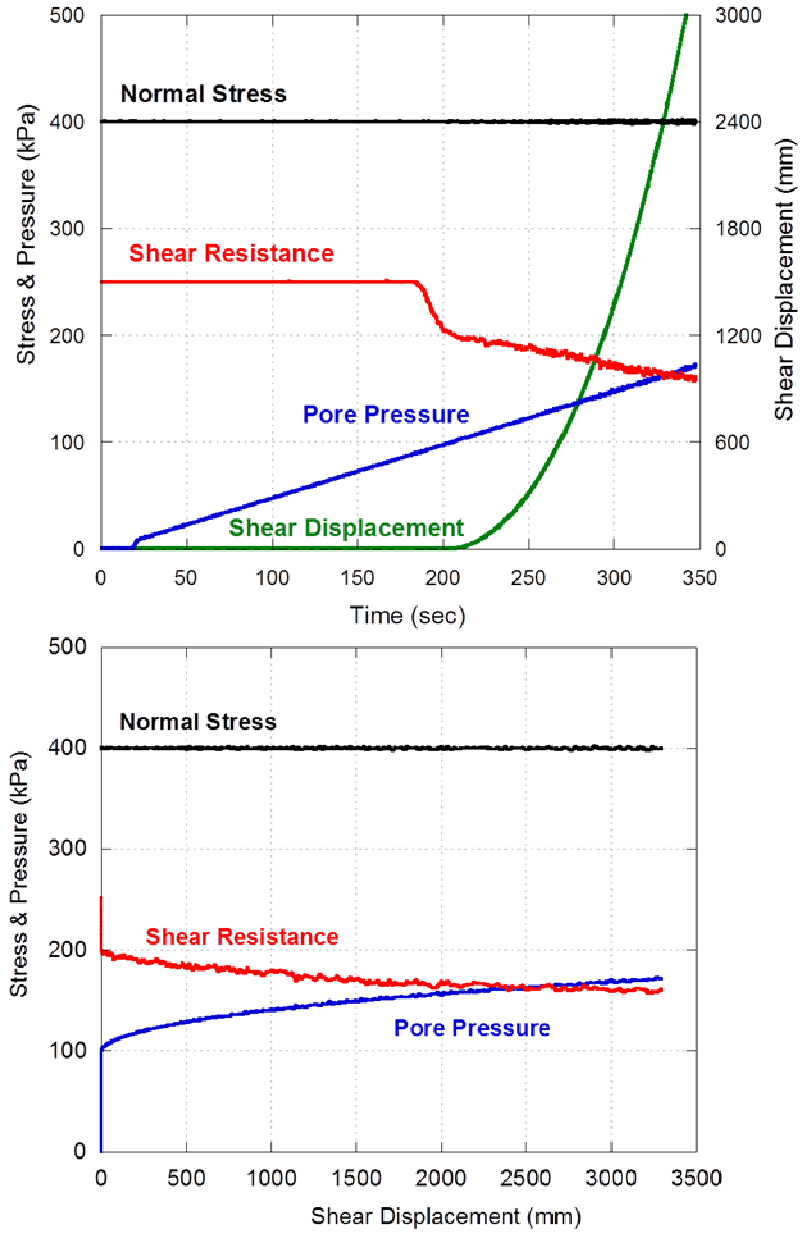

Figure 2.13 Time series and shear displacement data for initial stress I_3 (400 kPa, 250 kPa)

2.7 SUMMARY AND CONCLUSION

Although all the ring shear devices from the DPRI series were recognized as effective and powerful, their main disadvantage was that they are complex and expensive to produce (Sadrekarimi and Olson 2009). The transportable and compact high-stress undrained-loading ring shear apparatus presented in this paper (ICL-1) was developed by Sassa in 2011. The initial plan was to develop a transportable device to be donated to Croatia as a part of the Science and Technology Research Partnership for Sustainable Development (SATREPS)

This chapter has presented the principle of the design and the structure of the transportable ring shear apparatus ICL-1. Since one of the goals of this apparatus was to be transportable and used in Croatia, some of the modifications were made in order to be easily maintained outside of Japan. Most of these modifications have practical meaning. However, in the development of a new testing device, consideration had to be given to simplicity in the construction and operation of the testing apparatus, specimen preparation and to time required for testing. As stated by Bishop et al. (1971), the ring shear apparatus often fails in satisfying some of the criteria of simplicity of construction and operation, and the duration of tests. With some of the modifications in ICL-1, some of the criteria mentioned above are satisfied. Rubber edges are not fixed with glue to the lower pairs of rings, like in previous DPRI series, but with the Teflon and stainless steel rings and screws. This enables easy replacement of the damaged rubber edge with the new one. Also, the gutter can be opened for cleaning and change of metal filters and felt cloth. Depending on the material tested, annular metal filters with different pore sizes could be used. The height of the lower part of the shear box can be adjusted by adding porous metals. This is useful for test-time reduction in low permeable specimens.

By performing tests (undrained cyclic stress control test and naturally drained pore-pressure control test) on fine silica sand, related experimental procedures are presented in detail. Typical test results are presented to show the efficiency of this ring shear apparatus as well as its application for earthquake-induced landslides through the undrained cyclic loading test and the rain- induced landslide through the drained pore-pressure control test.

Although initially designed for sub-aerial landslides, ICL-1 was recently used for investigation of the hypothesis of an earthquake-induced submarine landslide in Suruga Bay (Sassa et al. 2012).

REFERENCES

Alarcon-Guzman, A., Leonards, G.A. and Chameau, J.L., 1988, "Undrained Monotonic and Cyclic Strength of Sands," *Journal of Geotechnical Engineering*, American Society of Civil Engineers, Vol. 114, No. 10, pp. 1089-1109.

Bishop, A.W., Green, G.E., Garga, V.K., Andersen, A. and Brown, J.D., 1971, "A New Ring Shear Apparatus and its Application to the Measurement of Residual Strength," *Géotechnique*, Vol. 21, No. 1, pp. 273-328.

Bromhead, E.N., 1979, "A Simple Ring Shear Apparatus," *Ground Engineering*, Vol. 12, No. 5, pp. 40–44.

Castro, G. and Poulos, S.J., 1977, "Factors Affecting Liquefaction and Cyclic Mobility," *Journal of Geotechnical Engineering Division*, American Society of Civil Engineers, Vol. 103, pp. 501-516.

Garga, V.K. and Infante Sedano, J.A., 2002, "Steady State Strength of Sands in a Constant Volume Ring Shear Apparatus," *Geotech. Test. J.*, Vol. 25, No. 4, pp. 414–421.

Hungr, O. and Morgenstern, N.R., 1984, "High Velocity Ring Shear Tests on Sand," *Géotechnique*, Vol. 34, No. 3, pp. 415-421.

La Gatta, D.P., 1970, "Residual Strength of Clays and Clay-Shales by Rotation Shear Tests," Ph.D. thesis reprinted as *Harvard Soil Mechanics Series* No. 86, Harvard University, Cambridge, MA, 204 p.

Meehan, C.L., Brandon, T.L. and Duncan, J.M., 2007, "Measuring Drained Residual Strengths in the Bromhead Ring Shear," *Geotech. Test. J.*, Vol. 30, No. 6, pp. 466-473.

Meehan, C.L., Brandon, T.L. and Duncan, J.M., 2008, "Measuring "Fast" Shear Strengths along Slickensided Surfaces in the Bromhead Ring Shear," *Geotech. Test. J.*, Vol. 31, No. 3, pp. 239-242.

Merchan, V., Romero, E. and Vaunat, J., 2011, "An Adapted Ring Shear Apparatus for Testing Partly Saturated Soils in the High Suction Range," *Geotech. Test. J*., Vol. 34, No. 5, pp. 1-12.

Okada, Y., Sassa, K. and Fukuoka, H., 2000, "Liquefaction and the Steady State of Weathered Granitic Sands Obtained by Undrained Ring Shear Tests: a Fundamental Study on the Mechanism of Liquidized Landslides," *Journal of Natural Disaster Science*, Vol. 22, No. 2, pp. 75-85.

Okada, Y., Sassa, K. and Fukuoka, H., 2004, "Excess pore pressure and grain crushing of sands by means of undrained and naturally drained ring-shear tests," *Engineering Geology*, Vol. 75, pp. 325-343.

Okada, Y., Sassa, K. and Fukuoka, H., 2005, "Undrained shear behaviour of sands subjected to large shear displacement and estimation of excess pore-pressure generation from drained ring shear tests," *Can. Geotech. J.*, Vol. 42, pp. 787-803.

Poulos, S.J., 1981, "The Steady State of Deformation," *Journal of Geotechnical Engineering Division*, American Society of Civil Engineers, Vol. 107, No. GT5, pp. 553-562.

Poulos, S.J., Castro, G. and France, J.W., 1985, "Liquefaction Evaluation Procedure," *Journal of Geotechnical Engineering Division*, American Society of Civil Engineers, Vol. 111, No. 6, pp. 772-792.

Sadrekarimi, A., and Olson, S.M., 2009, "A new ring shear device to measure the large displacement shearing behaviour of sands," *Geotech. Test. J.*, Vol. 32, No. 3, pp. 197-208.

Sassa, K., 1984, "The mechanism starting liquefied landslides and debris flows," *Proceedings of 4th International Symposium on Landslides*, Toronto, June, pp. 349-354.

Sassa, K., 1996, "Prediction of earthquake induced landslides," *Proceedings of 7th International Symposium on Landslides*, A.A. Balkema, Trondheim, 17–21 June, pp. 115-132.

Sassa, K., Fukuoka, H., Scarascia-Mugnozza, G. and Evans, S., 1996, "Earthquake-induced-landslides: distribution, motion and mechanisms," Special Issue for the Great Hanshin Earthquake Disasters, *Soils and Foundations*, pp. 53-64.

Sassa, K., Wang, G. and Fukuoka, H., 2003, "Performing Undrained Shear Tests on Saturated Sands in a New Intelligent Type of Ring Shear Apparatus," *Geotech. Test. J.*, Vol. 26, No. 3, pp. 257-265.

Sassa, K., Fukuoka, H., Wang, G. H. and Ishikawa, N., 2004, "Undrained Dynamic Loading Ring Shear Apparatus and its Application to Landslide Dynamics," *Landslides*, Vol. 1, No. 1, pp. 7-19.

Sassa, K., B. He , Miyagi, T., Strasser, M., Konagai, K, Ostric, M., Setiawan, H., Takara, K., Nagai, O., Yamashiki, Y. and Tutumi, S., 2012, "A hypothesis of the Senoumi submarine megaslide in Suruga Bay in Japan—based on the undrained dynamic-loading ring shear tests and computer simulation," *Landslides*, Vol. 9, No. 4, pp. 439-455.

Savage, S.B. and Sayed, M., 1984, "Stresses developed in dry cohesionless granular materials sheared in an annular shear cell," *Jorunal of Fluid Mech* , Vol. 142, pp. 391-430

Sedano, J.A.I., Vanapalli, S.K. and Garga V.K., 2007, "Modified Ring Shear Apparatus for Unsaturated Soils Testing," *Geotech. Test. J.*, Vol. 30, No. 1, pp. 39-47.

Stark, T.D. and Eid, H.T., 1993, "Modified Bromhead Ring Shear Test Procedure," *Geotech. Test. J.*, Vol. 16, No. 1, pp. 100-107.

Stark, T.D. and Poeppel, A.R., 1994, "Landfill Liner Interface Strengths from Torsional Ring Shear Tests," *Journal of Geotechnical Engineering Division*, ASCE, Vol. 120, No. 3, pp. 597-615.

Stark, T.D. and Contreras, I.A., 1996, "Constant Volume Ring Shear Apparatus," *Geotech. Test. J.*, Vol. 19, No. 1, pp. 3-11.

Tika, T.M., 1989, "The effect of rate of shear on the residual strength of soil," PhD thesis, University of London (Imperial College of Science and Technology), 494 p.

Tika, T.E., Vaughan, P.R. and Lemos, L.J., 1996, "Fast Shearing of Pre-existing Shear Zones in Soil," *Geotechnique*, Vol. 46, No. 2, pp. 197-233.

Chapter 3 Grohovo Landslide-Assessment of Triggers

3.1 INTRODUCTION

Different phenomena cause landslides. These phenomena can be grouped as preconditions, preparatory, and triggering factors. Preconditions (pre-disposing factors) are considered to be static, inherent factors (e.g. geological composition or structure, topographic geometry, etc.). Opposite to static, there are dynamic factors, such as preparatory and triggering factors that change with time. Preparatory factors decrease the stability of a slope over time without actually initiating movement and the triggering factors are those that initiate movement (Glade and Crozier 2005, Crozier et al. 2013).

Triggering by rainfall or more general hydrological triggering is commonly known as one of the principal natural landslide initiation mechanisms. Extensive literature on this subject exists (Terlien et al. 1998, Reichenbach et al. 1998, Glade et al. 2000, Iverson 2000, Jakob and Weatherly 2003, Jakob et al. 2006, Aleotti 2004, Cardinali et al. 2006, Guzzetti et al. 2004, 2007, 2008). Different approaches have been presented to determine the amount of precipitation needed to trigger landslide and to explain the relationship between rainfall and failures.

Rainfall thresholds (empirical or physically based) are often used and applied in early warning systems. Different rainfall and climate variables (and their combinations) are used for the definition of thresholds in rainfall-induced landslides. Guzzetti listed 25 rainfall and climate variables, but the ones that are most commonly used are: D- rainfall duration, E-cumulative event rainfall, C-critical rainfall, R-daily rainfall, I-rainfall intensity, A-antecedent rainfall (Guzzetti et al. 2008). They are characterized by an extreme temporal variability (Van Asch et al. 1999, Reichenbach et al. 1998, Pasuto and Silvano 1998, Guzzetti et al. 2008) and can be subdivided into short-term (short intense rainfall or rainfall

event) and long-term components (antecedent rainfall or pre-event conditions). The temporal occurrence of landslides and movement activities are controlled by rainfall patterns with different types of temporal resolution (from minutes to months). Both shallow- and deep-seated landslides can be triggered by rainfall. It is widely recognized that shallow failures (soil slips and debris flows with depth <2 m) can be triggered by high intensity and short rainfall duration, while most of the deep-seated landslides (≥5 m) are affected by long rainfall periods characterized by low to moderate average rainfall intensity (Corominas and Moya 1999, Aleotti 2004, Cardinali et al. 2006, Guzzetti et al. 2007). The general pattern could be explained by the definition of hydrological triggering as a decrease in shear strength due to an increase in pore-water pressure on the failure surface which results in a slope failure. Pore-water pressure increase may be directly related to rainfall infiltration and percolation (saturation from above) or indirectly, as the result of the build-up of a perched water table or a groundwater table (saturation from below) (Terlien 1998).

Beside the above mentioned conditions, short- and long-term rainfall conditions (rainfall event/ antecedent rainfall) that will affect reactivation or initiation of landslides, there is another group of conditions that are also important to consider, the most important being discharge (Reichenbach et al. 1998, Jakob and Weatherly 2003, Jakob et al. 2006).

The Grohovo landslide in Croatia, the biggest landslide on the Croatian coast, is selected as one of the study areas within Japanese-Croatian research project that was initiated in 2009. Research activities include real-time monitoring of landslides, laboratory soil testing, modeling of landslide behaviour, and an early warning system (Mihalic and Arbanas 2011, Arbanas and Mihalic 2012). For soil testing, the new, transportable ring shear apparatus, ICL-1 was designed. Two boreholes were drilled in order to install monitoring equipment and obtain soil samples for laboratory tests.

In this chapter an overview of the preparatory conditions of the Grohovo landslide are discussed by describing the geomorphologic setting and landslide itself. Furthermore, a detailed overview of the river's characteristics is given with emphasis on its torrential behaviour and flood occurrences that are related to mass movement occurrences in the past.

Slope failures can be triggered by a single event, such as an earthquake, rainstorm (intense rainfall) or prolonged rainfall period and a snowmelt (Guzzeti et al. 2007, 2008). To investigate the impact of rainfall as a trigger in reactivation of the Grohovo landslide in

1996, we performed rainfall data analysis. Both long-term and short-term rainfall data from Rijeka climatological station were used. The analysis of antecedent conditions is performed on monthly precipitation records for 2, 3 or 4 months in a period from 1948-2011. To analyze event rainfall, we used hourly precipitation data from the period of September to December of 1996, i.e., 3 months prior to the reactivation of the landslide. Although data of monthly discharge of Rjecina River exist from 1948, measurements for a profile of Grohovo in the period 1995-1997 are missing. Therefore, a detailed analysis of discharge on landslide reactivation was not possible. However, characteristics of the Rjecina River and the flood control problem are described as part of the study area description.

To investigate the other possible trigger, earthquake assessment was done by conducting ring shear tests on specimens taken from the Grohovo landslide. Ring shear apparatus, besides being used as a device for measurement of basic soil parameters, can be used for simulation of the landslide. A cyclic loading test was conducted on a sample from Grohovo landslide to simulate seismic loading.

3.2 STUDY AREA

Rjecina watercourse, in the northwestern Adriatic part of Croatia (Figure 3.1a), is a large torrential watercourse with its river mouth located in the center of the city of Rijeka (Figure 3.1b). The watercourse extends through two distinctive geomorphological units. The upstream and central parts of the river valley are relatively narrow and formed in flysch and limestone. Limestone rocks are situated on the top of the slopes, while flysch forms the lower parts, including the bottom of the valley. The downstream part of the watercourse flows through a canyon deep in carbonate rocks (Benac et al. 2005a, 2005b). The Valley is assumed to be younger in its morphogenetic development than the surrounding area, resulting in intensive recent mass movements (Benac et al. 2011). The central part of the valley is the most unstable part and here, mass movements occur mainly at the contact of carbonate rocks with the flysch rock complex. There are historic data of a few rockfalls and landslides on both slopes of the valley (Ostric et al. 2011, Vivoda et al. 2012).

Heavy precipitation and earthquakes may be potential triggers of rockfalls and rockslides. The historic data shows a strong correlation of flood/ rainfall events with mass movements (rockfalls and landslides) in the Rjecina River Valley. The contribution of these factors on landslide occurrence is discussed in the following section.

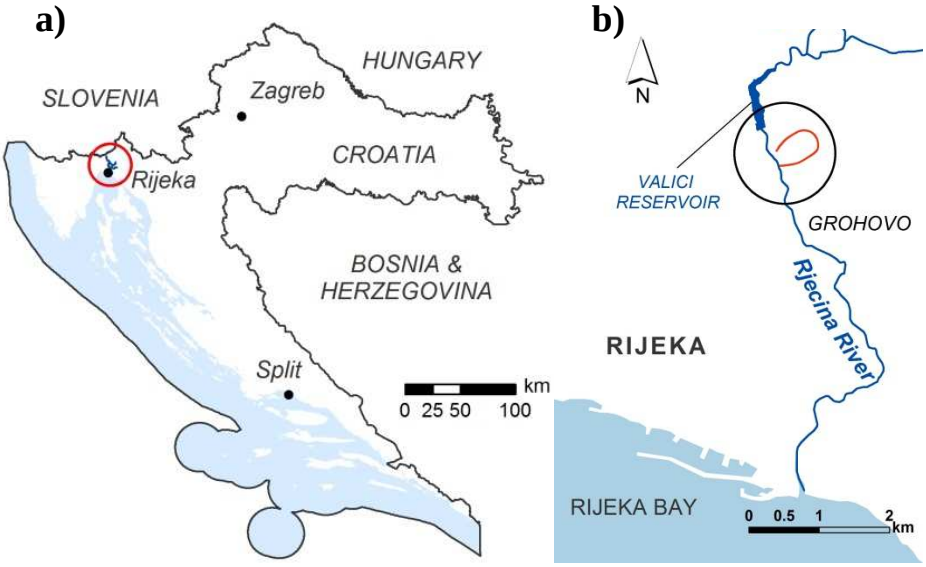

Figure 3.1 Location map of the Rjecina River (**a**) and Grohovo landslide (**b**).

3.2.1 Grohovo Landslide

Grohovo landslide is the biggest landslide in the valley and typical of landslides in the area, it is formed on the contact between flysch and carbonate rock formations (Figure 3.2). Geological composition and groundwater dynamics of the slope were the most important landslide causes (Benac et al. 2005a , 2006).

The landslide had several episodes of re-activation in the past. The most recent reactivation occurred on December 5, 1996, after a long rainy period that lasted for a few months. It started by undercutting two of the initial landslides at the bottom of the slope that caused retrogressive development up to the top of the slope (Benac et al. 2005a). With 13 different slide bodies identified, Grohovo landslide represents a complex composite landslide.

The failure surface is assumed at the contact between slope deposits (consisting of a clayey matrix from the flysch-weathered zone and the debris material from the limestone cliffs on the top) and flysch bedrock. Field investigations indicated a complex landslide

with thirteen separate slide bodies identified. Estimated dimensions and the geometry of this instability are (Benac et al. 2006):

- total length: L = 425 m;
- width of the displaced mass: W_d = 200 m;
- depth of the displaced mass: D_d = 6-20 m;

Figure 3.2 Photo of Grohovo landslide.

3.2.2 Characteristics of the Rjecina River and the flood control problem

The Rjecina River is an example of a large torrential watercourse typical for the coastal karst zone of Croatia. It is a typical karstic river originating from a strong karstic spring located at the foot of Gorski Kotar Mountains. The majority of Rjecina river discharge originates from the strong karst spring of the same name - Rjecina spring. The watercourse is 18.63 km long and has a direct (orographic) catchment area of app. 76 km^2, but the catchment area of all sources that nourish the Rjecina and its tributaries is much larger, app. 400 km^2 (Horvat and Rubinic 2006). Zvir is another important spring of the same catchment area that drains on a much lower level than Rjecina spring.

Part of the water balance from the Rjecina spring is used for the water supply of Rijeka, while part of the water from the Valici reservoir is used for electric power production. The annual average flow of the Rjecina spring is 7.8 m^3/s with maximal flow rates ranging from 0 to over 100 m^3/s (Karleusa et al. 2003, Rubinic and Saric 2005). These regular annual drought periods usually occur during summer and last from 1 to 4

months. Zvir spring located close to Rjecina river-mouth is very important for the water supply of the area. It is a permanent spring with an average annual discharge of 5.2 m^3/s, with minimal and maximal capacities varying from 0.5 to 20 m^3/s respectively.

The discharge of the river varies greatly during the year, from the minimum of 0 m^3/s in the profile directly below the spring (during summer) to the maximum ever recorded 439 m^3/s at the river mouth profile (calculation based on observations during the disastrous flood on September 19, 1898). After the great floods in late 19^{th} century, the river mouth was displaced and corresponding regulation works were carried out (Karleusa et al. 2009). The majority of regulation works were done to reduce flood effects, in order to prevent deepening of the channel and formation of landslides.

For hydropower purposes, the hydropower plant Rijeka was constructed in 1968, which uses water from the Valici reservoir and is located in the central part of the valley (Figure 3.1b). Grohovo landslide is located downstream from the reservoir. The construction of the dam significantly changed the runoff regime in the part of the Rjecina River near Grohovo landslide. To show the changes in the water regime of the Rjecina River after the reservoir (dam) construction, discharge in two profiles (Rjecina profile, upstream and Grohovo profile, downstream from the dam) before (up to 1967) and after (starting from 1969) the construction of the dam are shown in Figure 3.3. The hydrological monitoring at the Grohovo profile in the Rjecina catchment has been continuously performed beginning from 1947 until the present day with a few short interruptions (1976 - 1979 and 1995-1997). Hydrological data of the same period also exists for the profile at Rjecina spring.

Figure 3.3a shows a decreasing trend of mean discharges for both profiles, upstream and downstream from the reservoir, for the period 1947-2007. Mean annual discharge (m^3/s) is on the left axis and MAP for Rijeka station (mm) on the right axis of the Figure 3.3a. Mean annual discharges are represented by the green and red lines (Rjecina and Grohovo profile respectively), while MAP is represented by the blue line. Although the construction of the reservoir had significant influence by decreasing the mean discharge of the Rjecina River on the Grohovo profile, maximum discharges reached high values even after the construction (Figure 3.3b) (Rubinic and Saric 2005, Ostric et al. 2011). In Figure 3.3b, the maximum annual discharge (m^3/s) on the left axis and the

number of days with discharges higher than 50 or 100 m^3/s measured on Grohovo profile is on the right axis, shown by bars.

During 1996, when landslide re-activation occurred, several hydrological stations were active: Drastin station, Martinovo selo station, and Rjecina spring station, all located upstream from the Grohovo landslide and the Valici reservoir. Despite a significant amount of recorded rainfall that preceded the re-activation of the landslide, on the critical days (the 5th and 6th of December, 1996), very low values of maximum daily flow were recorded: 2.5 m^3/s at Rjecina spring, 3.7 m^3/s at Drastin, and 0 m^3/s at Grohovo profile.

It should be noted that at all the mentioned profiles, in mid-November 1996, maximal flows for that year were recorded. But even these maximum annual recorded flows were in the range of the average events: at the Martinovo selo profile, a maximum annual flow of 79.7 m^3/s was recorded (average annual flow being 69.1 m^3/s), and at the Drastin profile maximum annual flow of 107 m^3/s (average of 104 m^3/s).

From the presented data it can be concluded that the surface runoff of Rjecina River did not have an impact on the landslide re-activation, in the sense that the runoff caused erosion of the landslide toe and in that way decreased its stability. The landslide was the result of the force misbalance inside the landslide body which was caused by the change in groundwater level that was affected by rainfall. For this reason, in the following section, rainfall analysis is provided.

3.3 RAINFALL ANALYSIS

Mean annual precipitation (MAP) depends largely on the morphological characteristics of the area. In the mountainous areas MAP is up to 3500 mm, while closer to the coastal part of the wider area of Rijeka, it decreases to 1750 mm. The MAP for the station Rijeka is 1538 mm. Significant, very intensive, but short-term rainfall events have the major influence on water discharge for surface, as well as for groundwater (Rubinic et al. 2009). Therefore, the surface flows of the study area have torrential characteristics. The wet season lasts from September to January, with the dry season from May to August (Figure 3.5). The whole area is occasionally subject to very intense rainstorms, which can cause serious damage by flash floods and consequently mass movements.

Data used in the rainfall analysis are from the Rijeka climatological station, located in the most downstream part of the Rjecina River. For the analysis of long-term rainfall data (or antecedent, "pre-event") we used data of monthly precipitation records at Rijeka station for the period from 1948 to2011. For the short-term data analysis, we had daily precipitation for the period from 1993 to2006 of the same station as well as the continuous (i.e., every 5 min) rainfall record for the 3 month period that preceded landslide reactivation (September 1st- December 5th 1996).

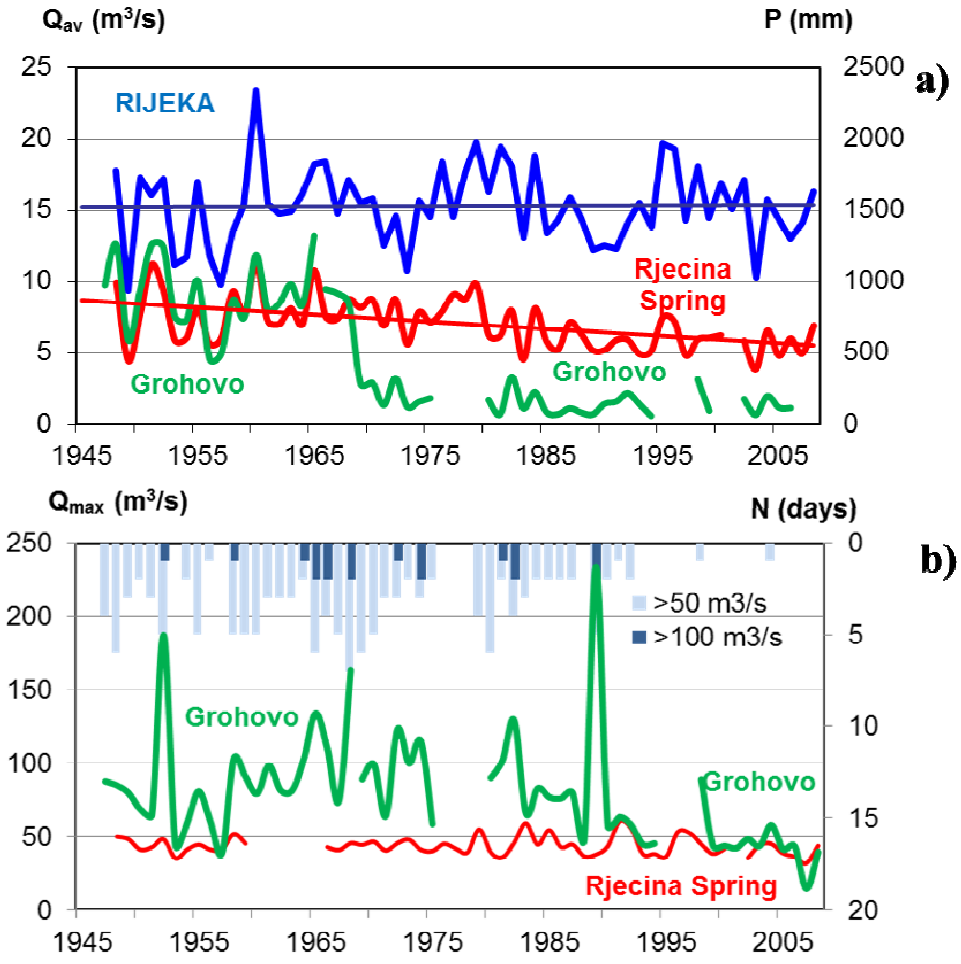

Figure 3.3 Changes in the water regime before and after the construction of a dam in 1968. (Modified from Rubinic and Saric 2005): **(a)** Mean annual discharge (m^3/s) **(b)** Maximum annual discharge (m^3/s).

3.3.1 Long-term analysis

The most recent larger displacement of Grohovo landslide was observed on December 5th, 1996. The landslide was triggered by a longer than usual rainy period that lasted for a few months. During that period, the regional mean annual precipitation (MAP) was 1929 mm, 26 % higher than the average MAP for the period between 1948 and 2011. The long rainy period resulted in a cumulative rainfall in the period from October to December which exceeded 900 mm, which is app. 74 % higher compared to the average cumulative rainfall (523 mm) calculated for the same period (Oct-Dec) in the period between 1948 and 2011. Figure 3.4 shows the cumulative rainfall measured at the Rijeka rain gauge in October, November, and December, 1996. During this period, the monthly rainfall was from 96% (October) to 66 % (November) higher than the long-term (1948–2011) monthly averages (red lines and italic numbers in Figure 3.4).

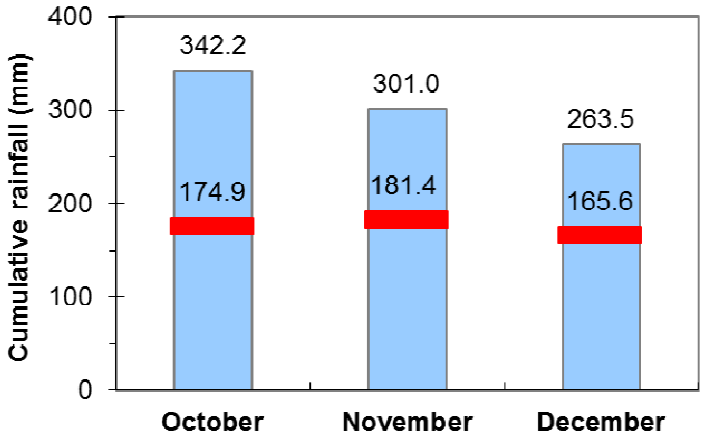

Figure 3.4 Cumulative rainfall at Rijeka station for October, November, and December 1996.

Analysis of the available historical record indicates that monthly rainfall at the Rijeka rain gauge exceeded 200 mm more than 90 times (of a total 134) in the period from September to December for the 65 year period (1948-2011), with a maximum monthly value of 526.7 mm in October 1998 (Figure 3.5). In Figure 3.5 the mean annual precipitation (MAP), minimum annual precipitation (MIN) and maximum annual precipitation (MAX) are shown for the period from 1948 to2011. The dashed, broken violet line shows monthly precipitation for 1996 (left axis). Bars show relative frequency of events when monthly rainfall exceeds 200 mm (right axis). Relative frequency is

calculated by dividing number of events exceeding 200 mm/ month by the observed period (1948-2011).

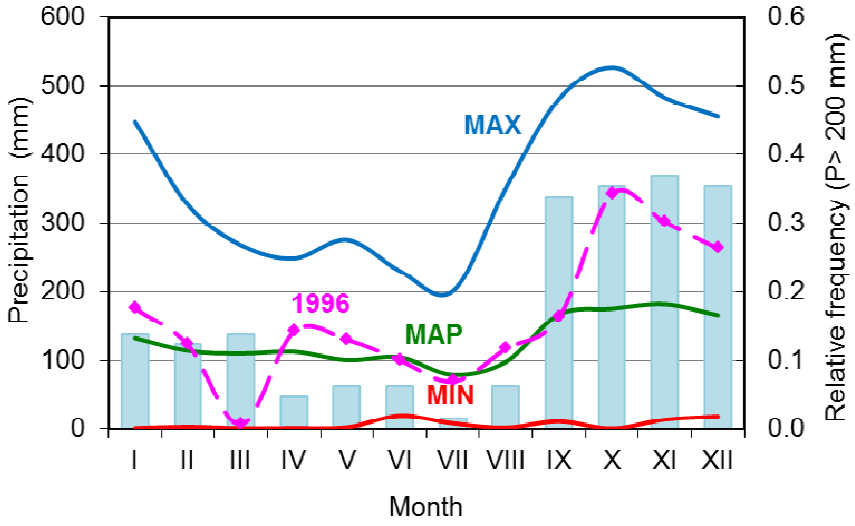

Figure 3.5 Monthly distribution of rainfall at Rijeka station.

However, analysis of the cumulative rainfall for the 2-month (Oct-Nov), 3-month (Oct-Dec) and 4-month (Sep-Dec) period (Figure 3.6ABC) indicates that only once (in 2000, 742 and 986 mm) the cumulative rainfall for the 2 (Oct-Nov) and 3-month (Oct-Dec) period exceeded the cumulative value measured in 1996 (643 and 907 mm respectively on Figures 3.6ab), and four times (in 1960, 1976, 1993 and in 2000) the cumulative precipitation for the 4-month period (Sep-Dec) (Figure 3.6c) exceeded the rainfall measured in 1996 (1069 mm). Bars on the Figure 3.6 are arranged from high (left) to low (right) values of cumulative yearly rainfall. Red bars show cumulative rainfall for the same 2, 3 and 4-months periods in 1996.

We also performed a probability analysis of the cumulative monthly rainfall for a 2-month period (Oct-Nov), a 3- month period (Oct-Dec) and a 4-month period (Sep-Dec). Based on the obtained results, we determined the character of the rainfall probability during the observed period in 1996. Several probability distribution functions were used (Galton, Gumbel, Gamma II, Pearson III, Log Pearson III and GEV) together with the Smirnov Kolmogorov test to estimate goodness of fit.

Table 3.1 summarizes the results of the analysis, showing the basic statistical indicators of the analyzed data series (average, maximum and minimum as well as the

annual data in 1996) and the values calculated for the characteristic return periods (2-100 yr).

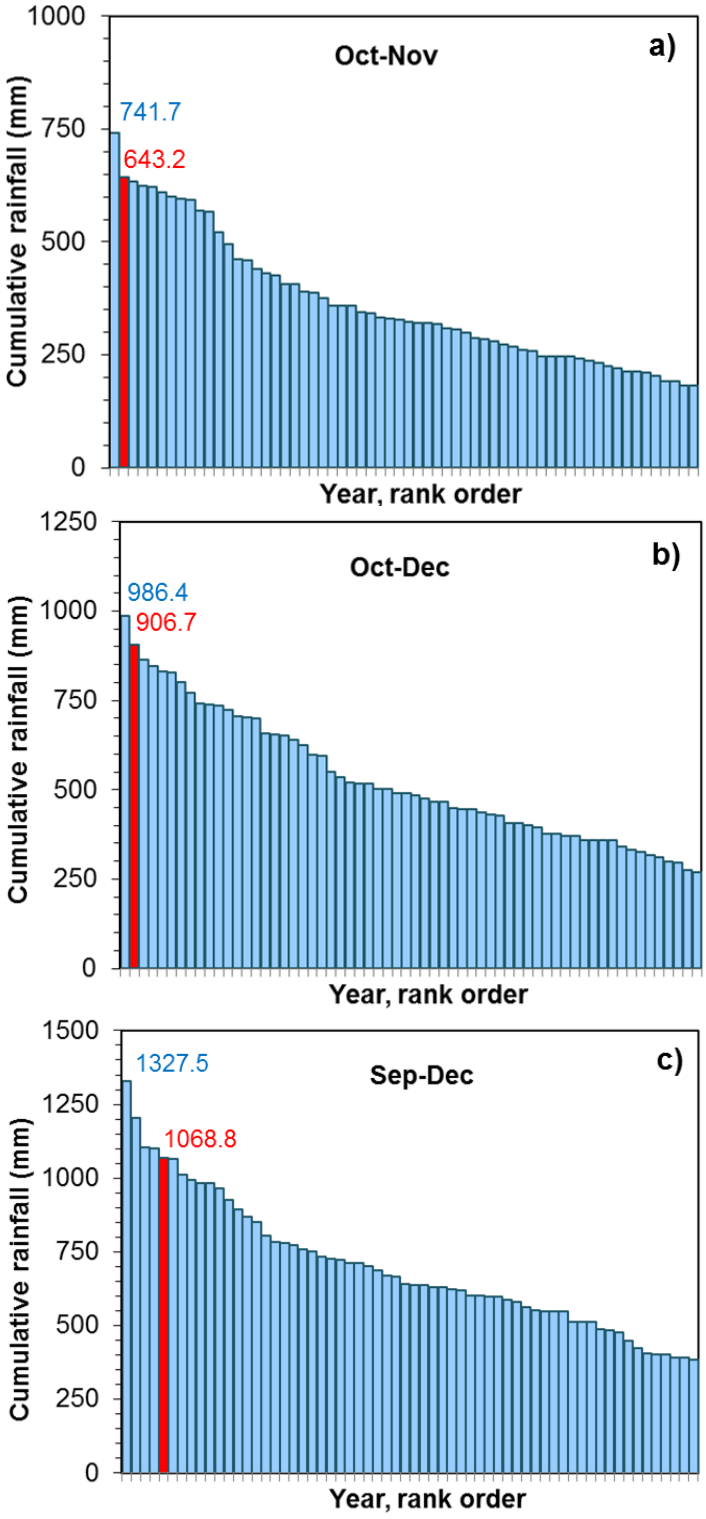

Figure 3.6 Cumulative rainfall at Rijeka station, for the period of: **a)** 2-months (Oct-Nov), **b)** 3-months (Oct- Dec) and **c)** 4-months (Sep-Dec) during 1948-2011.

According to the results of the analysis, the observed cumulative values of 2 months of rainfall (Oct-Nov) matches the rainfall with a 19 year return period (RP), cumulative 3- month rainfall (Oct-Dec) is adequate for 24 years RP, while cumulative 4-month rainfall (Sep-Dec) has the character of 15 years RP. Cumulative annual rainfall observed in 1996 has the character of a 12 year return period Depending on the duration of the analyzed critical period related to reactivation of the Grohovo landslide, it is obvious that the observed rainfall is relatively rare, but cannot be characterized as an absolutely extreme and exceptionally rare event.

Table 3.1 Results of the analysis of cumulative rainfall for the selected 2-, 3-, and 4-month periods and occurrence probability.

Analyzed Period (months)/ Distribution	**Po (mm)[a]**				**Pc (mm) -RP (year) [b]**					
	Av	**Min**	**Max**	**1996**	**2**	**5**	**10**	**20**	**50**	**100**
2 [c] / GEV	358	161	742	643	328	460	553	647	774	876
3 [d] / GEV	520	242	986	907	490	661	773	879	1013	1113
4 [e] / Gumbel	687	320	1328	1069	650	850	983	1111	1276	1399
12 [f] / Pearson III	1536	938	2339	1929	1529	1771	1902	2011	2136	2221

[a] Observed Precipitation, [b] Calculated Precipitation for the 2/5/10/20/50/100 year Return Periods (RP), [c] 2-month period (Oct-Nov), [d] 3-month period (Oct-Dec), [e] 4-month period (Sep-Dec), [f] 12-month period (Jan-Dec).

3.3.2 Short-term heavy rainfall

Short-term heavy rainfall describes rainfall occurring during 24 hours with scarce intensities (Bonacci 1994). One of the characteristics of a short- term rainfall is its huge spatial inhomogeneity and unsteadiness, which makes its estimation and the modeling of a

runoff process difficult (Rubinic et al. 2009). Short-term heavy rainfall especially refers to areas with distinctive orographic gradients, such as in the investigated Rijeka area. In addition, the Rijeka area is characterized with rainfall intensities that are among the highest in Croatia. Pluviographic measurements at the Rijeka climatological station have been made since 1957. Rainfall Depth-Duration-Frequency (DDF) curves (Figure 3.7) were defined on the base of those data for a duration up to 2 and 24 hours (Rubinic et al. 2009).

As part of the conditions that led to activating the Grohovo landslide in December 1996, we performed an analysis of probability and a return period of rainfall occurrence based on the pluviographic data observed at Rijeka gauging station (from 10 min to a 6h duration). Rainfall events that were analyzed started in September 1996 and continued until reactivation of the landslide on the 6th of December 1996. For illustration, Figure 3.8 shows a selected daily series for the period 3 months prior to reactivation (indicated with a red circle on the figure).

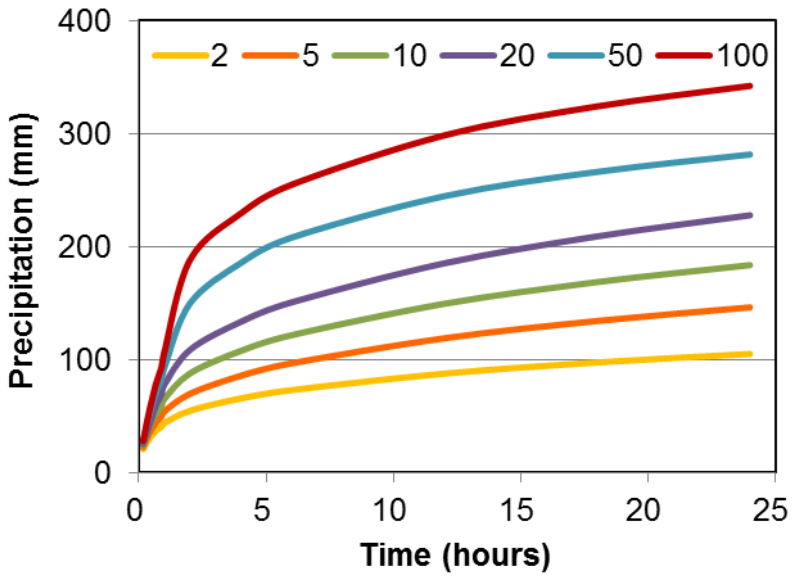

Figure 3.7 DDF curves defined for Rijeka station (modified from Rubinic et al. 2009); numbers in the legend representing Return periods in years (2, 5, 10, 20, 50 and 100 year return periods, respectively).

Table 3.2 shows the observed short-term rainfall with maximum intensities for different durations (10 min to 6 h). Each record is associated with the exact date and time the event started as well as the corresponding return periods according to DDF curves shown on figure 3.7. It is clear that short term rainfall observed during the 3- month period prior to the landslide reactivation (1st September 1996 – 6th December 1996), had the

characteristic of frequent events with a return period less than 1 year for the 2 h duration and an approximately 2-year return period for longer durations.

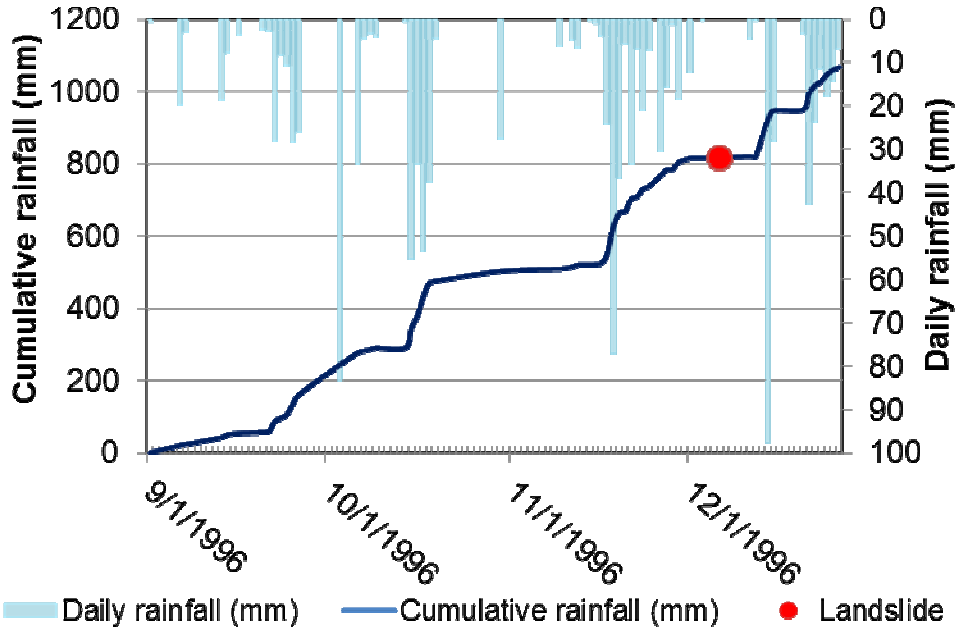

Figure 3.8 Daily rainfall observed during time period September 1st- December 31st at Rijeka station.

Table 3.2 Results of the analysis of short-term rainfall data (up to 24h).

Duration (min/h)	P (mm)	I (mm/h)	Event started (dd/mm/yy;hh:min)	RP (yr)
10 min	11.2	67.2	17.10.1996; 18:34	< 1
30 min	19.3	38.6	19.11.1996; 3:15	< 1
1 h	27.1	27.1	19.11.1996; 3:10	< 1
2 h	39.9	20.0	3.10.1996; 13:15	< 1
4 h	69.2	17.3	3.10.1996; 11:15	2
6 h	76.2	12.7	3.10.1996; 10.00	2

According to the results of both daily and hourly data, the long-term rainfall events (i.e. cumulative 2, 3 or 4 months rainfall) were characterized with much longer return periods (10-20 years), in comparison with the short-term rainfall events (i.e. up 24 h) which can be described as relatively frequent events with return periods less than 2 years.

3.4 RING SHEAR APPARATUS TESTING

ICL-1 Ring Shear Apparatus was used in this study. The testing procedure consisted of the following: gap adjustment; specimen setting and saturation; saturation checking by B_D measurement; specimen consolidation and shearing (by shear speed control and cyclic stress control). Detailed descriptions of each part of the testing procedure were given in previous chapter, Chapter 2.

First, the gap was adjusted by applying a vertical load of 1.5 kN. Secondly, the shear box without specimen was filled with CO_2 and de-aired water to expel entrapped air. Third, the specimen saturated by de-aired water during the night was slowly placed in the shear box. Because the specimen was previously saturated, water circulation was not necessary. The saturation of the specimen was then checked by measuring the B_D value that should be greater than 0.95 for fully saturated specimens. For both specimens, B_D=0.95 was obtained, which means that a fully saturated specimen was obtained without water circulation.

After full saturation was confirmed, the initial stress state of the specimen was created. Therefore, the specimen was normally consolidated under pre-decided normal and shear stress, depending on the specimen depth, slope angle, and unit weight of the soil. The estimated depth of the displaced mass varied from 6 m to a maximum 20 m (Benac et al. 2005a). According to published engineering-geological models (Benac et al. 2005a, 2005b) and the location of the sample, a sliding surface depth at 10 m, slope angle of 15°, and unit weight of 21 kN/ m^3 was assumed. These parameters were used in the calculation of initial stress (200 kPa for normal stress and 80 kPa for shear stress).

After consolidation, shearing was applied by stress-control mode (a cyclic test) and a speed-control test in undrained conditions.

3.4.1 Specimen

Surface samples from the landslides are usually taken from locations with outcrops of material where sliding surfaces are assumed. Grohovo surface sample (GS1) was taken from the flysch outcrop shown in Figure 3.9. Locations of boreholes (B1 and B3) that are drilled with the purpose of obtaining a sample for ring shear testing are also shown in the figure with red dots. The location of the surface sample (GS1) that was tested in this study is shown in a black triangle. A clayey sample of flysch was taken from the outcrop near the crown of one of the landslide bodies, from the central part of the slope. Basic parameters for this surface sample were obtained by standard laboratory tests (Table 3.3).

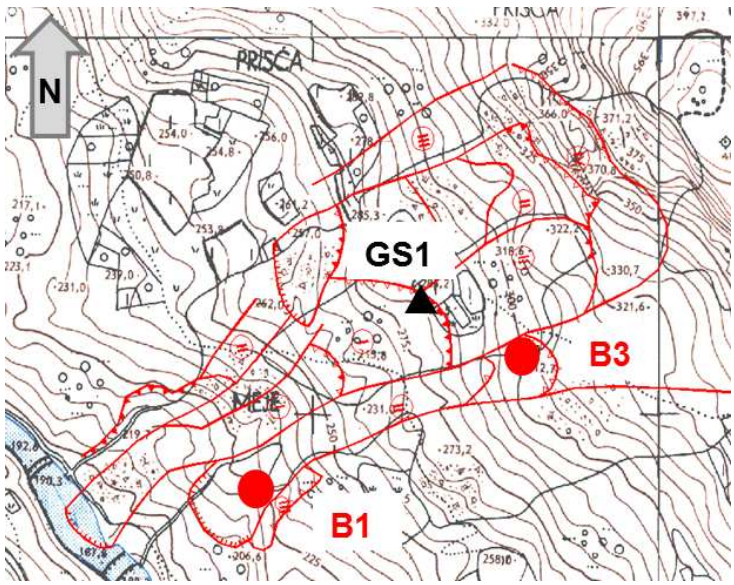

Figure 3.9 Location of surface sample and boreholes.

3.4.2 Results of Ring Shear Test

Speed Control Test

After consolidation of the specimen, a speed-control test was conducted under constant shear speed of 0.02 cm/s in an undrained condition. The specimen was sheared until a steady state condition was obtained at 2 m of displacement. Figure 3.10 shows the stress path that reached the failure line and moved down along the failure line, without an

observed peak failure line. The straight line fitting the stress path gave values of the friction angle during motion, and also at peak as $\Phi_p=\Phi_m=31.9°$ as well as the apparent friction angle, $\Phi_a=20.4°$. Cohesion was assumed to be zero.

Table 3.3 Specimen properties.

Prameter	Value
Specific gravity, *Gs* (g/cm^3)	2.66
Water content, *w* (%)	26.87
Wet unit weight, γt (kN/m^3)	20.11
Dry unit weight, γd (kN/m^3)	15.86
Porosity, *n*	0.26
Void ratio, *e*	0.35

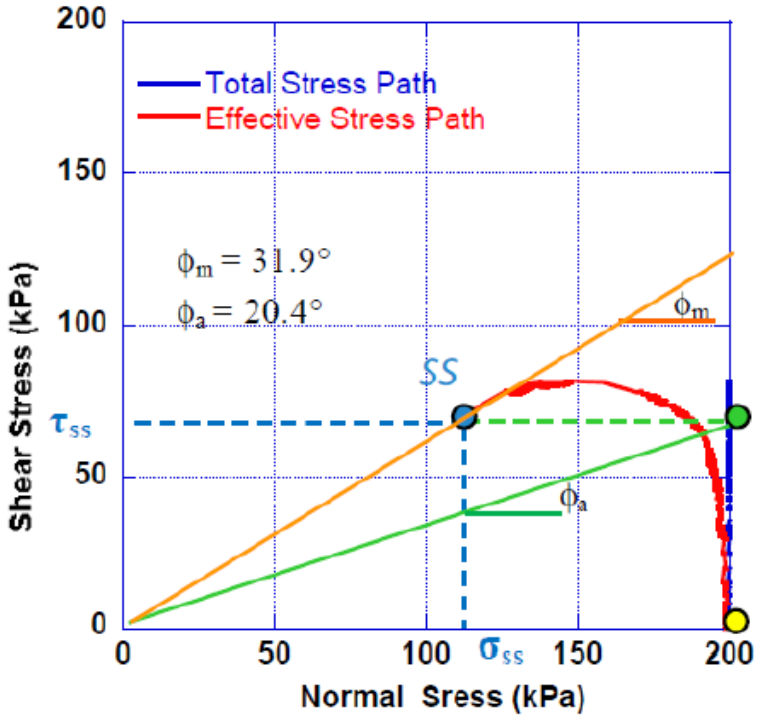

Figure 3.10 Stress path of undrained speed-control test on saturated clayey specimen from Grohovo landslide (B_D=0.95; ρ_d=1.51 g/cm^3).

Cyclic Stress Control Test

After the specimen was consolidated at 200 kPa of normal stress and 80 kPa of shear stress, cyclic shear stress was loaded with the amplification increment of 10 kPa/ cycle at 0.1 Hz. Due to the low permeability of the specimen, a slower cycle shearing of 2 cycles/ h was chosen, in order to obtain reliable pore pressure measurement data.

Figure 3.11a shows the time series data and 3.11b the stress path of the cyclic stress test. The sample failed, but without rapid failure motion. Figure 3.11a shows that displacement of 700 mm occurred after 6,000 sec and pore pressure of app. 20 kPa was generated. Both lines of the control signal for shear stress and the mobilized shear resistance were the same during the test.

Shear displacement occurred in the following mode: each time the shear stress given by the control signal reached the value of shear resistance, shear displacement occurred. When shear stress decreased, displacement stopped and shear resistance moved down with loaded shear stress lower than the failure line. The sample showed dilative behaviour, which is indicated by black arrows in Figure 3.11a, showing negative pore pressure generation at each displacement step. Consequently, the peak friction angle increased as well, from the initial value of 31.9° to 39.0° and 41.2° (Figure 3.11b). The sample showed strength-hardening behaviour.

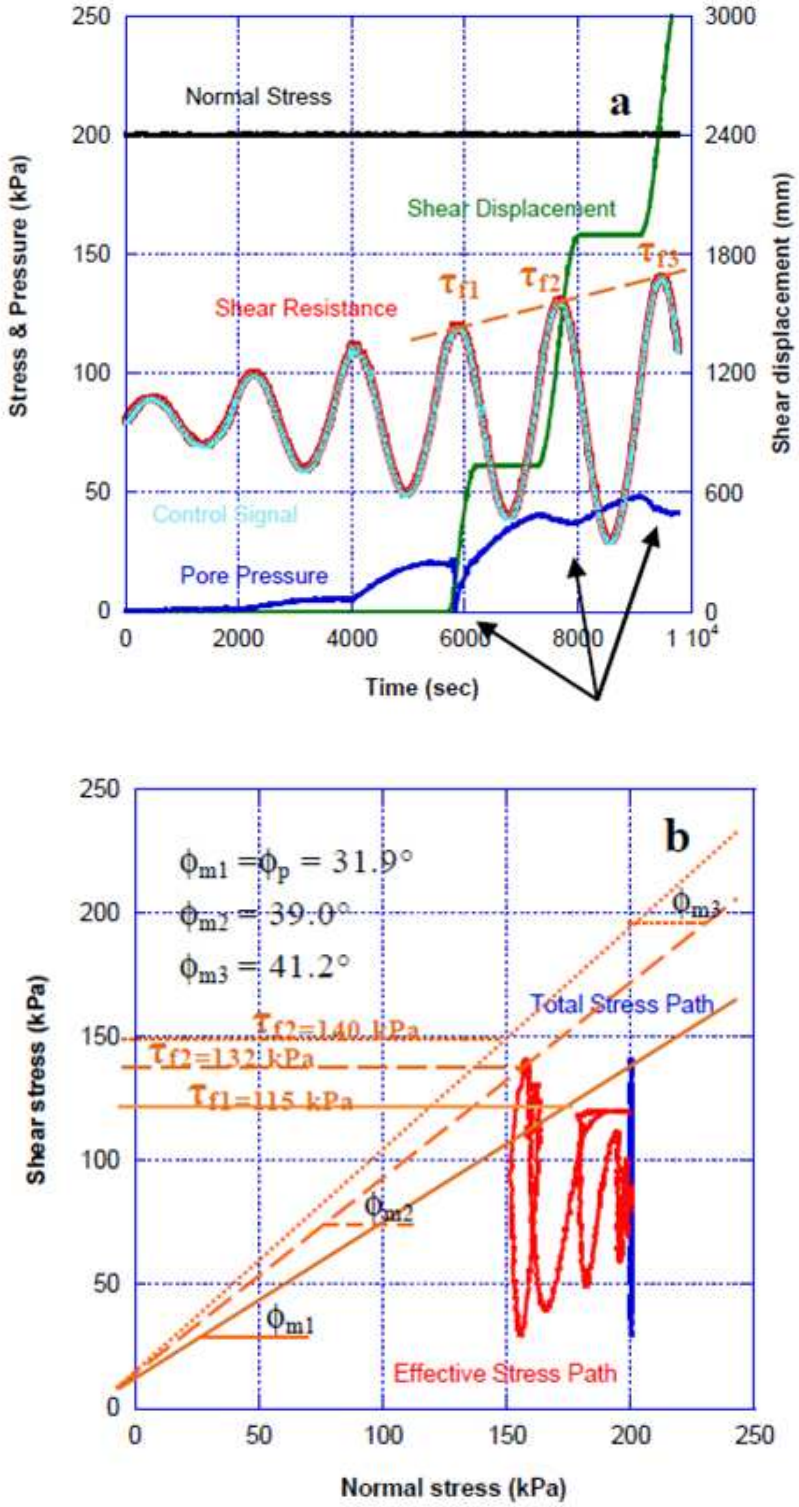

Figure 3.11 Undrained cyclic loading test on saturated clayey flysch specimen from Grohovo landslide (B_D=0.96; ρ_d=1.51 g/cm^3): **a)** Time series data for stress, pressure, and shear displacement and **b)** Stress path.

3.5 SUMMARY AND CONCLUSION

Grohovo landslide is one of the study areas chosen for investigation in Japanese- Croatian joint research project. It is a reactivated landslide formed on the contact zone of carbonate and flysch rock complexes. Flysch is a typical material of the area and due to its material properties is prone to erosion and other types of instabilities. Rainfall has been always considered a major trigger to these events; however, no comprehensive analysis of rainfall data was done in the past. Therefore, assessment of two possible triggers of this reactivated landslide: rainfall and earthquake was done. To investigate the rainfall conditions that resulted in the reactivation of landslides in 1996, rainfall data from the Rijeka climatological station was used. Both long-term and short-term rainfall data were analyzed and their impact on the Grohovo landslide was considered. The assessment of seismic triggering was done using the ring shear apparatus.

By analyzing the monthly precipitation data for the Rijeka station in a 65 yr. period (1948-2011), it was found that landslide reactivation was probably caused by cumulative rainfall in the rainy period during October and November. It is clear that in 1996 a very dry summer period (with precipitation lower than average for the 65 yr. period) was followed by a very wet period (exceeding average values by 75 %). However, by analyzing daily and hourly data of the same period (September-December 1996), no significant single event was observed in that period. The return period of the observed 2, 3, and 4 cumulative monthly rainfall in 1996 was 19, 24, and 15 years respectively. Short-term data analysis showed a much higher probability of occurrence, i.e., less than a 2-year return period. The analysis indicated that antecedent conditions are more important for the reactivation of a landslide or landslide initiation than short-term rainfall intensities alone.

Due to the low permeable properties of flysch material and to the behaviour of landslides in the same or in similar clay rich materials, it is reasonable to assume that cumulative rainfall for a longer period has a more important role in landslide formation and reactivation. This is also in accordance with previous investigations that generally emphasized the importance of soil moisture in landslide initiation of low permeable terrains (Pasuto and Silvano 1998; Glade et al. 2000; Jakob and Weatherly, 2003; Aleotti 2004, Guzzetti et al. 2008). Some argue that groundwater levels and soil moisture conditions cannot be considered as triggers, but as preparatory factors (Reichenbach et al.

1998, VanAsch 1999, Guzzetti et al. 2008). However, antecedent rainfall that influences both groundwater levels and soil moisture can be used to determine when landslides are likely to occur. The main difficulty is that the definition of the period over which rainfall accumulates and the considered periods vary from 3 days to 4 months (Cardinali et al. 2006). In our study, antecedent conditions of longer periods (60-120 days) showed to be the most important for landslide reactivation. Some researchers also found that the number of antecedent days is related to the depth of the potential failure surface and larger windows of antecedent precipitation periods have to be considered for the deeper landslides (Van Asch et al. 1999, Terlien 1998).

However, the role of short term events should not be ignored, especially in catchments where runoff reflects the short-term hydrological behaviour of the basin, particularly during extreme events (Reichenbach et al. 1998). In that way short-term events can also cause landslides, by erosion of the landslide foot that may result in reactivation. Unfortunately, discharges of the Rjecina River on the Grohovo profile (located upstream from the landslide) were not available for the period 1995-1997. Consequently, the evaluation of the effect of discharge on the reactivation of landslides in 1996 was not possible.

Although the analysis of rainfall indicated the importance of antecedent conditions in reactivation of the Grohovo landslide as is the case with the initiation of landslides of similar geological setting in Croatia (Dugonjic and Arbanas 2012), because of the lack of data it is difficult to establish an empirical threshold and instead, a physically based rainfall threshold should be determined.

The new, transportable ring shear apparatus, ICL-1, was applied for testing samples taken from the Grohovo landslide in Croatia. The apparatus was used for obtaining basic soil parameters by conducting an undrained speed-control test and as a simulation test for dynamic loading, by conducting a cyclic stress test. From the results of the cyclic stress test, assessment of a seismic trigger was done. According to the results of the cyclic ring shear test, clayey flysch specimen from the Grohovo landslide showed the following behaviour: an increase of friction angle and shear resistance that was caused by dilation and generation of negative pore pressure. This resulted in soil hardening behaviour. From this it was concluded that Grohovo soil is resistant to seismic loading. From these findings, earthquakes can be ruled out as possible triggers in the case of the Grohovo landslide.

REFERENCES

Aleotti, P., 2004, "A warning system for rainfall-induced shallow failures," *Engineering Geology*, Vol. 73, pp. 247-265.

Arbanas, Z. and Mihalic, S., 2012, "Progress in the Croatian–Japanese Joint Research Project On Landslides," *Proc. of the IPL Symposium*, Sassa, K., Takara, K. and Bin, He (Eds.), Kyoto, January 2012.

Benac, C, Dugonjic, S, Vivoda, M., Ostric, M. and Arbanas, Z., 2011, "A Complex landslide in the Rječina Valley: results of monitoring from 1998-2010," *Geologia Croatica*, Vol. 64, No. 3, pp. 239-249.

Benac, C., Jurak, V., Arbanas, Z., Ostric, M. and Ozanic, N., 2005a, "Complex landslide in the Rjecina River valley (Croatia): origin and sliding mechanism," *Bulletin of Engineering Geology and the Environment*, Vol. 64, No. 4, pp. 361-371.

Benac, C., Jurak, V. and Ostric, M., 2005b, "Qualitative assessment of geohazard in Rjecina Valley, Croatia," *Geophysical Research Abstract*, Vol. 7, pp. 1-6.

Benac, C., Jurak, V. and Ostric, M., 2006, "Qualitative assessment of geohazard in the Rjecina Valley, Croatia," *Proc. of the 10. IAEG International Congress*: IAEG Engineering geology for tomorrow's cities, 658 (1-7), The Geological Society of London.

Bonacci, O., 1994, "Rainfall-main input parameter in hydrological cycle," (in Croatian), Geoing, 341 p.

Cardinali, M., Galli, M., Guzzetti, F., Ardizzone, F., Reichenbach, P. and Bartoccini P., 2006, "Rainfall induced landslides in December 2004 in Southwestern Umbria, Central Italy,"*Nat Hazard Earth Sys Sci*, Vol. 6, pp. 237-260.

Corominas, J. and Moya, J., 1999, "Reconstructing recent landslide activity in relation to rainfall in the Llobregat River basin, Eastern Pyrenees, Spain," *Geomorphology*, Vol. 30, pp. 79-93.

Crozier, M.J., Preston, N. and Glade, T., 2013, "Antecedent conditions," *Encyclopedia of Natural Hazards*, Bobrowsky, P.T. (Ed.), Springer, pp. 10-13.

Dugonjic, S., and Arbanas, Z., 2012, "Recent landslides on the Istrian Peninsula, Croatia," *Natural Hazards*, Vol. 62, No. 3, pp. 1323-1338.

Glade, T., Crozier, M. and Smith, P., 2000, "Applying probability determination to refine landslide triggering rainfall thresholds using an empirical. Antecedent Daily Rainfall Model," *Pure Appl Geophys*, Vol. 157, No. 6, pp. 1059-1079.

Glade, T. and Crozier, M.J., 2005, "The nature of landslide hazard impact, "*Landslide hazard and risk*, Glade T, Anderson and M., Crozier, M.J. (Eds.), Wiley, New York, pp. 43-74.

Guzzetti, F., Cardinali, M., Reichenbach, P., Cipolla, F., Sebastiani, C., Galli, M. and Salvatia, P., 2004, "Landslides triggered by the 23 November 2000 rainfall event in the Imperia Province, Western Liguria, Italy," *Engineering Geology*, Vol. 73, pp. 229-245.

Guzzetti, F., Peruccacci, S., Rossi, M. and Stark, C.P., 2007, "Rainfall thresholds for the initiation of landslides in central and southern Europe," *Meteorol Atmos Phys*, Vol. 98, No. 3-4, pp. 239-267.

Guzzetti, F., Peruccacci, S., Rossi, M. and Stark, C.P., 2008, "The rainfall intensity–duration control of shallow landslides and debris flows: an update," *Landslides*, Vol. 5, No. 1, pp. 3-17.

Horvat, B. and Rubinic, J., 2006, "Annual runoff estimation– an example of karstic aquifers in the transboundary region of Croatia and Slovenia," *Hydrological Sciences Journal*, Vol. 51, No. 2, pp. 314-324.

Iverson, R.M., 2000, "Landslide triggering by rain infiltration," *Water Resour. Res.*, Vol. 36, No. 7, pp. 1897-1910.

Jakob, M. and Weatherly, H., 2003, "A hydroclimatic threshold for landslide initiation on the North Shore Mountains of Vancouver, British Columbia," *Geomorphology*, Vol. 54, No. 3-4, pp. 137-156.

Jakob, M., Holm, K., Lange, O. and Schwab, J.W., 2006, "Hydrometeorological thresholds for landslide initiation and forest operation shutdowns on the north coast of British Columbia," *Landslides*, Vol. 3, No. 3, pp. 228-238.

Karleusa, B., Ostric, M. and Rubinic, J., 2003, "Water Management Elements in Regional Planning in Karst, Rjecina Catchment Area – Case Study," *Proc.: Voda u krsu slivova Cetine, Neretve i Trebisnjice* (in Croatian), University of Mostar, pp. 85-94.

Karleusa, B., Magas, O., Rubinic, J. and Palinic N., 2009, "Rjecina River Basin Restoration (Croatia)," *Proc. of International Symposium on Water Management and Hydraulic Engineering*, 2009.

Mihalic S. and Arbanas Z., 2012, "The Croatian–Japanese joint research project on landslides: activities and public benefits," *Landslides: Global Risk Preparedness*. Sassa, K. (Ed.), Springer-Verlag, Berlin- Heidelberg, pp. 345-361.

Ostric, M, Yamashiki, Y., Takara, K. and Takahashi, T., 2011, "Possible scenarios for Rjecina River Catchment – on the example of Grohovo landslide," *Annuals of Disaster Prevention Research Institute, Kyoto University*, Vol. 54 (B), pp. 63-69.

Pasuto, A. and Silvano, S., 1998, "Rainfall as a trigger of shallow mass movements. A case study in the Dolomites, Italy," *Environmental Geology*, Vol. 35, No. 2, pp. 184–189.

Reichenbach, P., Cardinali, M., De Vita, P. and Guzzetti, F., 1998, "Regional hydrological thresholds for landslides and floods in the Tiber River Basin (central Italy)," *Environmental Geology*, Vol. 35, No. 2, pp. 146-159.

Rubinic, J. and Saric, M., 2005, "Hidrology of water resources in Rjecina catchment area," *Proc. of Proslost, sadašnjost i buducnost vodoopskrbe i odvodnje - Iskustva i izazovi*. Ilinic A. (Ed.). Opatija: Vodovod i kanalizacija Rijeka, pp. 199-207.

Rubinic, J. Lukaric, S. and Rukavina, J., 2009, "Engineering Analysis Of Short- Term Heavy Rainfall- Rijeka Area Case Study," *Proc of Suvremene Metode odvodnje oborinskih voda urbanih sredina na obalnim podrucjima* (in Croatian), Rijeka.

Vivoda, M., Benac, C., Zic, E., Domlija, P. and Dugonjic-Jovancevic, S., 2012, "Geohazard in Rjecina River valley in the past and today," (in Croatian), *Croatian Waters*, Vol. 81, pp. 105-116.

Terlien, M.T., 1998, "The determination of statistical and deterministic hydrological landslide triggering thresholds," *Environmental Geology*, Vol. 35, No. 2, pp. 124-130.

Van Asch, T.W.J., Buma, J. and Van Beek, L.P.H., 1999, "A view on some hydrological triggering systems in landslides," *Geomorphology*, Vol. 30, pp. 25-32.

Chapter 4 Negative Rate Effect in Sand-Bentonite Mixtures

4.1 INTRODUCTION

The measurement of strength parameters is necessary for stability analysis. Peak shear strength is used when analysis is made for first time slides. Peak shear strength is defined as the highest shear strength measured, and this strength is measured by triaxial, direct shear, and simple shear apparatus. Small displacement is usually necessary for the soil to reach its peak strength. After peak strength was reached, the strength gradually decreased until reaching a constant minimum value at a large displacement. According to Skempton (1985) this is the definition of residual shear strength. However, the concept of residual strength is meaningful only for soils that contain platy particles and consequently, can form a shear zone or shear surface with highly oriented platy particles (Mesri and Cepeda-Diaz 1986, Bromhead 1992, Stark and Eid 1994, Wood 1990). According to Skempton, the effect of particle reorientation is felt only in soils having a clay fraction exceeding 20-25%. Skempton also differentiates between critical state (or fully softened state) and residual strength, which corresponds to the orientation of platy particles along the shear plane.

Ring shear apparatus was designed for the purpose of determining residual strength because it allows shearing at almost unlimited displacement. Unlimited displacement is necessary because it enables gradual reorientation of clay particles parallel to the direction of the shear. The measurement of residual strength is significant in soil stability problems where the existence of shear zones is known (re-activated landslides) or suspected. The residual behaviour is influenced by: mineralogy and the shape of the particles, applied stress, the type of shearing (turbulent or sliding), the rate of displacement and pore water chemistry (Lambe and Whitman 1979, Fell et al. 2000, Leroueil 2001).

The drained residual strength of cohesive soils has been studied extensively in the past (Bishop et al. 1971, Skempton 1964, 1985, LaGatta 1970, Lupini et al. 1981, Lemos 1986, Stark and Eid 1994, Tika et al. 1996, Tiwari and Marui 2004, 2005, Meehan et al. 2008, Saito 2008). Early investigations on the residual strength of cohesive soils focused on the measurement of the residual strength at relatively slow rates of displacement to prevent the generation of excess pore water pressure during shearing. Although rate effect on the residual strength was investigated even in those earlier studies (LaGatta 1970, Bishop et al. 1971), because of the narrow range of rates of displacement used, no rate effect was reported. The review of the previous investigations on the rate effect on the residual shear strength is given in more detail in the following section. An extensive literature review was done to determine proper percentages and types of clay material as well as the methods used.

However, in most of the previous studies the correct measurement of pore water pressure in ring shear tests was not possible, and thus, the influence of pore pressure on rate effect in cohesive soils remained unclear. Saito (2008) was the first to explain the mechanism of negative rate effect by conducting undrained ring shear test.

The following data were found in previous studies (Lupini et al. 1981, Skempton 1985, Lemos 1986, Tika et al. 1996, Saito 2008) and is used as a basis for further research in this thesis; namely, soils showing a negative rate effect have a drastic drop in shear resistance for the rates of displacements higher than the critical, attaining fast minimum values of 30- 50 % of the slow residual. Soils in the transitional shear mode range usually exhibit this type of behaviour.

The aim of this chapter is to investigate in more detail the reported drop in residual strength of transitional soil in the range of rates of displacement between 0.1 and 1 mm/s. A series of undrained single-stage and undrained, drained, and partially drained multi-stage ring shear tests were conducted to investigate this effect. The results and their significance are shown and discussed.

For simplicity, in this chapter we use the term "residual strength" for all specimens regardless of the clay fraction percentage, although as mentioned above, this term should be used only for soils that exhibit the effect of particle orientation. All rates of displacement are given in mm/s to be comparable with the international landslide

classification (WP/WLI, 1990). The residual effective friction angle is determined as a residual secant friction angle, assuming cohesion is zero.

4.2 REVIEW OF PREVIOUS EXPERIMENTAL WORK ON THE EFFECT OF RATE OF DISPLACEMENT ON RESIDUAL STRENGTH

Besides using the ring shear apparatus for the investigation of the rate effect, experimental studies in granular material have also been carried out by flume tests, and in cohesive material by a reversal direct shear test. However, in the following section, an overview of the rate effect on both granular and cohesive soils conducted on ring shear tests is given, by summarizing the most important findings from "old" papers with an update with recent research on this topic. The details of the specimens tested and methods used are described in detail.

4.2.1 Granular Soils

All earlier investigations on the rate effect by ring shear tests on granular soils reported no or slight rate effect (e.g., Hungr and Morgenstern 1984, Savage and Sayed 1984). The first tests were carried out on glass and plastic granular material (Savage and Sayed 1984, Sassa 1985). Hungr and Morgenstern (1984) carried out ring shear tests on sand specimens with varying normal stress (up to 200 kPa) and velocities (1, 160 and 1000 mm/s). All tests resulted in unique angles of friction, practically unaffected by the rate of displacement of the test.

Investigating the effect of grain crushing of sands on the generation of excess pore pressure, Okada et al. (2004) performed undrained and naturally drained speed-control ring shear tests on silica sand, under different normal stresses (50, 200 and 470 kPa) and at different rates of displacement (3, 5, and 100 mm/s). For silica sand No. 8, an almost constant value of friction angle was observed after failure, regardless of the shear rates of displacement used. For the silica specimens grain crushing was small in Okada et al. (2004) tests and no excess pore pressure was generated. However, in the tests in the Osaka

group, coarse sandy soils were present due to the grain crushing that occurred during the long shear displacement (60 m), and there was a drop in the shear strength with an increase in the rate of displacement.

Fukuoka et al. (2007) conducted a series of naturally drained ring shear tests on mixed sand and mixed beads under different normal stresses and rates of displacement to study the process of shear zone development. They used a normal stress of 22 and 200 kPa and rates of displacement of 90 and 2000 mm/s. The shear zone was visually observed (a ring shear apparatus with a transparent shear box was used) and the variation of grain size distribution along the specimen cross section was examined. The following results were obtained: large grains were concentrated in the central and upper part of the shear zone, and small particles deposited downward and upward from the shear zone. A possible explanation was suggested -larger grains tend to move into the moving layer that is in the shear zone. These results are consistent with those presented by Wafid et al. (2004). He studied the evolution of the shear zone and found that at steady state (shear displacement of 10 m) the shear zone was separated into two parts by a segregation process. The upper part consisted mainly of coarse grains, and the bottom of the of the shear zone where fine particles accumulated.

4.2.2 Cohesive Soils

Many papers have provided detailed reviews of investigations on the drained residual strength of cohesive soils (La Gatta 1970, Lupini et al. 1981, Skempton 1964, 1985 and Tika et al. 1996) and the effect of the rate of displacement on the residual strength is mentioned in some of them.

La Gatta (1970) conducted tests on three specimens (shale and clay) by initially shearing them at 0.001 mm/s until the residual strength was defined. Then he reduced the rate of displacement to 0.0001 mm/s with no significant change in the shearing resistance. Next, he increased the rate of displacement to 0.01 mm/s and reported the increase of resistance by only 3.5 %. Skempton (1985) also reported a negligible rate effect within the usual range of slow laboratory tests (0.00003-0.0002 mm/s). When those results were compared to field values, this variation appeared between -3 to +5%. Tiwari et al. (2005a)

obtained similar values for tests conducted on specimens from two landslides, under a normal effective consolidation stress of 250 kPa at rates of displacement of 0.002 and 0.02 mm/s. The value of the residual shear at the higher rate of displacement was about 2 and 3% higher than for the lower rate used.

Most of the previous investigations reported the significant change in the residual shear behaviour of cohesive soils with an increase in clay fraction. Many researchers tried to correlate the residual friction angle of soils with their index parameters (Skempton 1964, 1985, Voight 1973, Lupini et al. 1981, Mesri and Cepeda-Diaz 1986, Stark and Eid 1994, Tiwari and Marui 2005, Wesley 2003). The results showing a decrease of the residual effective friction angle with an increase in clay fraction, obtained by Lupini et al. (1981) were summarized by Skempton (1985) and are reproduced in Figure 4.1 along with the results obtained by Tiwari and Marui (2005). Figure 4.1 shows the change from "sand" to a "clay" type of behaviour and consequently, a decrease in the residual effective friction angle with the increase of the clay fraction. Clay fraction (CF) refers to percentage by weight of particles smaller than 0.002 mm, as determined by sedimentation. The percentage of CF that differentiate the "sand" and "clay" behaviour, obtained by Tiwari and Marui (2005) are lower, 8.5 % and 42.5 %, respectively, compared to 25 and 50 % obtained by Lupini et al. (1981).

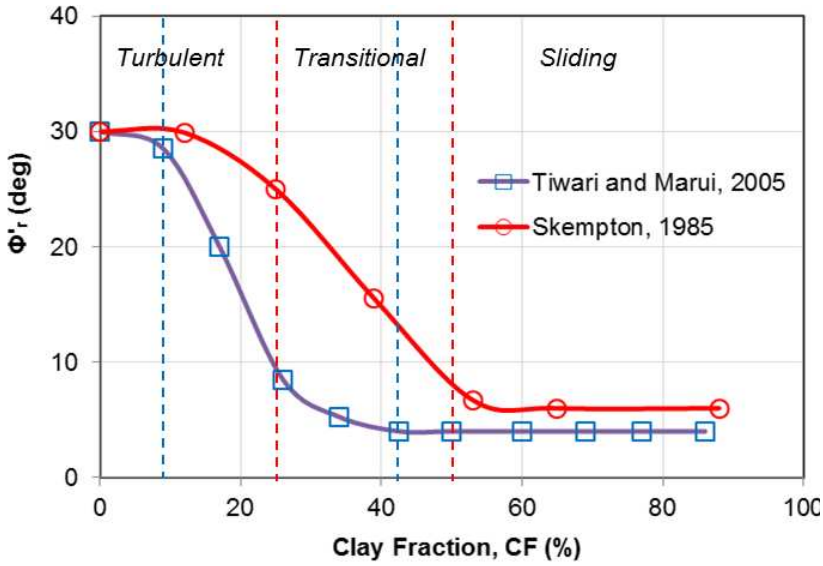

Figure 4.1 Residual effective friction angle as a function of clay fraction-from the drained ring shear tests on sand-bentonite mixtures (from Tiwari and Marui (2005) and Skempton (1985) after Lupini et al. (1981)).

Most of the authors recognized that the use of CF as an indicator of platy particles did not give real insight in the composition of soil. Measurement of the clay content proportion of total clay minerals indicates soil characteristics more comprehensively than CF (Tiwari and Marui 2005). However, for practical reasons, the use of CF for descriptions of soil behaviour is still more widely used.

Lupini et al. (1981) carried out a series of ring shear tests on sand-bentonite mixtures, and suggested two basic mechanisms in the development of residual strengths that mostly depend on clay fraction percentage. The authors called the mechanisms turbulent (rolling) and sliding shear with a transitional shearing between these two conditions. When soils containing both rotund and platy particles were sheared at large displacements, the following behaviour was observed:

- A turbulent (or rolling) mode was identified in soils with a high proportion of rotund particles, when the clay fraction is less than 20-25 % and soil behaves much like sand or silt, with higher friction angles (usually greater than 25°). The "residual strength" of these soils will be same as the critical state strength and they will exhibit almost classical critical state type behaviour. In the turbulent mode of shearing, preferred particle orientation does not occur, and the changes in shear zone are only concerned with change in porosity.
- A sliding mode was identified in soils formed by a high proportion of platy low friction particles, when the clay fraction is about 50% and residual strength is controlled by the sliding friction of the clay minerals. In the sliding mode, platy clay particles orientate in the direction of shearing. Therefore, a low strength shear surface is formed and results in low residual strength of a predominant clay mineral (15 ° for kaolinite, 10° for illite and 5° for montmorillonite).
- A transitional mode was identified in soils with no dominant particle shape, when the clay fraction is 25% to 50%. Shearing involves both turbulent and sliding behaviour of a shear zone with rotund particles that disrupt the development of a continuous shear surface.

In both sliding and transitional shearing mode, residual shear strength depends on the mineralogy and shape of clay particles (clays containing platy minerals are more likely to

orientate in shearing and show a decrease in shear resistance) and pore water chemistry (Lemos 2003, Tiwari et al. 2005b, Fell et al. 2000, Leroueil 2001).

Lupini was the first to identify the rate effect on the drained residual strength in cohesive soils and following his findings, several studies focused on the influence of fast rates of displacement on the residual shear strength (Lemos1986, 2003 and Tika 1989, Tika et al. 1996). The subsequent authors showed (and confirmed the findings of earlier studies) that residual strength is relatively insensitive to the rate of shearing for the slow rates of shearing. However, at faster rates (v> 1.67 mm/s according to Skempton (1985) and Tika et al. (1996)), the effect of rate of displacement on residual strength is significant and plays a role in the pattern of behaviour.

Lemos (1986, 2003) identified and described the pattern during fast shearing of a shear zone that was previously formed by slow drained shearing (when "slow" or " static" residual strength is obtained). The following behaviour is typically observed during fast shearing: an immediate increase in strength (threshold), a further increase in strength to a maximum (fast peak) and finally, a decrease of strength to a minimum value of fast residual strength. Three types of rate effects on the residual strength were identified (Figure 4.2), according to the relation of fast residual strength to slow residual strength: positive (POS) (fast residual>slow residual strength), neutral (NEU) (fast residual=slow residual strength) and the negative rate effect (NEG) (fast residual<slow residual strength). Soils with a turbulent shear mode exhibited a neutral or negative rate effect, soils with a sliding shear mode showed a negative or positive effect while the transitional shear mode showed a negative rate effect (Tika et al. 1996).

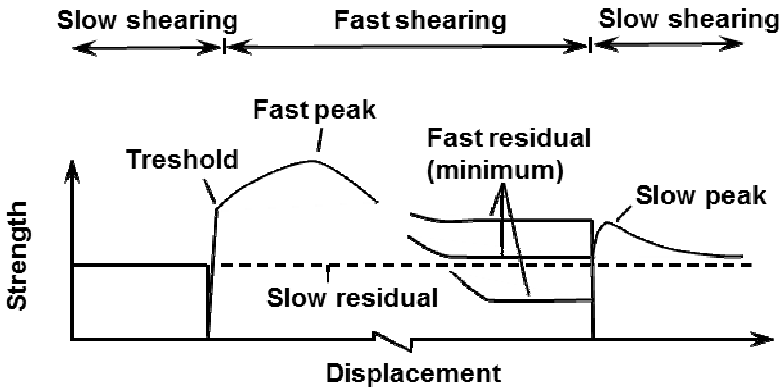

Figure 4.2 Three types of rate effects on the residual strength. Summary of the observed rate- displacement phenomena for residual strength (after Tika et al. 1996).

Tika et al. (1981) and Lemos (2003) also tried to investigate the causes of the negative rate effect and they suggested a possible mechanism. Causes of negative rate effect, such as pore pressure as the most important one, were investigated by using indirect (fast shearing with and without consolidation phase) and direct procedures (measuring of pore pressure and temperature immediately after fast shearing). These authors suggested the following mechanism of decrease in strength: fast shearing involves dilation of massive particles which results in increased void ratio and consequently, increased water content of the shear zone which leads to strength reduction (Tika et al. 1996, Lemos 2003).

Skempton (1985) concluded that there is a qualitative change in the behaviour of soils when they are sheared at rates exceeding 1.67 mm/s. He suggested that in soils with a positive rate effect this is probably due to the disturbance of the original structure and in soils with a negative rate effect, he assumed that negative pore pressures are generated, and as displacement continues, these pressures are dissipated within the specimen, thus leading to a decrease in strength. He also states: "It is surely significant that this material lies in the "transitional" zone, but why it should show increase in fast rates followed by an abnormal decrease is not clear. Clearly more research is needed better to define the limits of this phenomenon and for all types of soil, to measure pore pressures at fast rates of displacement and to explore the effects in rapid tests. The results and their significance in engineering design are obviously considerable" (Skempton 1985).

Meehan investigated shearing resistance that can be mobilized on slickensided rupture surfaces in clay slopes during earthquakes by conducting a series of ring shear tests, direct shear tests, and triaxial tests (Meehan 2006). The aim of his study was to investigate static and cyclic shear resistance of slickensided surfaces. A series of fast ring shear tests were conducted in the Bromhead ring shear device on Rancho Solano Fat clay specimens (CF >53 %). The purpose of these tests was to try to develop an understanding of the fast residual shear strength along existing slickensided discontinuities. He used same multi-stage testing approach proposed by Skempton (1985) by initial drained shearing at a slow rate (0.0003 mm/s), then rapidly shearing until app. 500 mm of shear displacement (0.74 mm/s), and then slowly again to re-establish the drained residual condition (Meehan et al. 2007, 2008). Test results indicated a positive rate effect that was in accordance with previous studies. However, there was a cyclic increase and decrease during that fast shearing stage that was likely caused by a shifting of the top platen during shearing. In

addition to this problem, he also pointed to the problem of the pore pressure response, which in the Bromhead ring shear apparatus, occurs differently than it would occur in the field, or in the Bishop type of apparatus. This is because in the Bromhead type of apparatus, shearing takes place at or close to the top platen so the generated pore pressure dissipates relatively quickly. He showed that the Bishop type of ring shear apparatus is better suited for testing at fast rates of displacement (Meehan 2006).

Saito (2008) conducted a series of undrained ring shear tests on silica sand and sand-clay mixtures (sand with 10 and 20 % of kaolin, illite and bentonite), in order to investigate the mechanism of the negative rate effect. He showed that there is an effect of the rate of displacement on the secant friction angle in bentonite-sand and illite-sand mixtures but not in silica sand and kaolin-sand mixtures. His results of undrained multi-stage test on silica sand and a 20 % bentonite specimen, showed a significant difference in effective friction angle between 0.01-0.1 mm/s. The rate effect on the effective secant friction angle was interpreted as a change in the degree of interlocking that was influenced by the change in the shear zone by the type of clay and the particle segregation.

4.3 APPARATUS AND TESTING PROCEDURE

In this study, ICL-1, a transportable and compact undrained ring shear apparatus designed by Sassa in 2010 is used. The details related to its mechanism and structures are explained in detail in the previous chapter. The maximum shear rate of displacement it can produce is 54 mm/s and the minimum is 0.01 mm/s.

4.3.1 Tested specimens

Three types of specimens were tested, one of pure silica sand No. 8 (SS 8) and two mixtures of silica sand and bentonite clay (SB 20, SB 30). Both silica sand and bentonite are commercially available and were mixed in different proportions; 20 % and 30 % of bentonite (by weight) was added to silica sand (SB 20 and SB 30 respectively).

Silica sand No. 8 is a silty sand mainly consisting of quartz and smaller amounts of feldspar while commercial bentonite contains mainly smectite and smaller amounts of

crystoballite, illite, and quartz. The bentonite clay used in this research is Na–bentonite with 97% of clay fraction, and plastic and liquid limits which were measured to be 85.7 and 357.9 (Gratchev et al. 2007). Specimen properties are given in Table 4.1 and grain size distribution is shown in Figure 4.3. Grain size distribution was determined according to Japanese soil testing practices. The Clay fraction (CF) determined by sedimentation seems to be overestimated due to the high percentage of silt in silica sand No. 8.

Table 4.1 Specimen properties

Specimen	Bentonite content (%)	*CF* (<2μm)	ρ_s (g/cm^3)	*LL* (%)	*PL* (%)	*Ip*
SS 8	0	5	2.59	-	-	NP*
SB 20	20	30	2.55	64.3	26.5	37.8
SB 30	30	40	2.45	70	20	50

*NP- Non Plastic

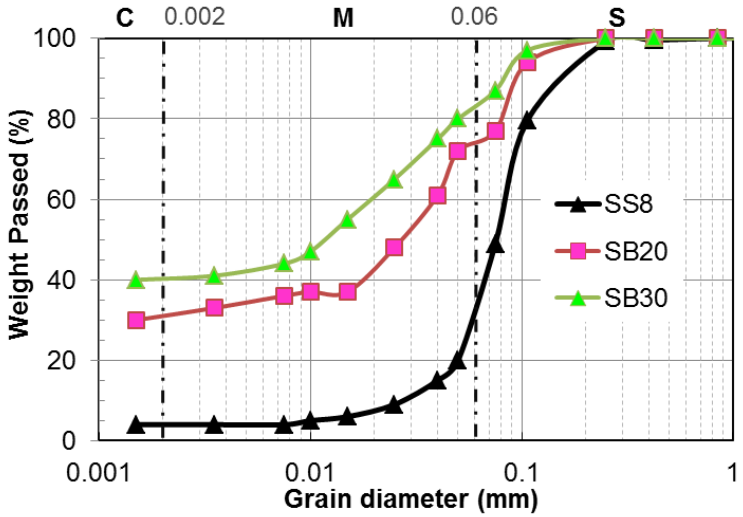

Figure 4.3 Grain size distribution.

In the previous ring shear tests with saturated specimens, dry samples were usually placed in the shear box and then saturated by water circulation. For low permeability

specimens, this process of water circulation took at least several days (Tiwari et al. 2004 mentioned 72 h).

To reduce the time of sample saturation, the sample was saturated outside of the shear-box. All the mixtures were first mixed dry, then saturated with de-aired water and finally mixed until they became slurry. Next, they were placed in a vacuum and left for at least two days (Figure 4.4). A similar procedure was reported by Toyota et al. (2009). Therefore, the already prepared saturated specimen was placed into the ring shear box filled with de-aired water. In this way, fully saturated samples were successfully prepared without water circulation, which was confirmed by $B_D \geq 0.95$.

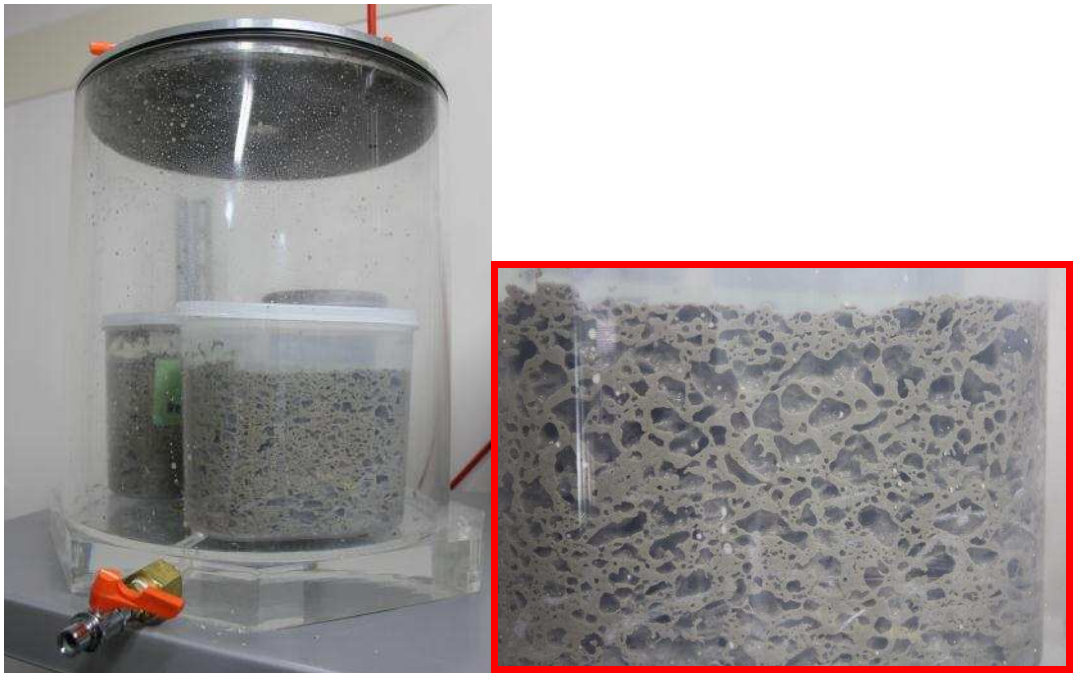

Figure 4.4 Silica sand-bentonite specimens in vacuum tank.

Silica sand–bentonite mixtures were chosen for testing because both are commercially available and the same mixtures were tested in ring shear tests by Lupini et al. (1981), Tiwari and Marui (2005) and Saito (2008). Also, the aim was to investigate in more detail soils in a transitional zone that show the negative rate effect.

4.3.2 Testing Procedure

The testing procedure consisted of; specimen saturation, consolidation, and shearing. The following procedure was employed to saturate the specimens for the ring shear tests. Here only a short description of each stage is given, because details of the procedure are explained in the previous chapter.

Gap adjustment and measurement of rubber edge friction: After the apparatus is set up without a sample, the gap value is adjusted by applying the vertical load of 0.8 kN. The shear box without a sample was filled with CO_2 and de-aired water to expel entrapped air. Then, the friction of the rubber edge was measured. The increment of shear resistance due to rubber edge friction was usually around 25 kPa, and that value was subtracted from the measured test values to obtain the true shear resistance of the specimen.

Next, a saturated sample was slowly spooned in the de-aired water inside the shear box. Preparation of saturated specimens has been previously described. The saturation was then checked by measuring the B_D value which should be greater than 0.95 for fully saturated specimens. For all specimens $B_D > 0.95$ was obtained (Table 4.2).

The sample was then consolidated in drained conditions, under a pre-decided normal stress of 400 kPa (or 500 kPa in some tests when the back pressure of 100 kPa was kept constant during the test). For all tests the same, initial effective stress of 400 kPa was used and normal stress was kept constant during test.

After consolidation, the shearing was applied by speed-control tests. To investigate and explain the decrease in shear resistance and the effective secant friction angle (Φ'_r), two series of speed-controlled ring shear tests were conducted on silica sand and silica sand-bentonite mixtures:

- **Single-Stage Shearing**-each individual specimen was sheared at one constant rate of displacement until a certain displacement in the undrained condition. Four different rates of displacement were used: 0.01 mm/s, 0.1 mm/s, 1 mm/s, and 10 mm/s. The first two rates of displacement are considered slow, and last two fast. By testing a new specimen at each shear rate, it was possible to avoid the effect of settlement that occurs during a multi-stage test.

- **Multi-Stage Shearing**-one specimen is sheared in several stages with different rates of displacement until 1m of displacement for each stage is achieved. To confirm previous rate effect findings, specimens were subjected to alternating slow and fast shearing stages, as shown in Figures 4.2 and 4.5. First, slow shearing was applied and was stopped after 1 m of displacement. Next, the specimen was re-sheared at a fast rate of displacement. Four types of multi-stage shearing were conducted, depending on the rates of displacement used and the draining conditions during shearing, and the pause that followed after shearing was stopped. For the first three types, three rates of displacement were used (0.1, 1 and 10 mm/s) in 8 stages, that is, until cumulative displacement of 8 m. Figure 4.5a shows the rates of displacement used in the 8-stage type of tests. In one type of multi-stage test, the specimen was sheared until 7 m, in 7 stages, using only two rates of displacement (0.1 and 1 mm/s), but with a gradual change between them. Rates of displacement used in this type of multi-stage test are shown in Figure 4.5b.

To avoid possible terminological confusion, different multi-stage tests were named by the state of the upper valve during shearing and pausing: as open or closed (C-O; C-C and O-O). The first letter refers to the position of the upper valve during shearing and the second letter refers to the valve position during the pausing, e.g C-O is the multi-stage test in which shearing is conducted with a closed upper valve and during pausing the valve is open. When silica sand is sheared with the upper valve open, shearing is considered to be drained. However, in the case of SB 20 and SB 30 specimens, shearing with the open upper valve is considered to be partially drained, because the pore-pressure generation rate is greater than the dissipation rate. And to be consistent, the same was done for the pause that followed after shearing was stopped: with the open upper valve, consolidation was allowed while with the closed upper valve, no consolidation was allowed. The following are the four types of multi-stage tests conducted:

1) **Undrained test with consolidation**- Multi-stage Test in 8 stages (I-VIII; C-O). Shearing in undrained conditions was conducted in 8 stages. After 1 m of displacement shearing was stopped and the upper valve opened for pore pressure to dissipate. The specimen was allowed to consolidate and after the pore pressure was zero, re-sharing at a different rate of displacement could start.

2) **Undrained test without consolidation**- Multi-stage Test in 8 stages (I-VIII; C-C). Shearing was conducted in undrained conditions and after shearing was stopped, the upper valve was kept closed and pore pressure could not dissipate. In this way consolidation of the specimen was not allowed.

3) **Drained/ Partially drained test with consolidation**- Multi-stage Test in 8 stages (I-VIII; O-O). The entire time during the test the upper valve was open enabling drainage during shearing. As mentioned earlier, shearing was drained in silica sand specimens and partially drained in the mixtures. After shearing was stopped, the valve remained open to allow full dissipation of pore pressure and specimen consolidation.

4) **Undraind test with consolidation**- Multi-stage Test in 7 stages (I-IV; C-O) with gradual change of the rate of displacement. Conditions of this test are the same as in the first case; namely, the undrained shearing is followed by consolidation, except the change between the slow (0.1 mm/s) and fast (1 mm/s) stages is gradual, as shown in Figure 4.5.b.

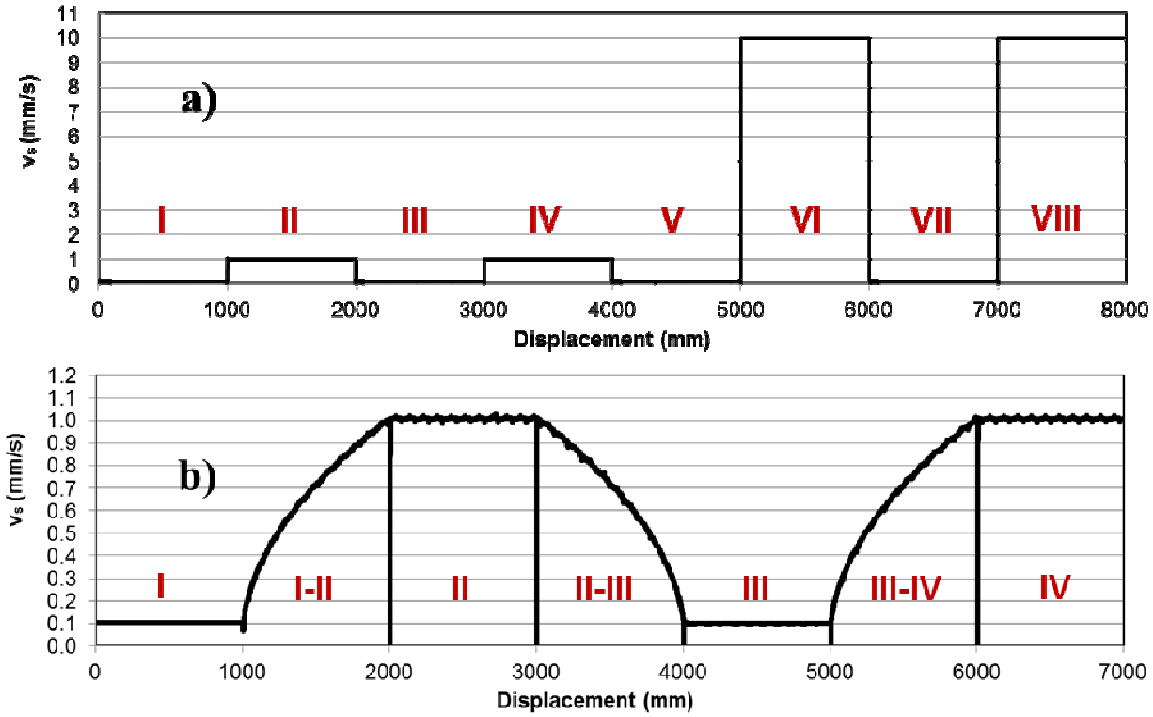

Figure 4.5 Multi-stage tests and rates of displacement applied: a) 8-stage test (I-VIII) and b) 7-stage test (I-IV).

Multi-stage ring shear tests have been used by many researchers in their investigation for both stress-dependent (Stark and Eid 1994, Tiwari et al. 2004) and rate-dependent (Skempton 1985, Lemos 1986, Tika et al.1996, Saito 2008) behaviour of the residual failure envelope. Although multi-stage ring shear tests have been reported as being useful, because they reduce testing time considerably, these tests are still not widely used, mostly due to problem of leakage during long shearing and due to the limitation in measuring peak shear strength.

Individual specimen testing is more commonly used although each specimen may not have the same properties (Tiwari et al. 2004). Even when specimens of the same mixture are used, different saturations can be obtained (B_D value) and the consolidation process may differ, which will result in variations of pore pressure generation and measured shear resistance. Due to the above mentioned reasons, a series of single and multi-stage ring shear tests were conducted for each specimen. Shear resistance, shear displacement, vertical displacement, and pore pressure were monitored continuously during each test. The results of both single-and multi-staged tests are shown and explained in the following section.

4.4 RESULTS

First, single-stage tests were conducted, in order to have preliminary results that would indicate the behaviour of the specimen sheared at different rates of displacement. The minimum displacement of 3 m was reached for the slowest test (0.01 mm/s) and 20 m for the fastest (10 mm/s). Four different multi-stage shearing tests were conducted for each type of specimen (SS 8, SB 20 and SB 30). The results are shown separately for all three specimens in the following section and the list of tests and test conditions are summarized in Table 4.2.

As mentioned in the introduction to this chapter, the results are interpreted using the secant phi approach, assuming that there is no residual cohesion, using the following formula for calculation of the effective secant residual friction angle (Figures 4.8, 4.11 and 4.14):

$$\Phi'_r = tan^{-1}\left(\frac{\tau_r}{\sigma'}\right). \quad \text{(Eq 4.1)}$$

where τ_r is residual shear resistance and σ' is effective stress.

Test results of each multi-stage test are shown in Appendices (A1-A12). In all figures in the Appendices, the same representation style was used; the slow rates of displacement are shown in the "cold" colors (blue and green) and the fast shear rates in "warm" (violet and red) colors. The results of four multi-stage tests conducted for SS 8, SB 20 and SB 30 are summarized and shown in the following way: the ratio of a friction coefficient to the corresponding residual value (R) as well as to the pore-pressure ratio (r_u) are plotted against the cumulative shear displacement (Figures 4.7, 4.10, and 4.13). The ratio of the friction coefficient to the corresponding residual value is expressed by Eq. 4.2. and is represented in the red lines in figures 4.7, 4.10 and 4.13. The pore-pressure ratio (r_u), which is represented by blue lines, is calculated by generated excess pore pressure (u) divided by total normal stress (σ) (Eq. 4.3).

$$R = R'/R'_{0.1} = \left(\frac{\tau_r}{\sigma'}\right)/\left(\frac{\tau_r}{\sigma'}\right)_{0.1}. \quad \text{(Eq. 4.2)}$$

$$r_u = u/\sigma\,. \quad \text{(Eq. 4.3)}$$

The residual friction coefficient ($R'_{0.01}$) refers to the value obtained at the end of the first slow stage when residual shear resistance was obtained. Results shown in this way allow changes to be seen compared to the residual value of the first stage when R=1 indicated in figures by the grey line.

Table 4.2 List of tests and test conditions.

Test No.	Specimen	v_s (mm/s)	σ_0' (kPa)	D_s (m)	B_D	Type of test	
T 1	SS 8	0.01	400				
T 2	SS 8	0.1	400	6	0.95	Single- stage	
T 3	SS 8	1	400	10	0.96		
T 4	SS 8	10	400	20	0.96		
T 5	SS 8	0.1 & 1 &10	400	8	0.97		C-O
T 6	SS 8	0.1 & 1 &10	400	8	0.97	Multi-stage	C-C
T 7	SS 8	0.1 & 1 &10	400	8	0.98		O-O
T 8	SS 8	0.1 & 1	400	7	0.97		C-O
T 9	SB 20	0.01	400	3	0.96		
T 10	SB 20	0.1	400	6	0.95	Single- stage	
T 11	SB 20	1	400	10	0.97		
T 12	SB 20	10	400	20	0.98		
T 13	SB 20	0.1 & 1 &10	400	8	0.97		C-O
T 14	SB 20	0.1 & 1 &10	400	8	0.98	Multi-stage	C-C
T 15	SB 20	0.1 & 1 &10	400	8	0.97		O-O
T 16	SB 20	0.1 and 1	400	7	0.94		C-O
T 17	SB 30	0.01	400				
T 18	SB 30	0.1	400	6	0.95	Single- stage	
T 19	SB 30	1	400	10	0.97		
T 20	SB 30	10	400	20	0.96		
T 21	SB 30	0.1 & 1 &10	400	8	0.95		C-O
T 22	SB 30	0.1 & 1 &10	400			Multi-stage	C-C
T 23	SB 30	0.1 & 1 &10	400	8	0.95		O-O
T 24	SB 30	0.1 and 1	400	7	0.95		C-O

v_s- rate of displacement, σ_0'- initial effective stress, D_s – shear displacement, C- Closed valve, O- Open valve (The first letter refers to the position of the upper valve during shearing and the second letter refers to the valve position during pausing). Tests 1, 17, and 22 were not conducted.

4.4.1 Silica Sand (SS 8)

As could be expected and according to previously published data on the rate effects of granular soils showing turbulent shear behaviour, there were no rate effects in the pure silica sand specimens. The results of both, single and multi-stage tests showed that the effective secant friction angle is independent of the rate of displacement used. Test results are presented and described separately for single and multi- stage shearing directly below:

Single-Stage Shearing Tests on SS 8

All single-stage tests results (T 2, T 3, and T 4) conducted on silica sand specimens are shown in Figure 4.6. The total normal stress of 400 kPa was kept constant during tests and each specimen was sheared at a different rate of displacement until 7, 10, or 20 m of displacement (Figure 4.6a). After failure, pore pressure increased and reached app. 250 kPa at the end of shearing, while shear resistance decreased to a minimum value (86 kPa to 70 kPa). The stress paths of these tests are shown in Figure 4.6 b. with the residual failure line showing the residual effective friction angle ($\Phi r'$) of 29.5°. The same can be seen on Figure 4.6c, which shows almost the same effective friction angle for all rates of displacement used.

Multi-Stage Shearing Tests on Silica Sand Specimens (SS 8)

In tests with undrained shearing and allowed consolidation (T 5, T 8), a gain in strength in each subsequent stage due to consolidation can be seen (Figure 4.7). The biggest change in sample height due to consolidation took place after the first stage and resulted in higher shear resistance in the beginning of the 2nd stage (Appendix A1 and A4).

When consolidation was not allowed (T 6), there was no such gain. The undrained shear resistance as well as the residual friction angle had the lowest values (Figure 4.8, Appendix A2). A decrease in pore pressure and consequent increase in resistance after stage IV occurred because the test was stopped during night. However, as soon as re-shearing started, strength was recovered, as well as pore pressure (Appendix A2). Almost constant values of all parameters were then observed.

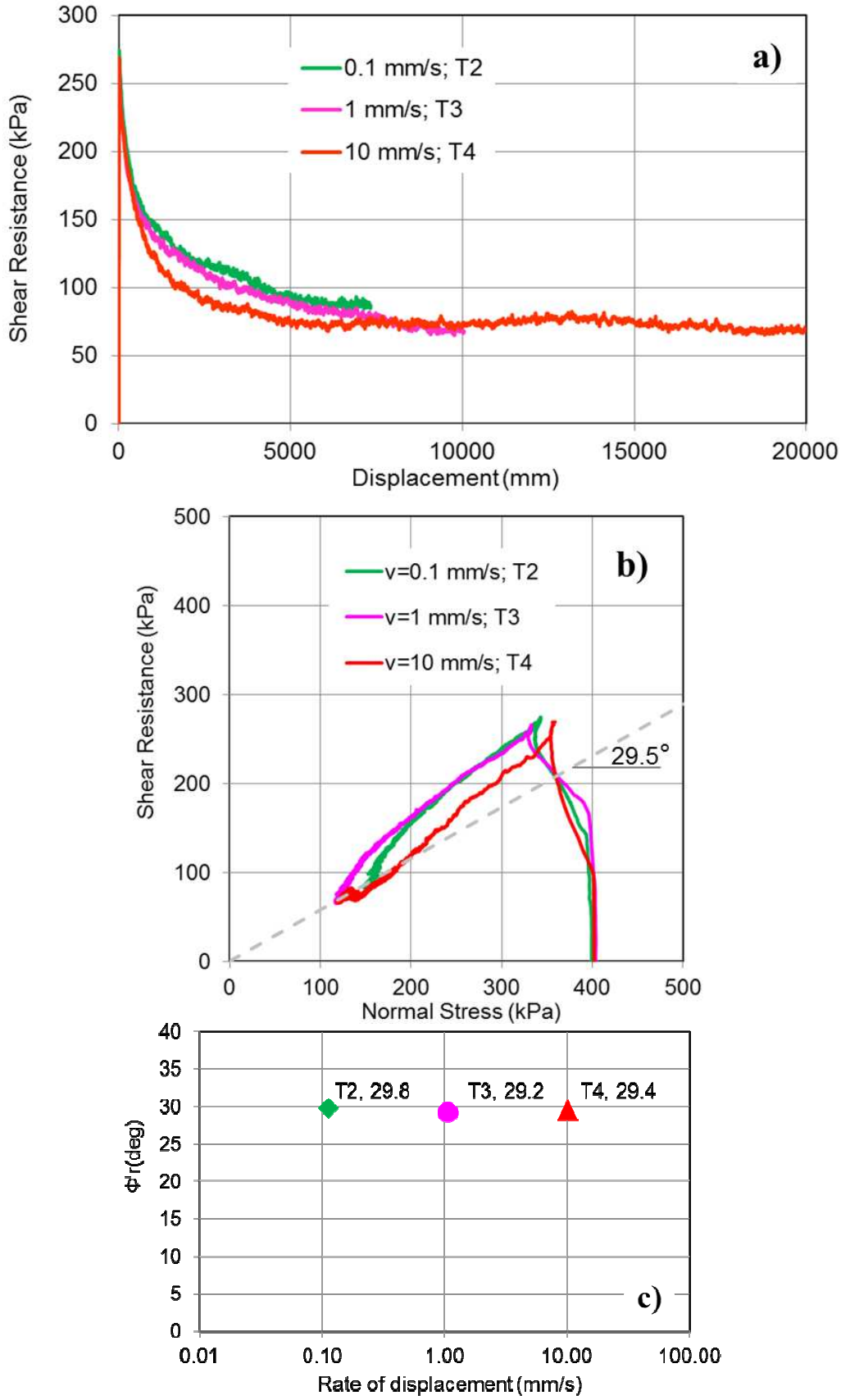

Figure 4.6 SS 8 single-stage tests results: a) Shear displacement, b) Stress Path and c) Rate of displacement.

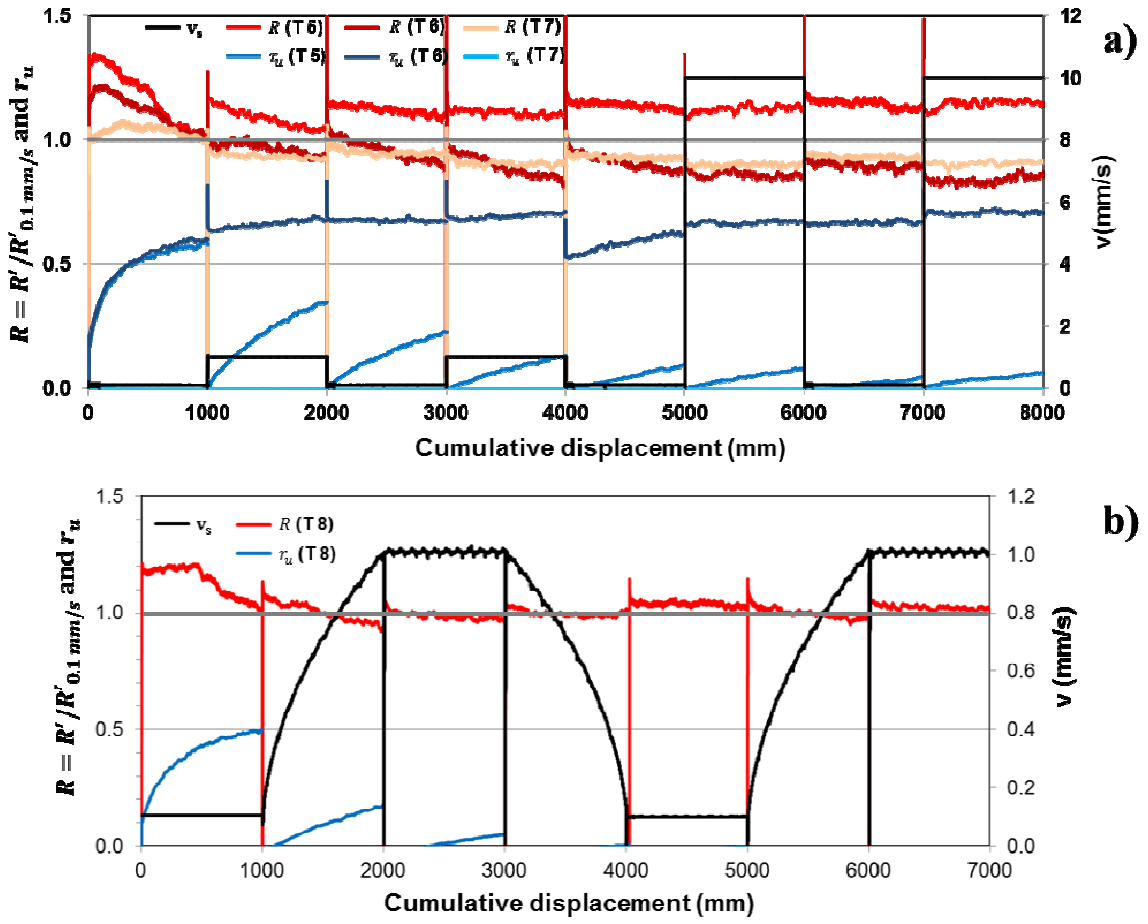

Figure 4.7 Cumulative displacement and friction coefficient and pore pressure ratio of multi-stage tests conducted on SS 8 specimens a) T 5-T 7 (8 stages) and b) T 8 (7 stages).

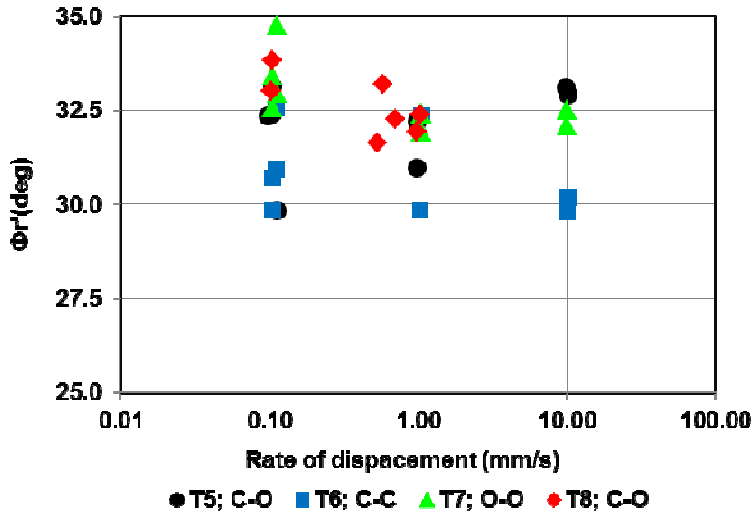

Figure 4.8 Rate of displacement and residual effective friction angle of multi-stage tests conducted on SS 8 specimens (T 5-T 8).

In the case of the drained shearing with allowed consolidation (T 7), similar behaviour as in T 6 occurred; the ratio of a friction coefficient to the corresponding residual value decreased after the first stage (Figure 4.7). Also, there was no generation of any excess pore pressure and vertical displacement increased gradually during shearing and the consolidation phase. This resulted in the highest shear resistance and effective friction angle (Figure 4.8). This cannot be seen in Figure 4. 7 because relative change compared to the first stage is given, but in Figure 4. 8 and Appendix A3.

However, the changes of the friction coefficient ratio were in the range of 10 % and as a result the residual effective friction angle varied around 3°, showing rate independent behaviour (Figure 4.8). This can be clearly visible from the test of the gradual change of the rate of displacement (T 8) that is shown in Figure 4.7b and Appendix A4.

4.4.2 Silica Sand and 20 % Bentonite Mixture (SB 20)

In the tests conducted on this specimen, a negative rate effect was observed, which was in accordance with reports of other authors (Tika et al. 1996, Saito 2008). As explained in the discussion, regardless of the displacement used, in the generated pore pressure and other factors, shear resistance was lower in both single and multi-stage ring shear tests, thus confirming that residual strength depends on the rate of displacement.

Single-Stage Shearing Tests on SB 20

In order to confirm results of single-stage tests (T 9-T 12 in Table 4.2), additional tests were conducted for each rate of shearing (in Figures T 9a-T 12a). As can be seen in Figure 4.9a, shear resistance measured at 1 mm/s was the lowest, and for 0.1 mm/s, the highest. Figure 4.9b shows the effective stress paths of all 8 single-stage undraned tests. In that graph, two distinctive failure lines could be drawn, one for tests at slow rates of displacement (0.01 and 0.1 mm/s) with the $\Phi'r$=29°, and in the other one for tests at fast rates of displacement (1 and 10 mm/s) with the $\Phi'r$=16°. When residual effective friction angles of all tests are drawn in relation to the rates of displacement (Figure 4.9c) a very clear tendency of decrease could be seen.

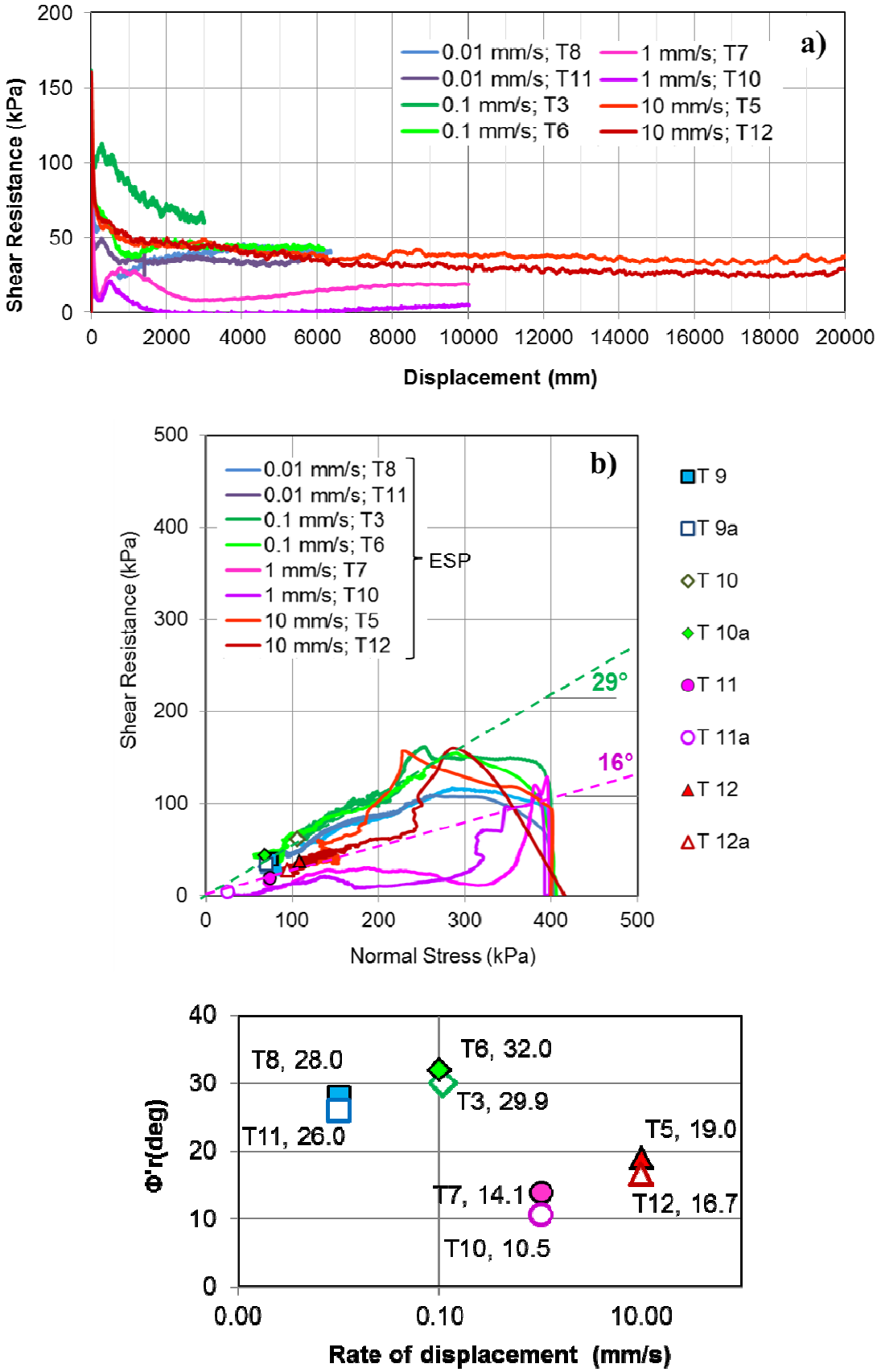

Figure 4.9 SB 20 single-stage tests results: a) Shear displacement, b) Stress Path and c) Rate of displacement

Multi-Stage Shearing Tests on SB 20

Multi-stage tests on SB 20 specimens showed changes in effective friction angle, shear resistance and pore pressure, especially during fast shearing stages (II, IV, VI and VIII). This change was the most significant in the case of tests with undrained shearing with allowed consolidation (T 13 and T 16). This can be more clearly seen in the figures of each test that are given in the Appendix (A5- A8). Figure 4.10 shows a cumulative displacement graph in terms of the change of friction coefficient and pore pressure ratio.

In an undrained test without consolidation (T 14), there was negligible change in specimen height (Appendix A6). High pore pressure was maintained during the test, but as can be seen in Figure 4.10a, it varied during fast stages, especially during VI and VIII stage. Due to the height of the pore pressure, shear resistance was the lowest (Appendix A6).

In the SB20 specimen, unlike in the pure silica sand specimen, a test with the open upper valve was partially drained (T 15). As can be seen from Figure 4.10a, there was excess pore pressure generated during shearing. However, the generated pore pressure was much lower than in the case of the undrained multi-stage shearing tests (T 13 and T 14). Keeping the valve open during all tests allowed consolidation to take place and resulted in the highest specimen height reduction of 3.8 mm (Appendix A7). The higher effective friction angles are also the result of the higher compaction and consolidation that was enabled by keeping the value open (Figure 4.11).

The multi-stage test with a gradual change of rate of displacement (T 16), showed similar results with T 13, due to the similar conditions used (but with a more pronounced difference of the slow and fast stages, and the gradual change between these stages (Figure 4.10b). The drop in the friction coefficient ratio is obvious from the value obtained at the end of 1st slow shearing stage (R=1). The value drops at 50 % of the initial value during a gradual increase of the rate of displacement between 0.1 and 1 mm/s, after 1.2 m of cumulative displacement. The value is then constant during the fast stage at 1 mm/ sec (2 to 3 m of cumulative displacement). Then, the friction coefficient ratio slowly increases up to R=0.7 during the decrease of the rate of displacement from 1 to 0.1 mm/s. The increase continues during the slow stage, from R=0.7 to R=1.1 (until 5 m of cumulative displacement). Similar behaviour occurred when a gradual increase of the rate of

displacement was repeated. This resulted in two distinctive failure lines in the stress path graphs of T 16 (Appendix A8).

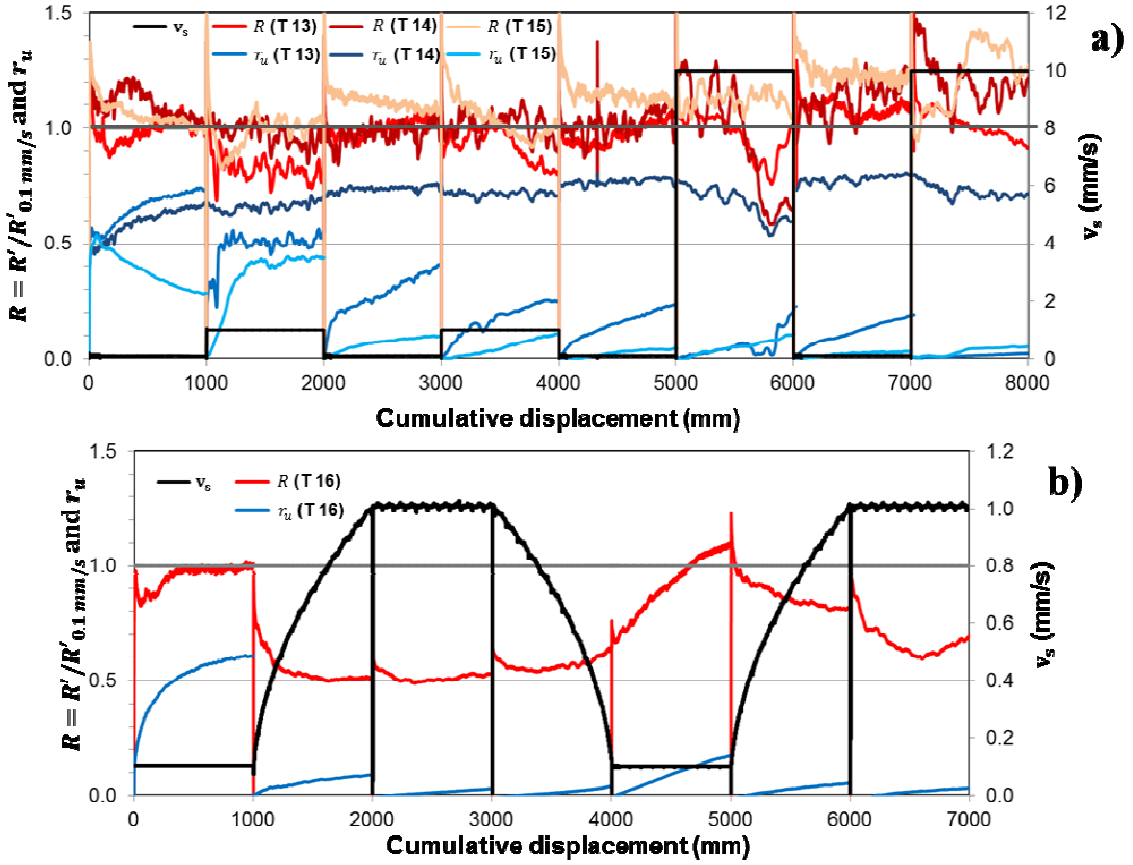

Figure 4.10 Cumulative displacement and friction coefficient and pore pressure ratio of multi-stage tests conducted on SB 20 specimens a) T 13-T 15 (8 stages) and b) T 16 (7 stages).

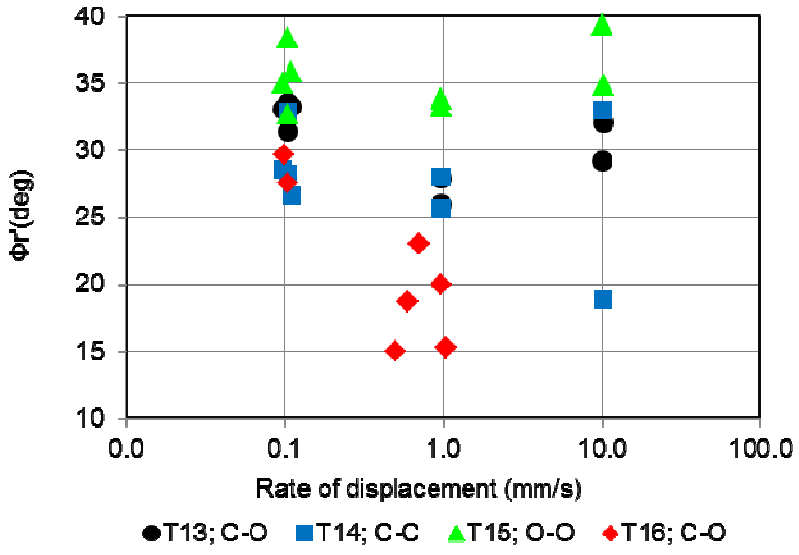

Figure 4.11 Rate of displacement and residual effective friction angle of multi-stage tests conducted on SB 20 specimens (T 13-T 16).

When effective friction angles of all stages are compared (Figure 4.11), it is obvious that there is a decrease in the faster shearing stages compared to the slow shearing stages.

4.4.3 Silica Sand and a 30 % Bentonite Mixture (SB 30)

Tests on mixtures of silica sand 30% bentonite were, due to the higher CF content and lower permeability, much slower and more difficult to conduct. The time needed for consolidation was app. 4 days. Because of larger height reduction in this specimen, there were problems with the vertical load, because the minimum specimen height was limited and was reached in some stages before the end of the tests. Because of the above mentioned difficulties and the duration of SB 30 specimen tests, only a few single-stage undrained shearing tests were conducted and only 3 of 4 multi-stage tests. Although these tests are listed in Table 4.2, they will be conducted additionally (T 17 and T 22).

In all conducted multi-stage tests, negative pore pressure occurred in fast stages which reflected the results obtained. In spite of the questionable reliability of these results, the results of these tests are shown and described. Their reliability and meaning as well as possible reasons for this negative pore pressure will be described and explained in the discussion.

Single-Stage Shearing Tests on SB 30

Figure 4.12a shows the shear resistance of tests T 18, T 19, and T 20. As can be seen, at a slow rate of displacement (0.1 mm/s), higher shear resistance was obtained compared to a test at 10 mm/s with lower resistance. Test T 19, at the rate of 1 mm/s shows the highest value of shear resistance, which is according to previous results questionable and should be repeated. This can also be seen in the stress path graph (Figure 4.12b) with obvious abnormalities in ESP of test T 19. When residual effective friction angles of all tests are drawn in relation to the rates of displacement (Figure 4.12c), it can be seen that lower effective friction angles are obtain compared to the SB 20 specimen as expected ($\Phi r'$=17.9° for SB 30 compared to the average $\Phi r'$=31° for SB 20 at 0.1 mm/s, and $\Phi r'$=7.6° for SB 30 compared to the average $\Phi r'$=18° at 10 mm/s).

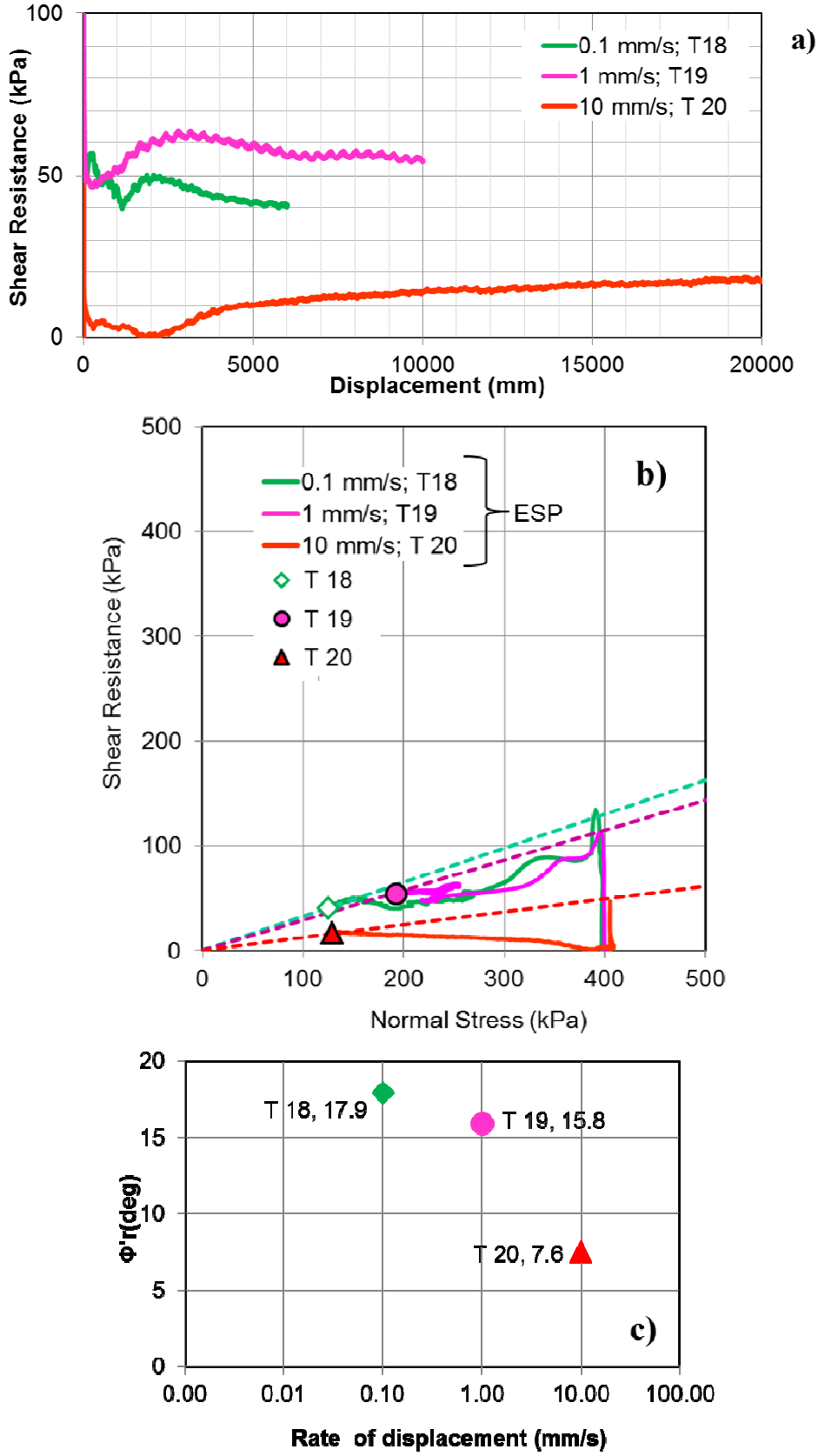

Figure 4.12 SB 30 single-stage tests results: **a)** Shear displacement, **b)** Stress Path and **c)** Rate of displacement.

Multi-Stage Shearing Tests on SB 30

Figure 4.13 shows a cumulative displacement graph with significant changes in the friction coefficient and pore pressure ratio of multi-stage tests on the SB 30 specimen. In the test of undrained shearing with consolidation (T 21), a small dilation occurred in stages II and IV, and the drop of pore pressure was probably caused by the dilation. Also, in stages VII and VIII there was a significant change in vertical displacement, probably caused by leaking, or undulation of the formed shear zone that caused the loading plate to move up and down (the cyclic shape indicates this). The variation in vertical displacement, as well as shear resistance, can be seen in the figures of T 21 given in Appendix A9. Even if leakage occurred, it did not affect the results of stages I-VI. Figure 4.13a shows a decrease of the friction coefficient ratio in stages II and IV and an increase of friction coefficient ratio in the slow stages (III and V).

In Test T 23, the valve was open during the test and shearing was partially drained as in the SB 20 specimen. Figure 4.13a shows excessive pore pressure in stage I that suddenly decreases in stage II and becomes negative possibly due to dilation or cavitation. Regardless of pore pressure, Figure 4.13a indicates a drop in the friction coefficient ratio between slow and fast stages. The comparison regarding the first stage, when R=1 shows much bigger variations compared to the SB 20 specimen. In the case of the SB 20 specimen, the consolidation that followed the first stage resulted in the maximum height reduction of the specimen (more than 50 % of all height changes occurred until 2 m of displacement), while in the case of the SB30 specimen, this height reduction was more evenly distributed.

The results of the test with a gradual change in the rate of displacement show a similar pattern to that in the SB 20 case, and are similar with Test T 21, because of the same conditions used (undrained shearing and consolidation), but with a more pronounced difference of slow and fast stages, and the gradual change between these stages (Figure 4.13b).

The effective friction angles of the end of each stage of all multi-stage tests are shown in Figure 4.14, indicating a decreasing trend.

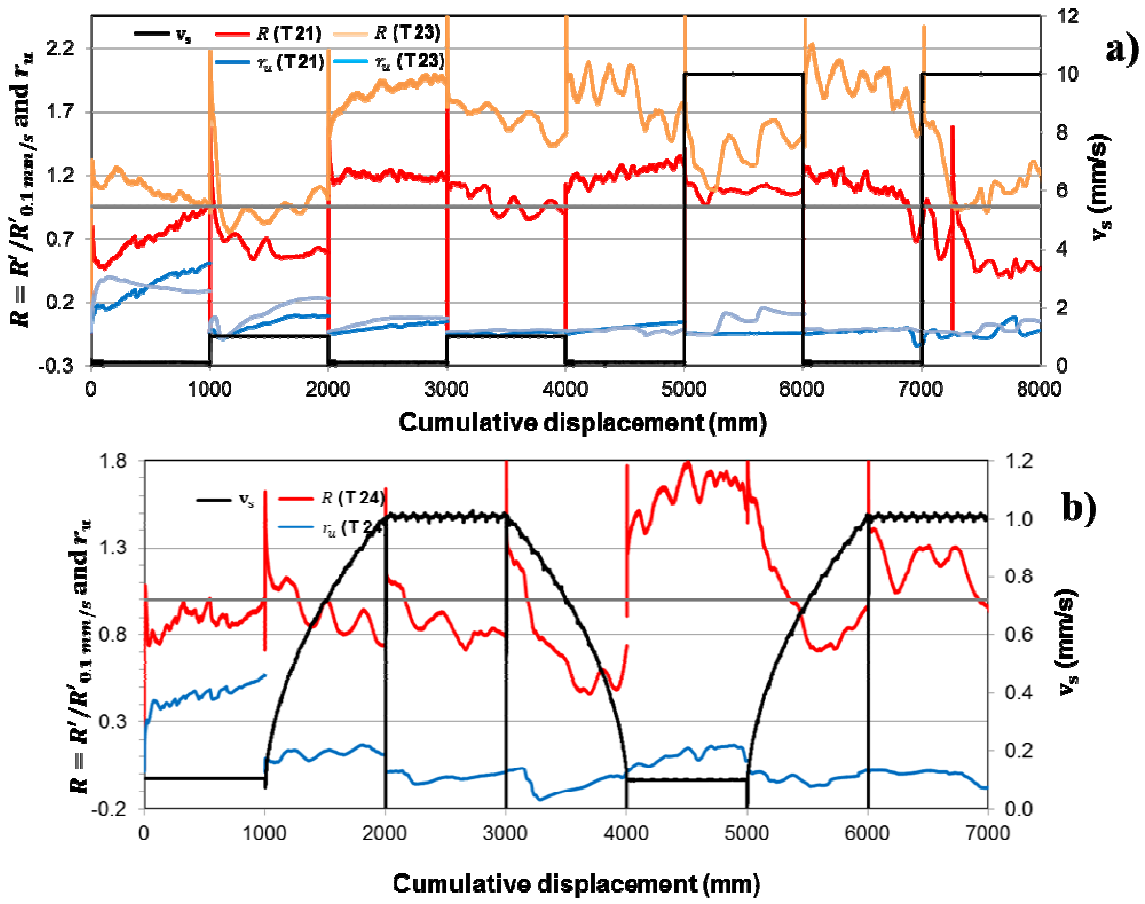

Figure 4.13 Cumulative displacement and friction coefficient and pore pressure ratio of multi-stage tests conducted on SB 30 specimens a) T 21 and T 23 (8 stages) and b) T 24 (7 stages).

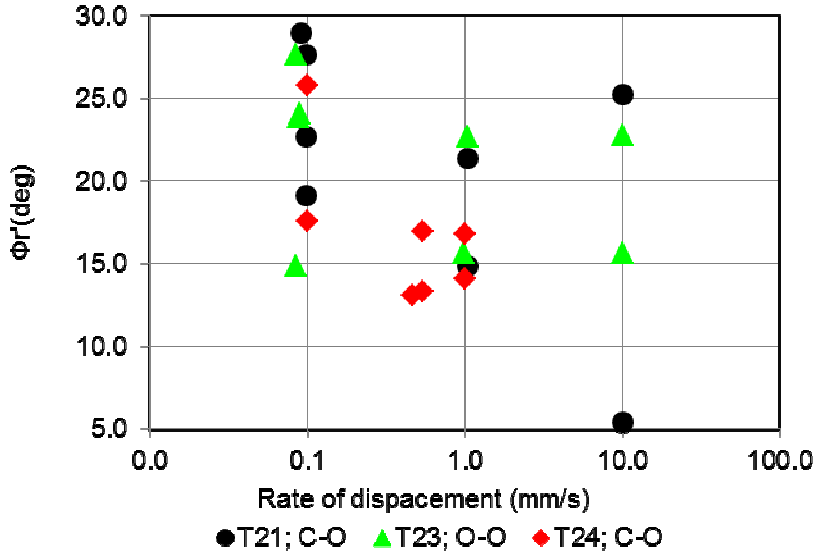

Figure 4.14 Rate of displacement and residual effective friction angle of multi-stage tests conducted on SB 30 specimens (T 21, T 23 and T24).

4.4.4 Shear zone examination

The structures of post-failure test specimens were examined only by visual examination after shearing. Slickensides were not found; only shear zones of 4-6 mm were observed when the specimen was cut (Figure 4.15). Similar shear zones were observed in sand and 15 and 30 % bentonite mixures (16- 26 % CF) by Lupini et al. (1981). The formation of well-polished slickensides was reported only for soils with a clay fraction higher than 40% (Tiwari and Marui 2005, Meehan 2006, Lupini et al. 1981) which was in contrast to what Saito (2008) observed in the SB 20 specimens. For some tests when shearing was much longer, this zone was even thicker (Figure 4.15c, as expected knowing that the thickness of the shear zone increases with an increase in the shear displacement (Tika et al. 1996, Tiwari and Marui 2004).

Figure 4.15 Photo of shear zones after shearing: **a**) SB 20 at 0.1 mm/s until 5 m, **b**) SB 30 at 1 mm/s until 10 m and **c**) SB 30 multi-stage test with total displacement of 30 m.

4.5 DISCUSSIONS

Published data of similar tests conducted on the same material exist. Silica sand is used as standard material in laboratory tests in Japan and the results obtained in our study are quite similar to those. However, there are few comparable sources for silica sand- bentonite mixtures, and the test conditions and apparatus used are quite different.

Investigating the influence of the rate of displacement on the shear behaviour associated with grain crushing, Okada et al. (2004) conducted speed-controlled tests at different rates of displacement (3, 5 and 100 mm/s) under a total normal stress of about 470 kPa. The authors observed the almost constant value of the residual friction angle (32-34°) after failure, for all rates of displacement used. This was in accordance with results

obtained on the same specimen in this thesis. Okada et al. (2004) observed no excess pore pressure generated, but observed some grain crushing.

The results of the silica sand–bentonite mixtures are to some degree comparable to previous research (Lupini et al. 1981, Tiwari et al. 2005, Saito 2008). First, these authors' tests were conducted on slow rates of shearing in drained conditions. In spite of some difficulties in comparing those results, a comparison is given for the slow stages (at 0.1 mm/s) of multi-stage tests because of the similar displacement used (1 m and 1.5 m). Assuming no excess pore pressure is generated in the slow drained test, the normal stress of 352 kPa can be calculated. Lupini et al. (1981) obtained a residual value of 30.5° for the 15 % mixture; and 23.3° for the 30 % mixture, respectively. Tiwari and Marui (2005) showed a residual failure envelope at 250 kPa of normal stress, at which the residual friction angle for 20 and 30 % mixture could be calculated as 20.8° and 9.5°, respectively. Tiwari and Marui (2005) used a linear regression friction angle value instead of the secant friction angle used in Lupini et al. (1981). This is true in Saito (2008) and our work as well.

Our multi-stage tests on SB 20 specimens resulted in a residual friction angle of 28-32° for the first slow stage and slightly higher values for the other slow stages, due to consolidation. For the SB 30 specimens, the residual friction angle of the first slow stage, varied from 15° to 22°. As for the other slow stages (III, V, VII), the angle was approximately 25°. Single-stage test at 0.1 mm/s, showed a lower value of 18° due to longer displacement.

We used a similar multi-stage testing procedure to the one used by Saito (2008) and the results were quite similar. Saito also determined the highest drop in shear resistance in the SB 20 specimen between 0.1 and 1 mm/s. However, values obtained in his tests show larger difference between the fast and slow failure envelope. He obtained $\Phi'r \approx 33°$ for slow stages and $\Phi'r \approx 14°$ for fast stage (19° difference). The results for the same specimen used in this thesis gave the same value for slow stages, but a much higher value for fast stages $\Phi'r \approx 26°$ (7° difference). However, in the multi-stage test with a gradual change in the rate of displacement, this difference was more distinctive, but still lower than in the Saito test (11° difference compared to 19° in results obtained by Saito). A possible explanation is that the pore pressure measurement in his test is probably not reliable. Two facts indicate this: first, the B_D value he obtained was 0.92, which implies that the specimen cannot be considered fully saturated; second, from stage 4 he had negative pore pressure, which

indicates a possible cavitation and making questionable pore pressure measurement from that point.

Obvious discrepancy in results exist, but it is difficult to compare results obtained by using different methods, drainage conditions, rates of displacements as well as shearing displacement. All these factors will affect the final result and are discussed in more detail in the following sections on cohesion, steady state condition and reliability of pore pressure measurement.

It is also worth noting that CF determined by sedimentation in this study seems to be overestimated, due to the silty sand used in mixtures. Overestimation in CF is very probable in soils containing silt due to the presence of clay-sized particles of silt (Mesri and Cepeda-Diaz 1986). The opposite occurred in the case of specimens tested by Lupini et al. (1981) and Tiwari and Marui (2005); the CF was lower than the percentage of mixtures (13% CF for SB15, 26 % CF for SB 30 in Lupini et al. (1981), and 8.5 % CF for SB10, 17 % for SB 20, and 26% for SB 30 in Tiwari and Marui (2005)).

In the following sections, other issues important for the interpretation and meaning of the results are discussed in detail.

Cohesion

We used a secant effective friction angle by assuming the cohesion is zero and thus, a residual strength envelope passes through the origin. Although this is a widely accepted assumption, there have been arguments on its accuracy (Tiwari et al 2005a). In Tiwari et al.'s (2005a) tests on natural soils, residual strength envelopes resulted in low values of cohesion. When comparing these results of tests with sand-bentonite mixtures, Tiwari et al. (2005a) explained the difference with Lupini's results by using a different strength interpretation, i.e., secant or the linear regression $\Phi'r$.

The residual-steady state problem (the problem of appropriate shear displacement)

Ideally, the residual shear strength is obtained when there is no change in shear stress or specimen volume/ pore pressure (in the case of drained/undrained tests, respectively) with increasing shear displacement. However, the problem of ascertaining the true residual has

long been known and is usually solved by the selection of the appropriate shear rate (slow enough to allow dissipation of excess pore pressure) or by achieving adequate displacement (long enough to ensure excess pore pressure dissipation in the drained test or by obtaining constant pressure and effective stress in the undrained test). Achieving adequate total displacement can be estimated well by plotting the stress-displacement behaviour on a semi-logarithmic base (Bishop et al. 1971, La Gatta 1970, Stark and Eid 1994).

In previous rate effect studies, this condition was not always achieved, especially during fast shearing (only 200-400 mm for rates 1.67- 6.67 mm/s, Skempton 1985, Lupini et al. 1981). However, in order to explain the role of generated pore pressure during fast shearing, the authors conducted a prolonged shearing for longer displacement (4 m and 15 m for shear rates of 2.67 and 5 mm/s). These tests showed low shear resistance that remained low until the end of displacement (Tika et al. 1996, Lemos 2003). In the multi-stage tests conducted by Saito (2008), the specimen was first slowly sheared at 0.01 mm/s until 100 mm of displacement. Since during the first stage, shear surface or zone should be formed and residual state obtained, it seems that this displacement was not appropriate. Also, according to previous research, a minimum displacement of 500 mm is required before residual strength is reached (Skempton 1985, Lupini et al. 1981, Tiwari and Marui 2004).

Figure 4.16 shows shear displacement in a semi-logarithmic scale for all single-stage tests conducted on SB 20 and SB 30 specimens. It is obvious that residual state in the SB 20 specimen was obtained only when the lowest shear rate was used (0.01 mm/s) at app. 1 m of displacement. All other shear rates show that the residual state was reached with a much longer displacement or not at all.

Our tests did not differ in this sense from the ones mentioned before. It is clear that in multi-stage tests residual strength (as it is "strictly defined"- minimum resistance at constant effective stresses, or pore pressure) was not obtained. Although aware of that fact, the use of longer displacement in fast stages was estimated as affecting shear strength (by increasing the shear zone) more than the case of the "non" residual condition. The emphasis was the rate effect; therefore, the effect of other factors that could influence the result had to be eliminated.

Reliability of pore water pressure monitoring

ICL-1 enables the monitoring of pore pressure by pore pressure transducers, connected to the valves placed in the gutter located 2 mm above the shear zone. In the low permeable materials such as in the clay mixtures used in this thesis, there is a high possibility that the pore-pressure transducers are not reliable because they show the value of the pore pressure along the shear surface (or within the shear zone). Also, there is the possibly of a time lag in pore pressure monitoring. Considering both factors, the results of tests conducted on SB 20 specimens appear reliable, and on the SB 30 may be considered not reliable. The right side of Figure 4.16 shows the results of the single-stage tests on the SB 30 specimens. As can be seen, the pore pressure varies more than in the SB 20 specimens. Also, multi-stage tests on the SB 30 specimens resulted in negative pore pressure during fast shearing stages, which did not occur in the case of the SB 20 specimen.

It should also be mentioned that permeability of the specimen during shearing changes (usually decreases) due to the structural changes in the shear zone (grain crushing of sand and/or particle orientation of clay). This will consequently result in a slower dissipation rate for generated excess pore pressure from the shear zone (Okada et al. 2004).

Density

The shear behaviour will depend on the change of density during shearing in the case of drained shearing. In undrained shearing, volume change hardly takes place and the variation of density in the shear zone is limited and might be neglected. However, the problem of influence of density change on shear behaviour should also be considered in undrained multi-stage tests with allowed dissipation, due to the volume change that takes place during consolidation. Figure 4.17 show that the change in density in Test T 16 did not influence the rate-dependent behaviour of that specimen. In test T 16, the change between slow (0.1 mm/s) and fast stages (1 mm/s) was gradual and the difference in residual friction angle was the most distinctive (between I and II stages around 13° and between III and IV, 10° respectively)

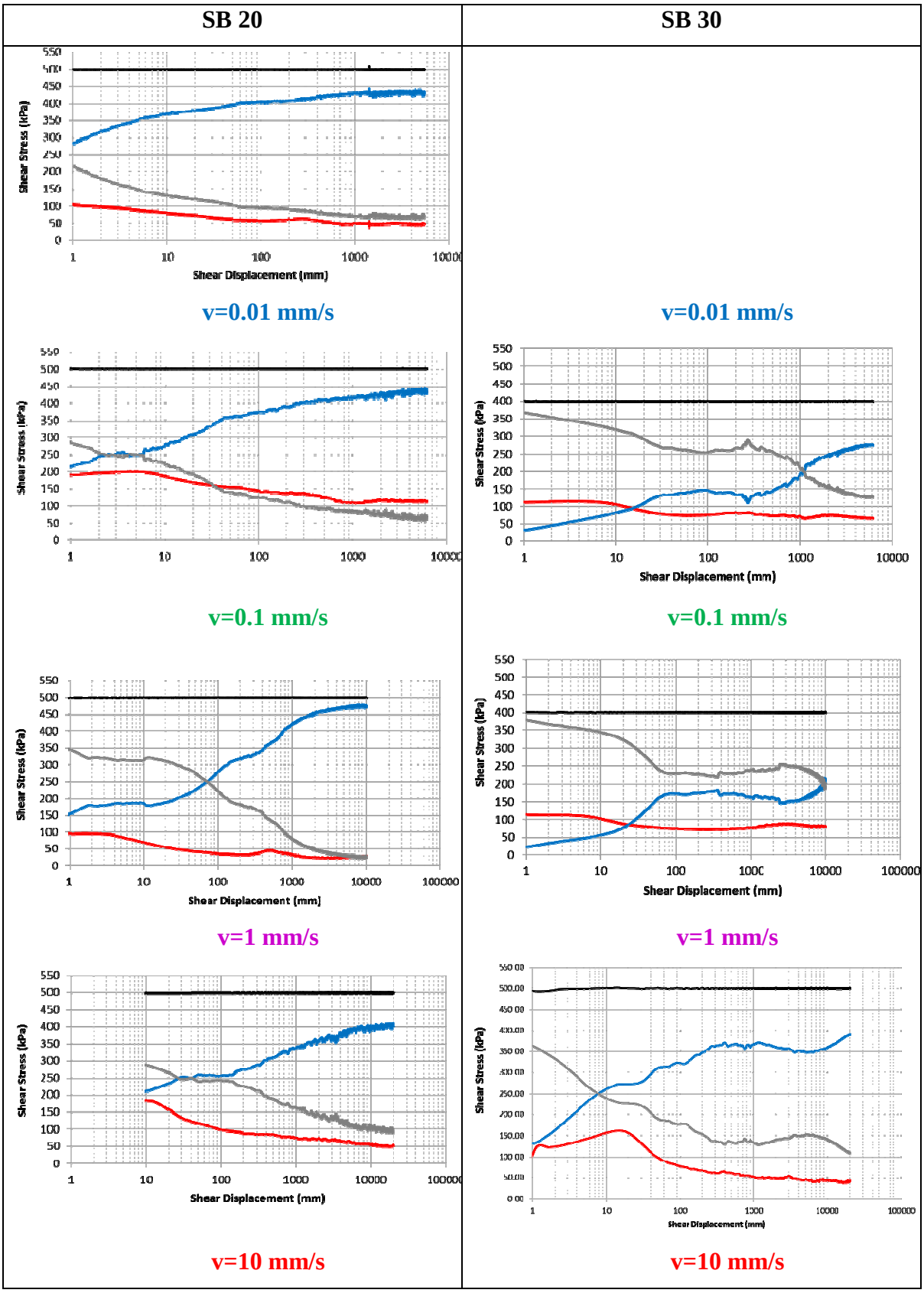

Figure 4.16 Shear displacement in log scale for single-stage tests on SB 20 (left side) and SB 30 (right side).

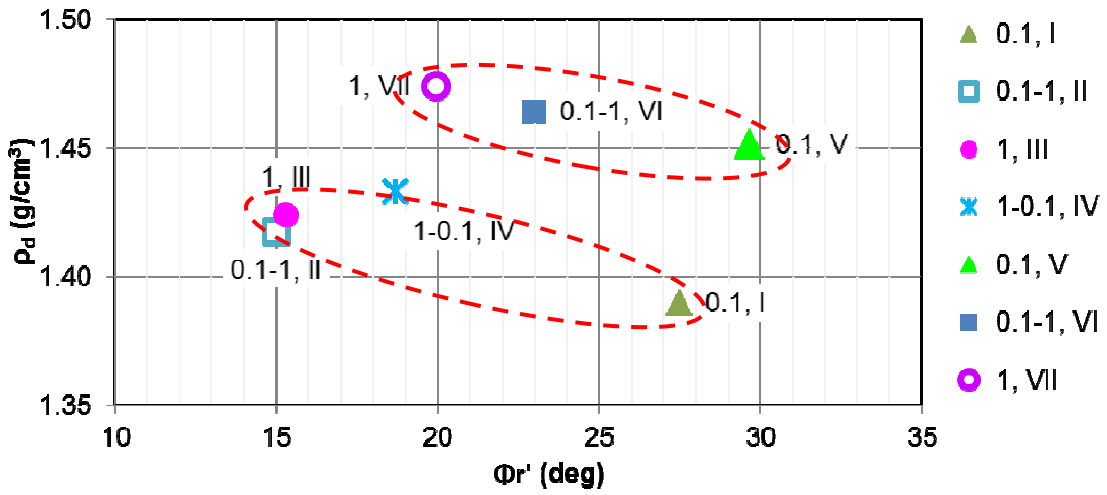

Figure 4.17 Residual friction angle and density, T 16.

Change in the failure line

As was shown in the results of multi-stage tests, residual strength in the SS 8 specimen was independent of the shear rate used, but SB 20 and SB 30 specimens showed a negative rate effect, by decreasing residual strength with the increase of the rate of displacement.

Figure 4.18 shows stress paths of these two types of behaviour. When effective stress paths (ESP) of all stages in the multi-stage test on SS 8 specimen are drawn, they all trace one failure line with the average residual effective friction angle of 32.6° (Figure 4.18). Black circles represent the end of each stage.

However, in the SB 20 specimen, there are two very distinctive failure lines; the slow shearing stages with $\Phi'r$=28.6°, and the fast stages with $\Phi'r$=17.6° (Figure 4.18b). These are the average values of slow stages (I and III) and fast stages (II and IV), respectively. The same was obtained in other SB 20 and SB 30 multi-stage test results with different variations between the failure lines of slow and fast stages.

Change of strength with gradual change of the rate of displacement

The aim of this study was to investigate in more detail the reported drop in the shear resistance and residual effective friction angle between 0.1 and 1 mm/s (Skempton 1985, Tika et al. 1996 and Saito 2008). In previous reports, the authors all noticed and mentioned a critical rate beyond which, structural changes take place. However, the main goal of

those studies was an explanation of the mechanism that causes the drop in resistance, and consequently the effective friction angle, and not the change itself.

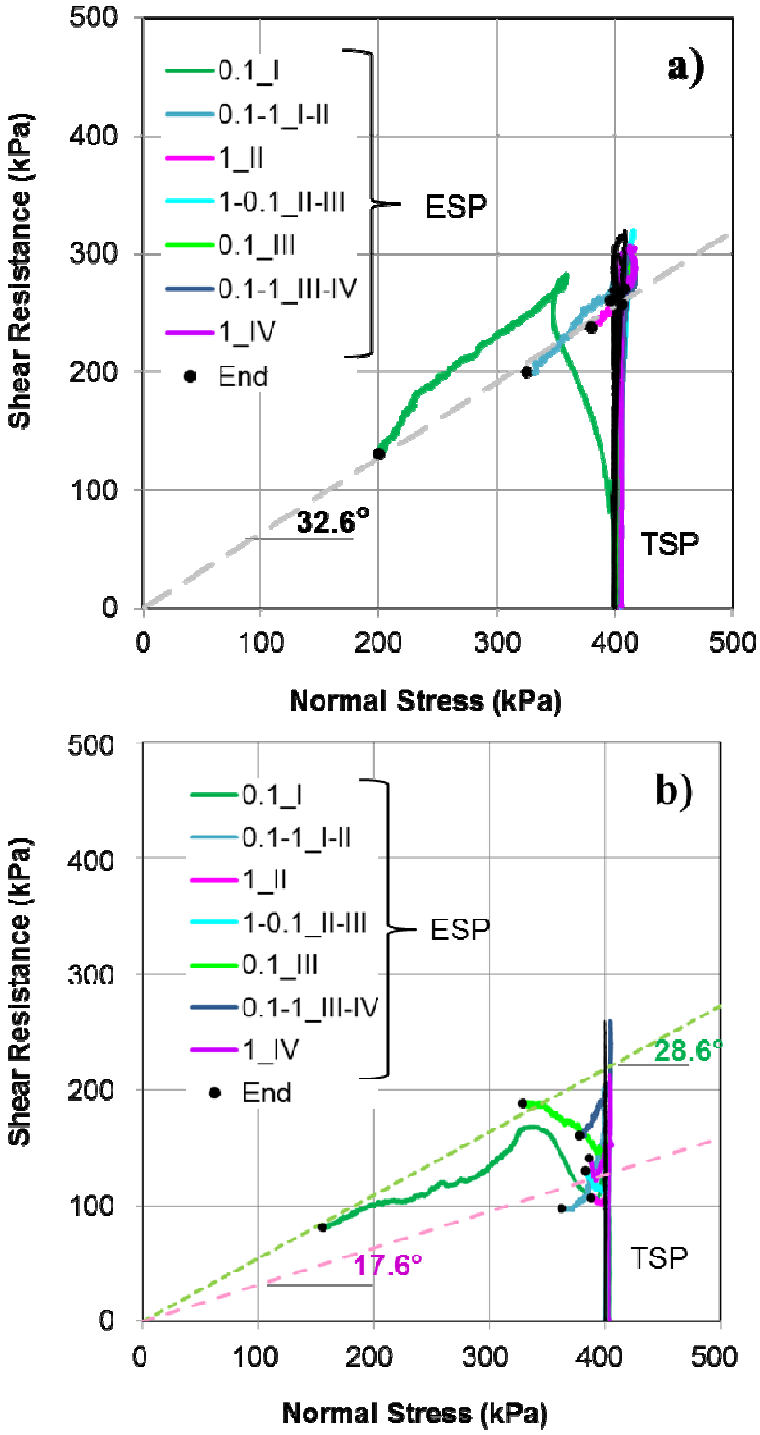

Figure 4.18 Stress path of multi-stage tests: a) SS 8 specimen (T 8) and b) SB 20 specimen).

To investigate this claim, multi-stage tests were conducted with the gradual change in the rate of displacement to observe a continuous change of soil behaviour with the increase/ decrease of the rate of displacement. Unfortunately, although some tests, using the wider range of rates of displacement, were conducted (0.1-10 mm/s), due to the large displacement (more than 30 m), the tests resulted in leakage and were not taken into account in this interpretation.

Figure 4.19 shows the continuous change of the effective friction angle between 0.1 and 1 mm/s for all multistage tests with a gradual change of the rate of displacement (T 8, T 16 and T 24). The decreasing trend in the effective friction angle in the case of the gradual increase of the rate of displacement is clearly visible. The trend is distinctive in the case of the SB 20 and SB 30 specimens, and negligible in the case of silica sand Both the SB 20 and SB 30 specimens showed a similar pattern, for both "increasing" stages (I-II and III-IV) (Figure 4.19a). The trend is expressed by the equations shown in Figure 4.19. However, in the "decreasing" stage (II-III), only specimen SB 20 showed an increasing trend (Figure 4.19b), but the trend was much milder than in the case of "increasing" stages (I-II and III-IV) for the same specimen. A gradual increase/ decrease of the rate of displacement is indicated by the arrow on the x-axis of Figure 4.19a and b.

Figure 4.19 shows that the residual friction angle changes linearly with the logarithm of the rate of displacement. A similar behaviour was observed by others (Ruina 1983, Wedage et al. 1998) and is well known in geophysics. It should be mentioned that this findings mostly refers to solid state mechanics and fault mechanics.

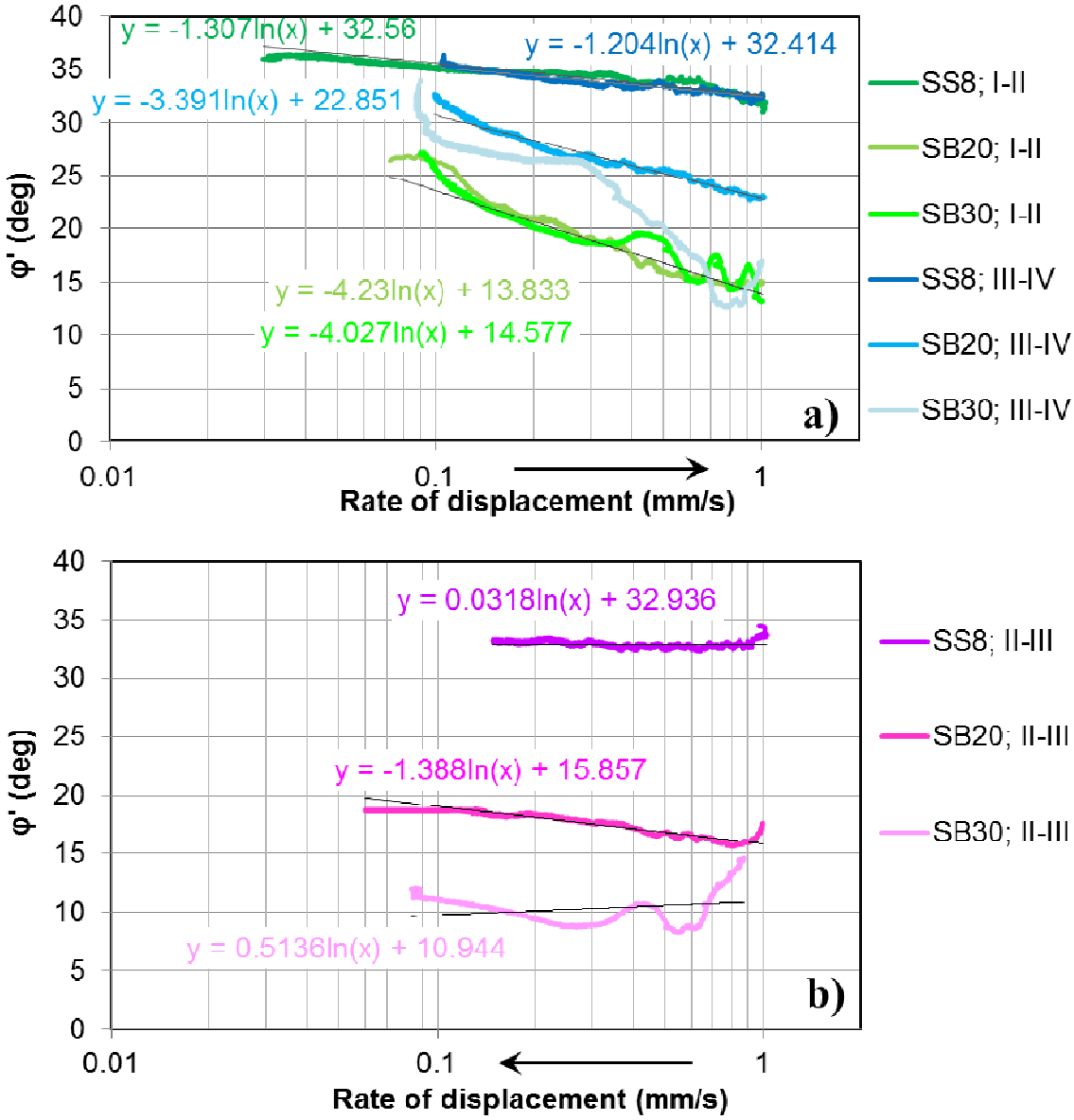

Figure 4.19 Residual friction angle and rate of displacement (T 8, T 16 and T 24)

4.6 SUMMARY AND CONCLUSION

The residual strength of soil is an important parameter--- one that controls behaviour when the shear plane already exists, as in re-activated landslides. On an existing shear surface, the shear strength is considerably changed and consequently affects the future behaviour of that soil (Bromhead 1992). Previous investigations reported a negative rate effect in soils showing transitional shear behaviour. However, in those studies, the pore pressure measurement was or: was neither possible nor reliable.

A series of ring shear tests were conducted on sand-bentonite mixtures to investigate the drop in strength between 0.1 and 1 mm/s. Two series of tests were conducted for each specimen (SS 8, SB 20 and SB 30). Single-step shearing in undrained conditions and multi-stage shearing in varying conditions (drained/ undrained/ partially drained, with or without consolidation). In multi-stage tests, shear zones were formed by slow shearing and then were tested at alternately fast and slow rates of displacement.

To avoid the influence of shear displacement on the shear strength, it was estimated that 1 m of displacement for each stage should be applied. Results on the SB 20 specimens showed a clear drop in shear resistance and in the effective secant friction angle. This was especially clear from the multi-stage test with a gradual change of the rate of displacement. The highest drop in strength occurred between 0.1 and 1 mm/s, which confirmed findings of earlier studies (Skempton 1985, Tika et al. 1996, Saito 2008). The issue of adequate shearing displacement in order to obtain a residual state of soil was discussed previously. Even if multi-stage displacement of 1 m for each stage was not adequate, and the drop in strength could be questionable, the findings of the multi-stage tests were confirmed with the results of the single-step shear tests. Undrained single-stage tests resulted in a lower shearing resistance even at large shear displacements. The results of multi-stage tests on the SB 30 specimens are considered unreliable due to negative pore pressure that occurred during fast shearing. However, the results do indicate a decrease in strength with an increasing rate of displacement.

Comparison of the multi-stage tests with the gradual change of the rate of displacement (T 8, T 16, and T 24), showed the following: in the case of an increased rate of displacement, there is a significant decrease of shear resistance and effective friction

angle in the SB 20 and SB 30 specimens. The results showed that the residual friction angle decreases linearly with the increase of the logarithm for the rate of displacement.

There are two existing explanations for the change in the strength of cohesive soils: 1) the change in strength is caused by the influence of excess pore water pressure or by a change in the shear mode in the shear zone (Lemos 1986, Tika et al. 1996, Saito 2008). Possible mechanisms of the change were not explained in this thesis because such explanation was outside of the scope of the thesis. However, it would be necessary to clearly understand the mechanism of both the positive and negative rate effect of cohesive soils. Saito (2008) tried to explain the mechanism of negative rate effect by clay enrichment during fast stages, by the mechanism of particle segregation. To confirm his work, it is necessary to conduct additional measurements, like the measurement of grain size distribution of the shear zone after shearing at different rates of displacement and at certain displacements.

Practical implications of these findings are important because the soils that show a negative rate effect will result in accelerating movement which usually results in negative consequences. Traditional limit equilibrium analysis does not take into account rate effects in weak soils, but considers the friction angle as static and constant.

REFERENCES

Bromhead, E.N., 1992, "The stability of slopes," Blackie Academic.

Bishop, A.W., Green, G.E., Garga, V.K., Andersen, A. and Brown, J.D., 1971, "A New Ring Shear Apparatus and its Application to the Measurement of Residual Strength," *Géotechnique*, Vol. 21, No. 1, pp. 273-328.

Fell, R., Hungr, O., Leroueil, S. and Riemer, W., 2000, "Keynote Lecture - Geotechnical engineering of the stability of natural slopes, and cuts and fills in soil," *GeoEng 2000*, Vol.1, Invited Papers, Technomic Publishing, Lancaster, pp. 21-120.

Fukuoka, H., Sassa, K. and Wang, G., 2007, "Influence of shear speed and normal stress on the shear behaviour and shear zone structure of granular materials in naturally drained ring shear tests," Landslides, Vol. 4, pp. 63-74.

Gratchev, I.B., Sassa, K., Osipov, V.I., Fukuoka, H. and Wang, G., 2007, "Undrained cyclic behaviour of bentonite–sand mixtures and factors affecting it," Geotech Geol Eng, Vol. 25, pp. 349-367.

Hungr, O. and Morgenstern, N.R., 1984, "High Velocity Ring Shear Tests on Sand," *Géotechnique*, Vol. 34, No. 3, pp. 415-421.

La Gatta, D.P., 1970, "Residual Strength of Clays and Clay-Shales by Rotation Shear Tests," Ph.D. thesis reprinted as Harvard Soil Mechanics Series No. 86, Harvard University, Cambridge, MA, 204 p.

Lambe, T.W. and R.V. Whitman, 1979, "Soil Mechanics", SI Version, John Wiley, New York, 553 p.

Lemos, L.J.L., 1986, "The effect of rate on residual strength of soil," Ph.D. thesis, University of London.

Lemos, J.L.J., 2003, "Shear behaviour of pre-existing shear zone under fast loading-insights on the landslide motion," *Proc. International workshop on occurrence and mechanisms of flow-like landslide motion*, pp. 229-236.

Leroueil, S., 2001. "Natural slopes and cuts: Movement and failure mechanism," *Geotechnique*, Vol. 52, No. 3, pp. 197-243.

Lupini, J.F., Skinner, A.E. and Vaughan, P.R., 1981, "The drained residual strength of cohesive soils," *Géotechnique*, Vol. 31, No. 2, pp.181-213.

Meehan, C.L., 2006, "An Experimental Study of the Dynamic Behaviour of Slickensided

Slip Surfaces," Ph.D. thesis, Virginia Tech, 281 p.

Meehan, C.L., Brandon, T.L. and Duncan, J.M., 2007, "Measuring Drained Residual Strengths in the Bromhead Ring Shear," *Geotech. Test. J.*, Vol. 30, No.6, pp. 466-473.

Meehan, C.L., Brandon, T.L. and Duncan, J.M., 2008, "Measuring "Fast" Shear Strengths along Slickensided Surfaces in the Bromhead Ring Shear," *Geotech. Test. J.*, Vol. 31, No. 3, pp. 239-242.

Mesri, G. and Cepeda- Diaz, A.F., 1986, "Residual shear strength of clays and shales," *Géotechnique*, Vol. 36, No. 2, pp. 269- 274.

Okada, Y., Sassa, K. and Fukuoka, H., 2004, "Excess pore pressure and grain crushing of sands by means of undrained and naturally drained ring-shear tests," *Engineering Geology*, Vol. 75, pp. 325-343.

Ruina, A.L., 1983, "Slip instability and state variable friction laws," *J. Geophys. Res*, Vol. 88, pp. 359-370.

Saito, R., 2008, "The Mechanism of the Negative Rate Effect on the Residual Strength of Clayey soil," PhD thesis, Kyoto University, Japan, 51 p.

Savage, S.B. and Sayed M., 1984, "Stresses developed in dry cohesionless granular materials sheared in an annular shear cell," *Jorunal of Fluid Mech* , Vol. 142, pp. 391-430.

Skempton, A.W., 1964, "The Long-term stability of clay slopes," *Géotechnique*, Vol. 14. No. 2, pp. 77-101.

Skempton, A.W., 1985, "Residual Strength of Clays in Landslides. Folded Strata and the Laboratory," *Géotechniqu*e, Vol. 35. No. 1, pp. 3-18.

Stark, T.D. and Eid, H.T., 1994. "Drained residual shear strength of cohesive soils," *J. Geotech. Geoenviron. Eng*., Vol. 120, No. 1, pp. 269-273.

Tika, T.E., 1989, "The effect of rate of shear on the residual strength of soil," PhD thesis, University of London (Imperial College of Science and Technology), 494 p.

Tika, T.E., Vaughan, P.R., and Lemos, L.J., 1996, "Fast Shearing of Pre-existing Shear Zones in Soil," *Geotechnique*, Vol. 46, No. 2, pp. 197-233.

Tiwari, B. and Marui, H., 2004,"Objective-oriented multistage ring shear test for shear strength of landslide soil," *J. Geotech. Geoenviron. Eng.*, Vol. 130, No. 2, pp. 217-222.

Tiwari, B. and Marui, H. 2005, "A new method for the correlation of residual shear strength of the soil with mineralogical composition," *J. Geotech. Geoenviron. Eng.*, Vol. 131, No. 9, pp. 1139-1150.

Tiwari, B., Brandon, T.L., Marui, H. and Tuladhar, G.R., 2005a, "Comparison of Residual Shear Strengths from Back Analysis and Ring Shear Tests on Undisturbed and Remolded Specimens," *J. Geotech. Geoenviron. Eng*., Vol. 131, No. 9, pp. 1071-1079.

Tiwari, B., Tuladhar, G.R. and Marui, H. 2005b, "Variation in Residual Shear Strength of the Soil with the Salinity of Pore Fluid," *J. Geotech. Geoenviron*. Eng., Vol. 131, No. 12, pp. 1445-1456.

Toyota, H., Nakamura, K., Sugimoto, M. and Sakai, N., 2009, "Ring Shear Tests to evaluate strength parameters in various remolded soils," *Geotechnique*, Vol. 59, No. 8, pp. 649-659.

Voight, B., 1973, "Correlation between Atterberg plasticity limits and residual shear strength of natural soils," *Geotechnique*, Vol. 23, No. 2, pp. 265-267.

Wafid, M.A., Sassa, K., Fukuoka, H. and Wang, G., 2004, "Evolution of shear-zone structure in undrained ring-shear tests," *Landslides*, Vol. 1, No. 2, pp. 101-112.

Wedage, A.M.P., Morgenstern, N.R. and Chan, D.H., 1998, "A strain rate dependent constitutive model for clays at residual strength," *Can. Geotech. J*., Vol. 35, pp. 364-373.

Wesley, L.D., 2003, "Residual strength of clays and correlations using Atterberg limits," Geotechnique, Vol. 53, No.7, pp. 669-672.

Wood, D.M., 1990, "Soil Behaviour and Critical State Soil Mechanics,"Cambridge University Press.

WP/WLI, 1990, International Geotechnical societies' UNESCO Working Party on World Landslide Inventory, "A suggested method for reporting a landslide," International Association Engineering Geology Bulletin, Vol. 41, pp. 5-12.

Chapter 5 Conclusions and Future Research

A transportable and compact high-stress undrained-loading ring shear was designed by Professor Sassa in 2010 (Sassa et al. 2012) as a part of a Japanese-Croatian Research Project. It was developed and modified through 2011. Although smaller in dimensions compared with previous versions, it has high capacity; it can load normal stress and keep to the undrained condition of pore water pressure up to 1 MPa. In **Chapter 2** the concept, design, and construction of ICL-1 was presented. The results of the tests on silica sand, as well as the experimental procedure, are described in detail. Typical test results are presented to show the efficiency of this ring shear apparatus as well as its application for earthquake induced landslides through undrained cyclic loading tests and rain-induced landslide through drained pore-pressure control tests.

The ring shear apparatus has two purposes: it can be used for basic soil tests (for determination of soil parameters) and for the landslide simulation test. In this thesis, ICL-1 was applied for both purposes. In **Chapter 3** we applied ICL-1 to the case of a real landslide, the Grohovo landslide. The assessment of two triggers was performed; namely, rainfall and earthquakes. The rainfall analysis was performed for long and short-term rainfall data as well as for the probability of their occurrence. The assessment of seismic triggering was done using the ICL-1. The surface samples from Grohovo were used in seismic loading simulation by conducting a cyclic loading test. The conducted test indicated soil hardening behaviour that has to be investigated further. Also, tests on borehole samples from the assumed sliding surface, need to be conducted, both as basic tests; i.e., as a speed-control test to obtain soil parameters and as a simulation test. According to the results from Chapter 3, a pore pressure control test that will simulate groundwater rise would be desirable. Although the rainfall data analysis performed in Chapter 3 showed that the influence of a cumulative, long rainy period has a much higher impact on landslide reactivation, the role of short term events shouldn't be neglected. If hydrological triggering is defined as a decrease in shear strength due to an increase in pore-

water pressure on the potential failure surface, then pore-water pressure increase may be related to rainfall infiltration and percolation (saturation from above), or may be the result of the groundwater table rising (saturation from below) (Terlien 1998, Iverson 2000, 2005). Therefore, a more detail hydrological analysis should be performed to define threshold values for reactivation of the Grohovo landslide. Also, internal and boundary pore-water pressures are among material properties such as strength, viscosity, and relative density, and are main factors that may affect landslide velocity (Schultz et al. 2009).

Ring shear apparatus was also applied for the investigation of basic soil characteristics, specifically in **Chapter 4**, for the investigation of a negative rate effect on sand-bentonite mixtures. There is a significant drop in shear strength of SB 20 and SB 30 mixtures between 0.1 and 1 mm/s rate of displacement. The tests on SB 20 specimens showed to be reliable regarding the measurement of pore pressure. Both single-stage undrained tests as well as multi-stage shearing tests in varying conditions (undrained/ partially/ drained; with/ without consolidation) showed a decrease of strength with an increasing rate of displacement. This was most evident in multi-stage tests with undrained shearing by gradual change of the rate of displacement from 0.1 to 1 mm/s. From the results of the same tests, the same trend for SB 20 and SB 30 specimens was obtained, in which the residual friction angle increases linearly with the logarithm of the rate of displacement. Practical implications are obvious for both first-time slides and reactivated ones: if the critical displacement rate is exceeded in the soil that shows negative rate effect, the strength drops below the slow residual and accelerates. There is an argument about the significance of negative rate effect in the rates of displacement that are used at fast rates of displacements. However, landslides exhibit a great diversity of movement styles and rates, ranging from centimeters per year to meters per second (WL/WPI 1990). Velocity is also the most important parameter determining the destructive potential of landslides (Hungr 2007). As professor Skempton pointed out, the rates of displacement in reactivated landslides can vary by many orders of magnitudes (very fast for ones induced by earthquakes) and the knowledge of rate effects should be an important part of residual strength studies (Skempton 1985).

Although cyclic tests on the Grohovo landslide showed soil-hardening behaviour that should consequently result in the decelerating behaviour of a reactivated landslide, it is necessary to conduct additional tests to confirm soil-hardening behaviour Most of the

instabilities in the coastal part of Croatia occur in the flysch deposits. Due to variability in mineralogical composition of flysch deposits, they could be in the group that shows transitional shearing behaviour (CF 10-40 %). Laboratory work on typical sand or clay behaviour is extensive; however, for the transitional zone this is not the case.

Therefore, the investigation of rate effect should be applied to natural samples that show transitional shear behaviour. Also, one important parameter that was not addressed properly in our rate effect study is pore water chemistry. Usually, laboratory tests are conducted by using distilled water or de-aired water as in our case. However, if pore water chemistry is changed it will affect the measured residual strength of soil and consequently, slope stability (DiMaio 1996, Leroueil 2001, Tiwari et al. 2005). From a practical point of view, this means that the residual strength parameters should be evaluated with pore water chemistry close to the pore water chemistry existing *in situ.*

REFERENCES

Di Maio, C., 1996, “Exposure of bentonite to salt solution: Osmotic and mechanical effect,” *Geotechnique*, Vol. 46, No. 4, pp. 695-707.

Hungr, O., 2007, “Dynamics of Rapid Landslides”, In: *Progress in Landslide Science*, Sassa, K., Fukuoka, F., Wang, F. and Wang, G. (Eds.), Springer Verlag, pp. 47-57.

Iverson, R.M., 2005, “Regulation of landslide motion by dilatancy and pore pressure feedback,” *Journal of Geophysical Research*, Vol. 110, No. 02, doi 10.1029/2004JF000268.

Iverson, R.M., 2000, “Landslide triggering by rain infiltration,” *Water Resour. Res*., Vol. 36, pp. 1897-1910.

Kenney, T.C., 1977, “Residual strengths of mineral mixtures,” *Proc., 9th Int. Conf. Soil Mechanics and Foundation Engineering*, pp. 155-160.

Leroueil, S., 2001, “Natural slopes and cuts: Movement and failure mechanism,” *Geotechnique*, Vol. 52, No. 3, pp. 197-243.

Terlien, M.T., 1998, "The determination of statistical and deterministic hydrological landslide triggering thresholds," Environmental Geology, Vol. 35, No. 2, pp. 124-130.

Tiwari, B., Tuladhar, G. R. and Marui, H., 2005, “Variation in Residual Shear Strength of the Soil with the Salinity of Pore Fluid,” *J. Geotech. Geoenviron. Eng*., Vol. 131, No. 12, pp. 1445-1456.

Sassa, K., B. He , Miyagi, T., Strasser, M., Konagai, K, Ostric, M., Setiawan, H., Takara, K., Nagai, O., Yamashiki, Y. and Tutumi, S., 2012, “A hypothesis of the Senoumi submarine megaslide in Suruga Bay in Japan—based on the undrained dynamic-loading ring shear tests and computer simulation,” *Landslides*, Vol. 9, No. 4, pp. 439-455.

Skempton, A.W., 1985, "Residual Strength of Clays in Landslides, Folded Strata and the Laboratory," *Géotechnique*, Vol. 35. No. 1, pp. 3-18.

Schulz, W.H., McKenna, J.P., Kibler, J.D., Biavati, G., 2009, “Relations between hydrology and velocity of a continuously moving landslide – evidence of pore-pressure feedback regulating landslide motion*?”* *Landslides*, Vol. 6, No. 2, pp. 181-190.

WP/WLI, 1990, International Geotechnical societies’ UNESCO Working Party on World Landslide Inventory, “A suggested method for reporting a landslide,“ *International Association Engineering Geology Bulletin*, Vol. 41, pp. 5-12.

Appendix: Results of Multi-stage Tests

The Appendix contains figures of all multi-stage tests conducted (listed in Table 4.2). In Chapter 4 they were explained separately for SS 8, SB 20 and SB 30 specimens. However, because figures in the text compared results of more multi-stage tests, some of the data could not be presented. Here, results of all multi-stage tests are compiled for cumulative displacement, shear displacement of 1 m, stress paths of all stages and rate of displacement and effective friction angle.

A.1 Test T 5-SS 8-Undrained shearing with consolidation (I-VIII; C-O)

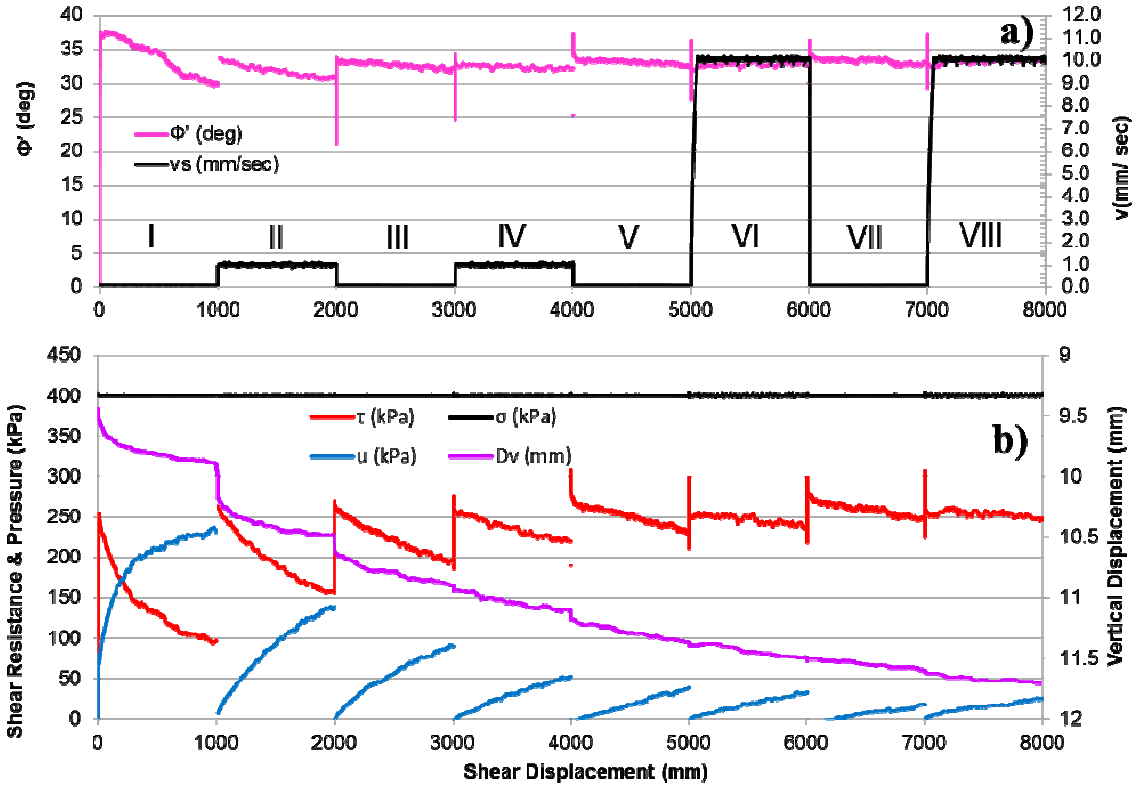

Fig. A.1.1 Cumulative shear displacement and a) Effective friction angle (Φ') and rate of displacement (v_s), b) Shear resistance (τ) , pore pressure (u) and vertical displacement (D_v).

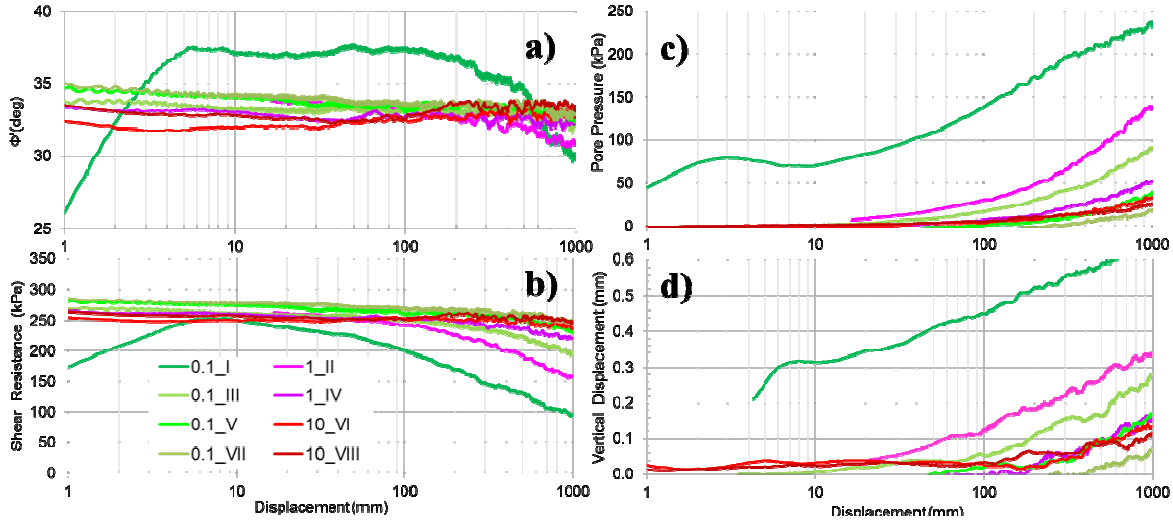

Fig. A.1.2 Shear displacement and a) Effective friction angle (Φ'), b) Shear resistance, c) Pore pressure and d) Vertical displacement.

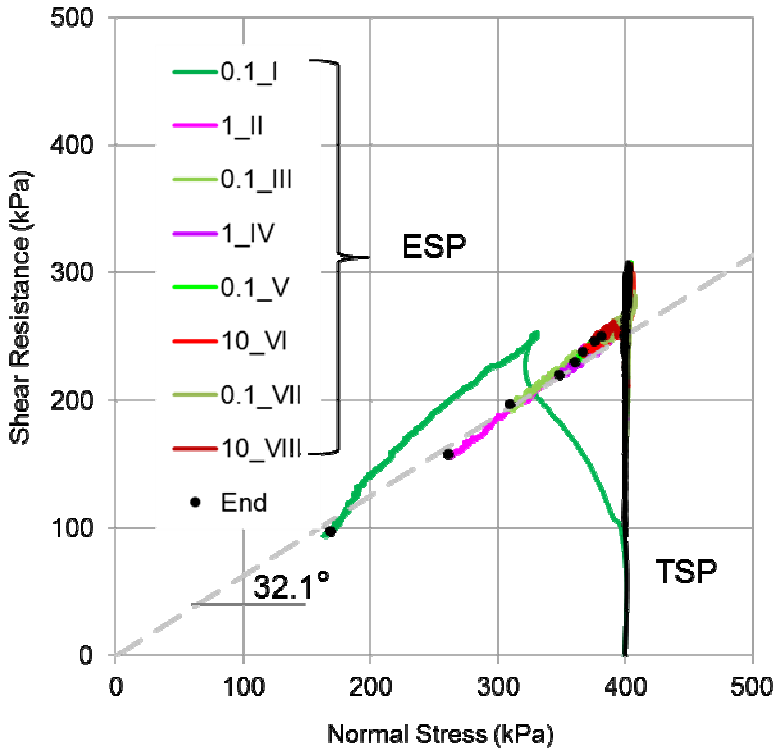

Fig. A.1.3 Stress path of all Stages (I-VIII), TSP- total stress path, ESP- effective stress path.

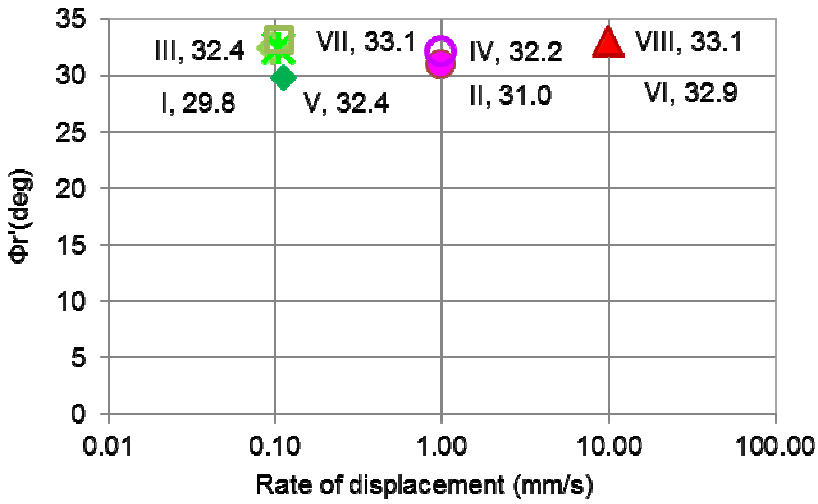

Fig. A.1.4 Rate of displacement and effective friction angle.

A.2 Test T 6-SS 8-Undrained shearing without consolidation (I-VIII; C-C)

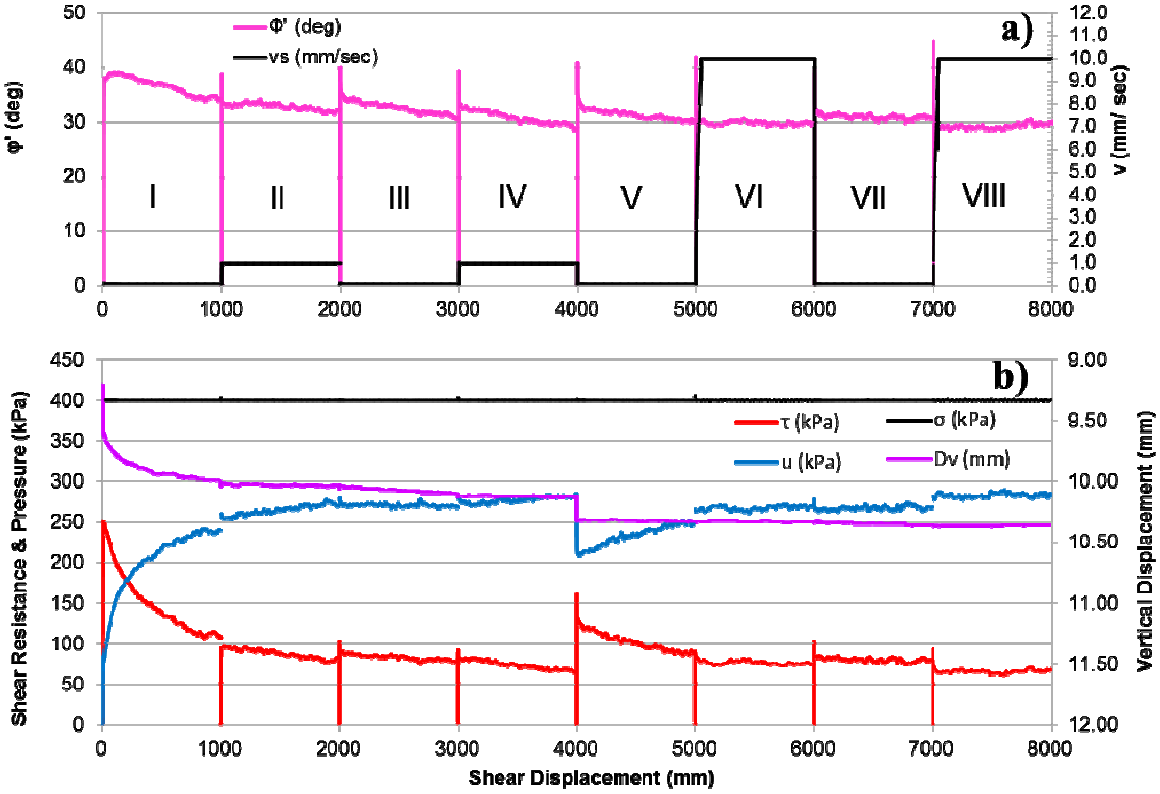

Fig. A.2.1 Cumulative shear displacement and a) Effective friction angle (Φ') and rate of displacement (v_s), b) Shear resistance (τ) , pore pressure (u) and vertical displacement (D_v).

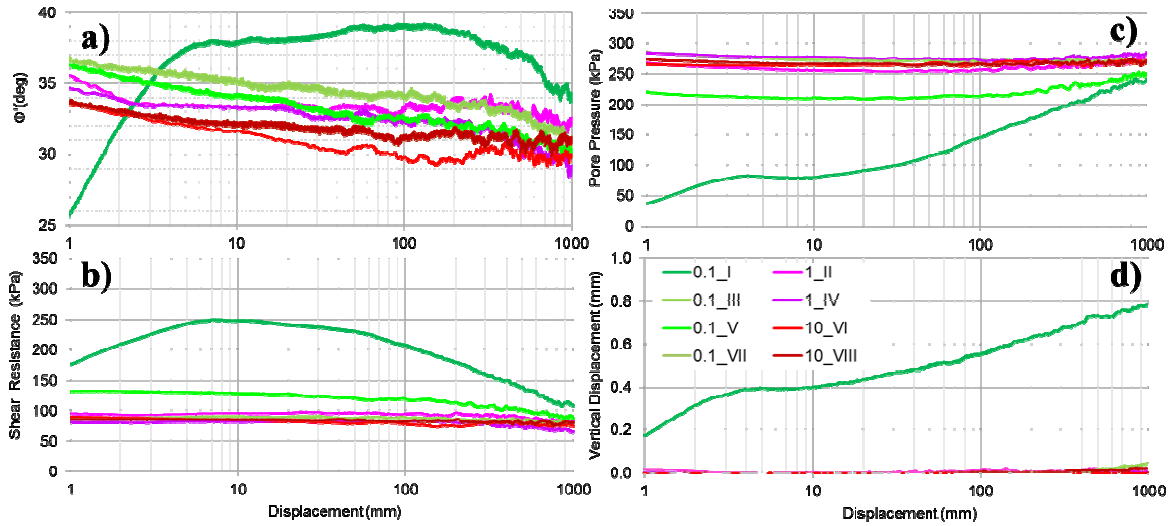

Fig. A.2.2 Shear displacement and a) Effective friction angle (Φ'), b) Shear resistance, c) Pore pressure and d) Vertical displacement.

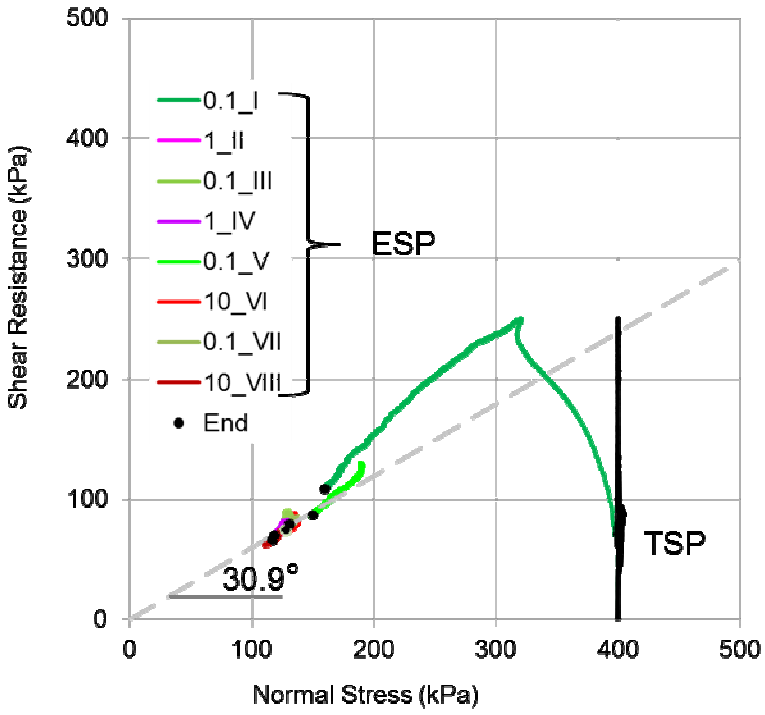

Fig. A.2.3 Stress path of all Stages (I-VIII), TSP- total stress path, ESP- effective stress path.

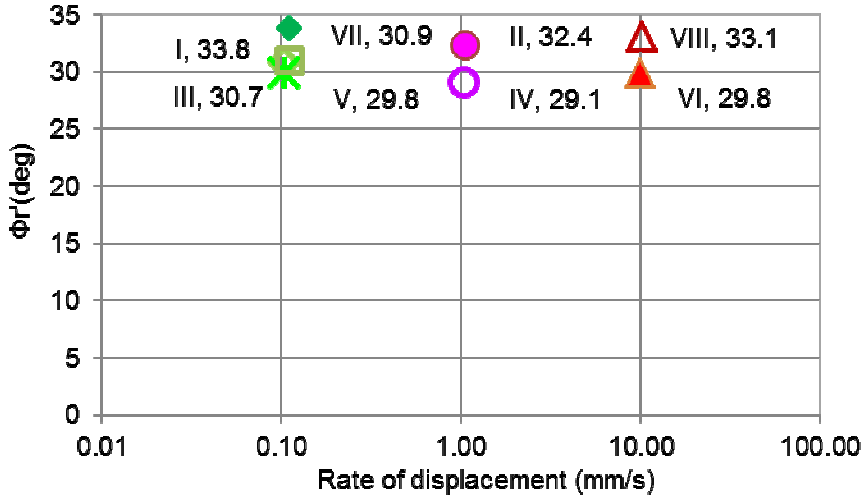

Fig. A.2.4 Rate of displacement and effective friction angle.

A.3 Test T 7-SS 8-Drained shearing with consolidation (I-VIII; O-O)

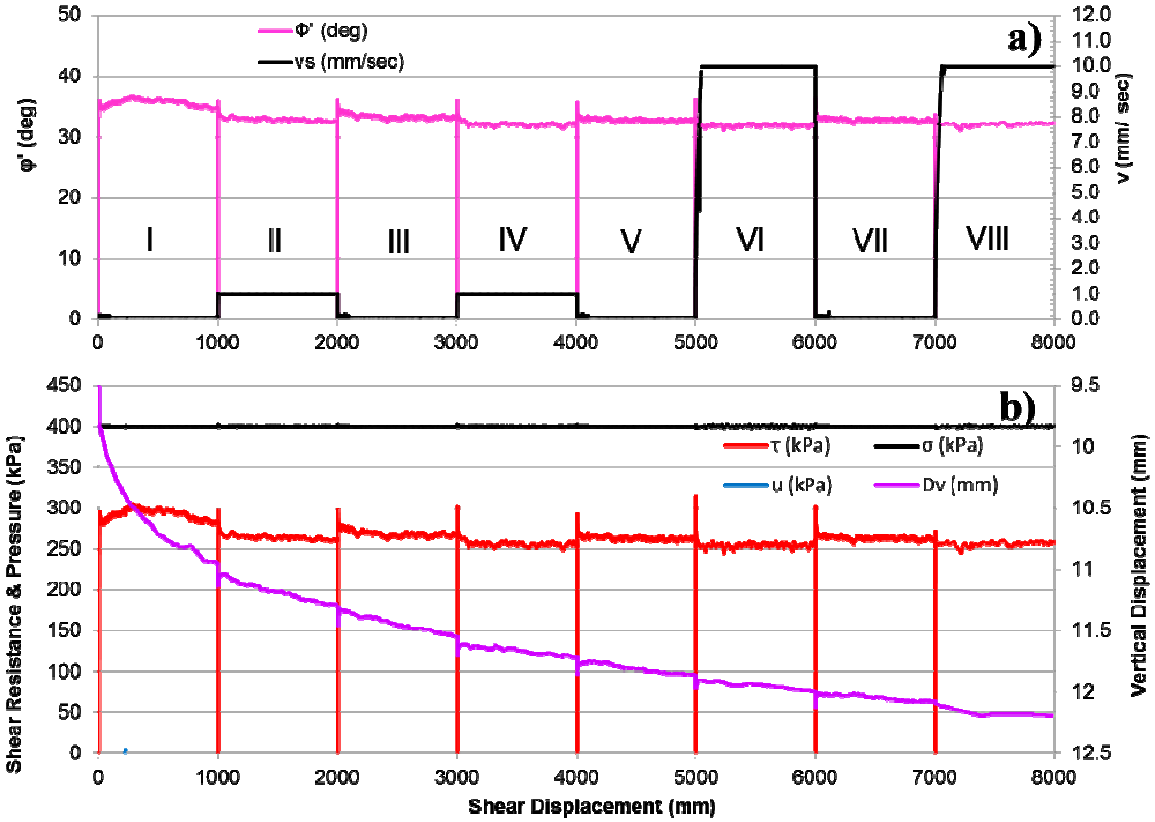

Fig. A.3.1 Cumulative shear displacement and a) Effective friction angle (Φ') and rate of displacement (v_s), b) Shear resistance (τ) , pore pressure (u) and vertical displacement (D_v).

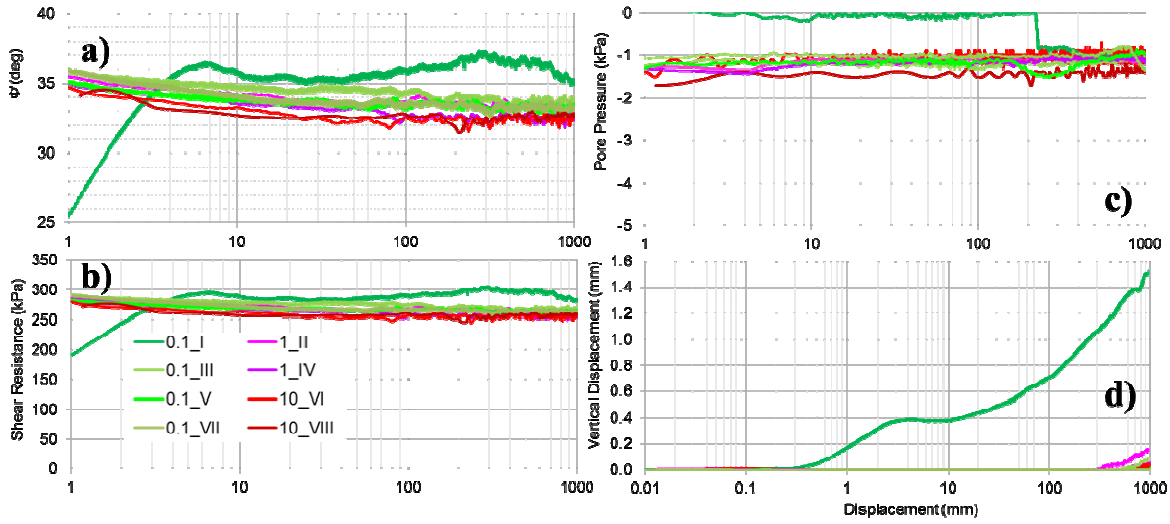

Fig. A.3.2 Shear displacement and a) Effective friction angle (Φ'), b) Shear resistance, c) Pore pressure and d) Vertical displacement.

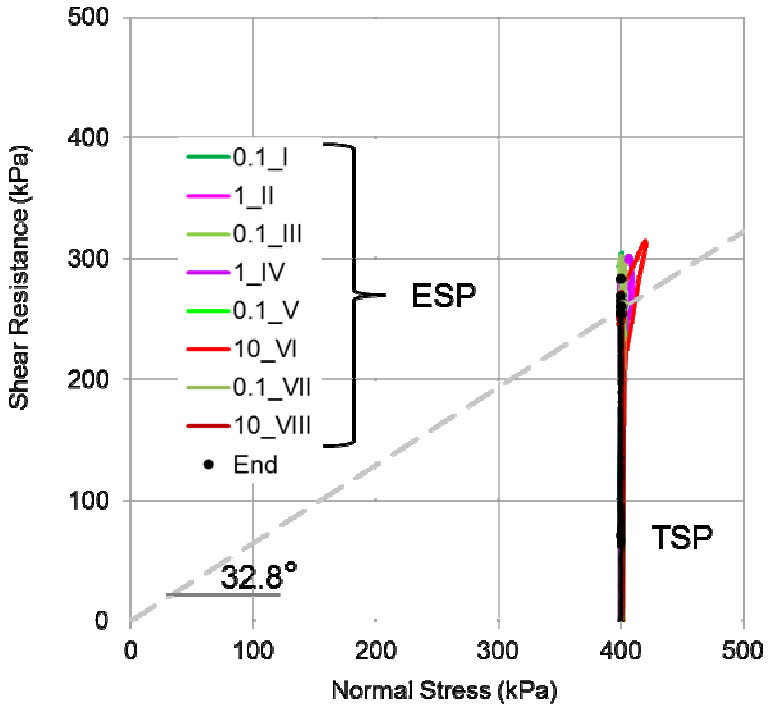

Fig. A.3.3 Stress path of all stages (I-VIII), TSP- total stress path, ESP- effective stress path.

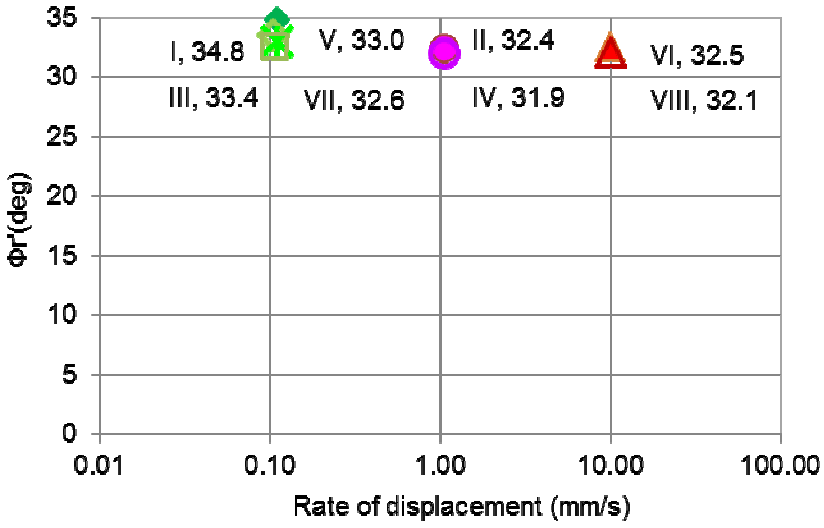

Fig. A.3.4 Rate of displacement and effective friction angle.

A.4 Test T 8-SS 8-Undrained shearing with consolidation (I-V; C-O)

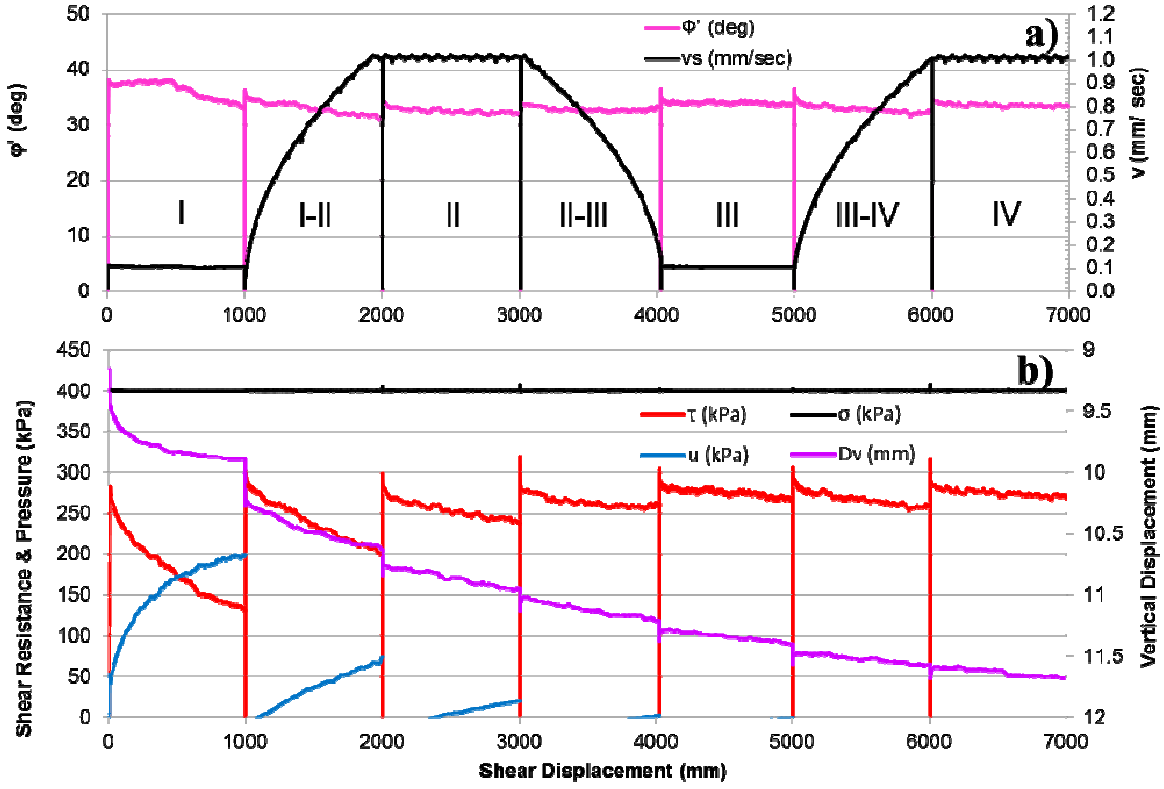

Fig. A.4.1 Cumulative shear displacement and a) Effective friction angle (Φ') and rate of displacement (v_s), b) Shear resistance (τ) , pore pressure (u) and vertical displacement (D_v).

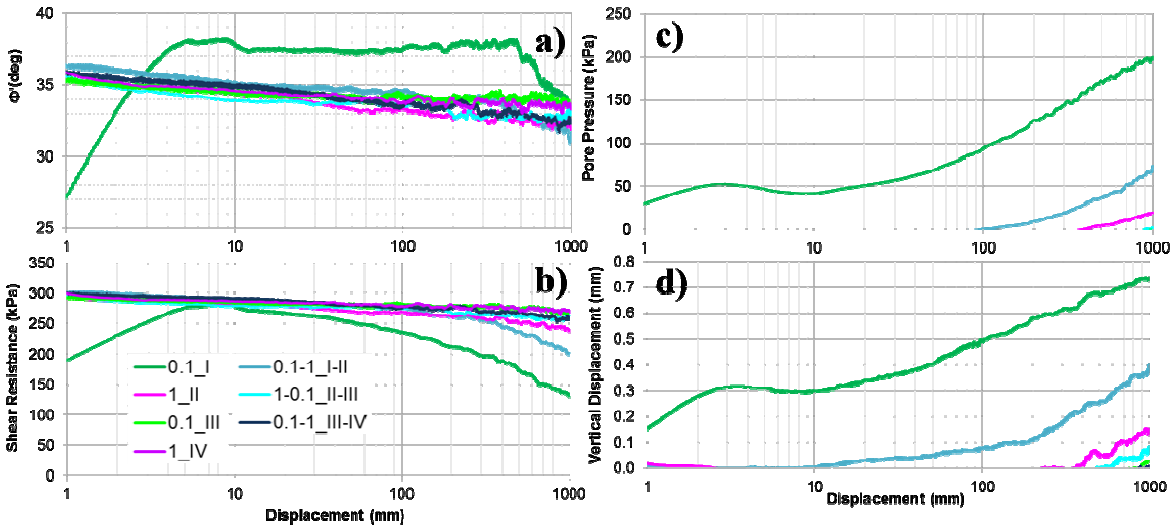

Fig. A.4.2 Shear displacement and a) Effective friction angle (Φ'), b) Shear resistance, c) Pore pressure and d) Vertical displacement.

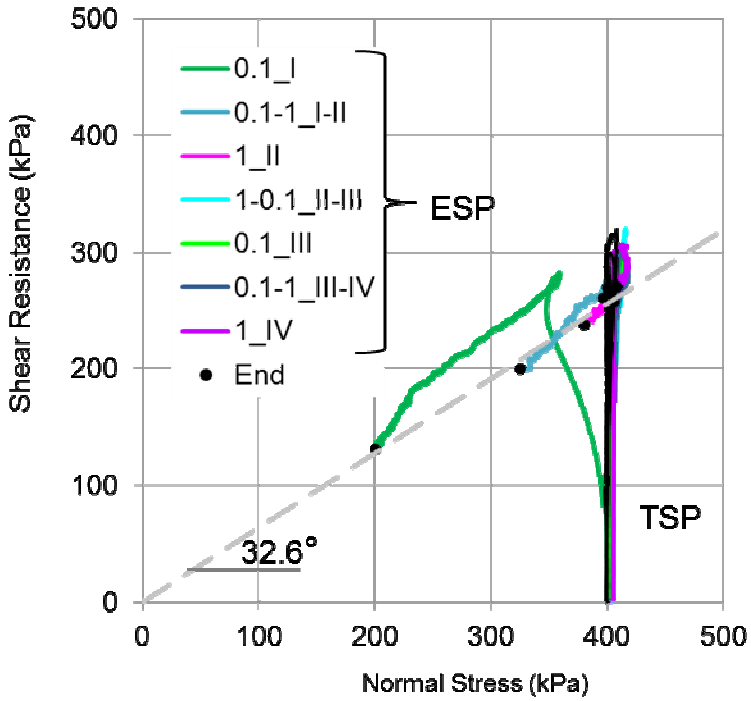

Fig. A.4.3 Stress path of all stages (I-VIII), TSP- total stress path, ESP- effective stress path.

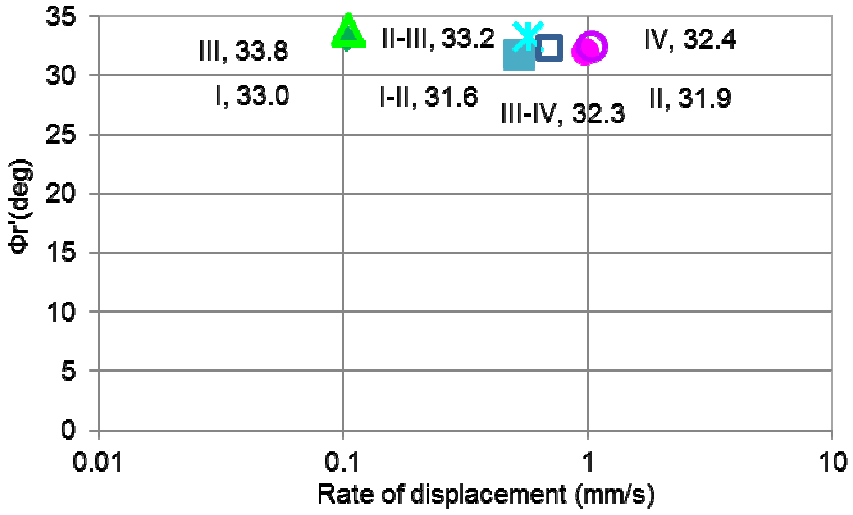

Fig. A.4.4 Rate of displacement and effective friction angle.

A.5 Test T 13-SB 20-Undrained shearing with consolidation (I-VIII; C-O)

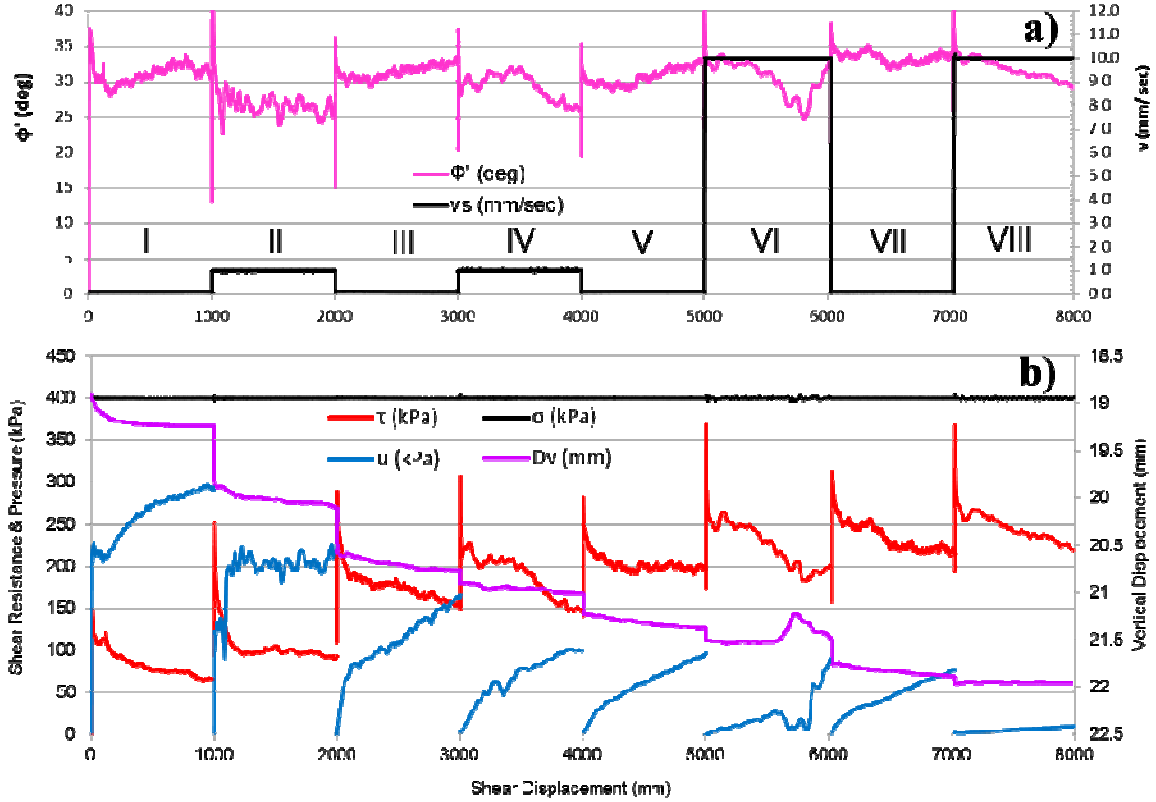

Fig. A.5.1 Cumulative shear displacement and a) Effective friction angle (Φ') and rate of displacement (v_s), b) Shear resistance (τ) , pore pressure (u) and vertical displacement (D_v)

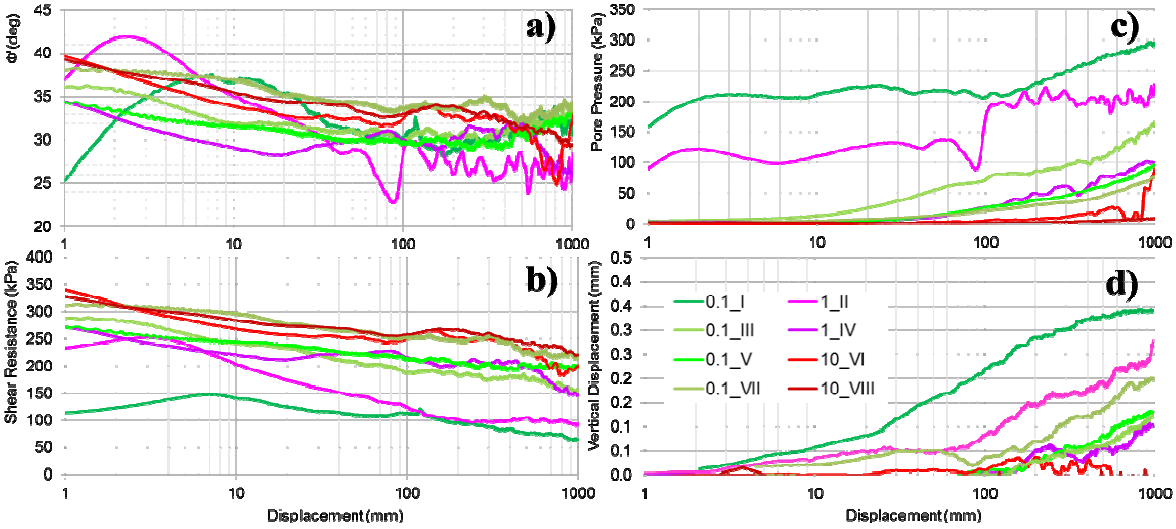

Fig. A.5.2 Shear displacement and a) Effective friction angle (Φ'), b) Shear resistance, c) Pore pressure and d) Vertical displacement.

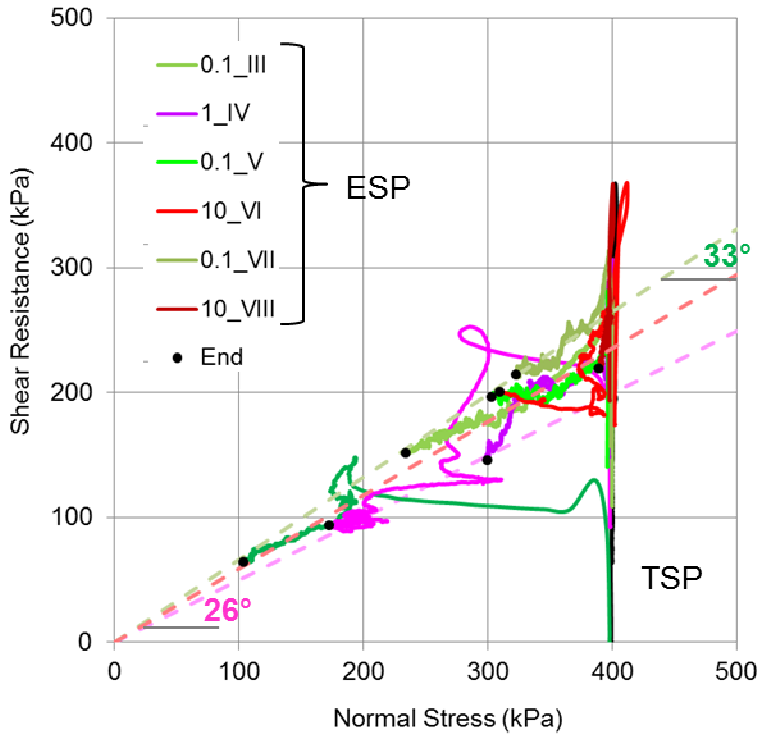

Fig. A.5.3 Stress path of all stages (I-VIII), TSP- total stress path, ESP- effective stress path.

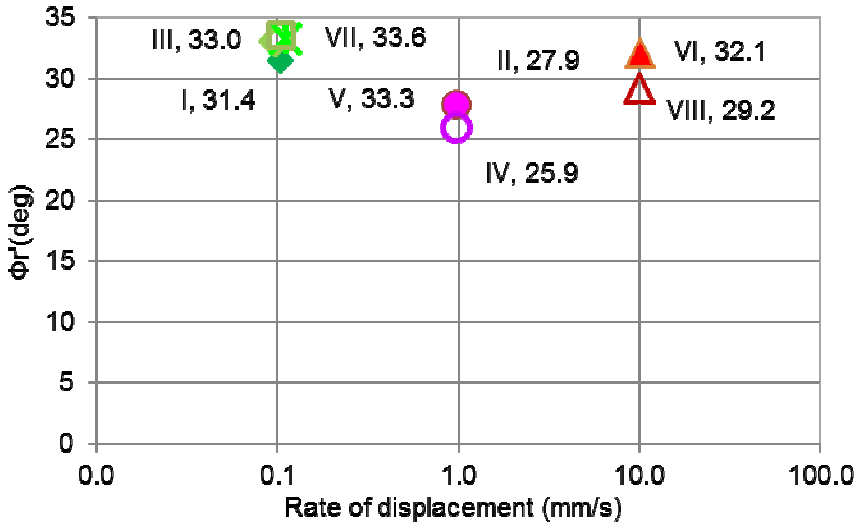

Fig. A.5.4 Rate of displacement and effective friction angle.

A.6 Test T 14-SB 20-Undrained shearing without consolidation (I-VIII; C-C)

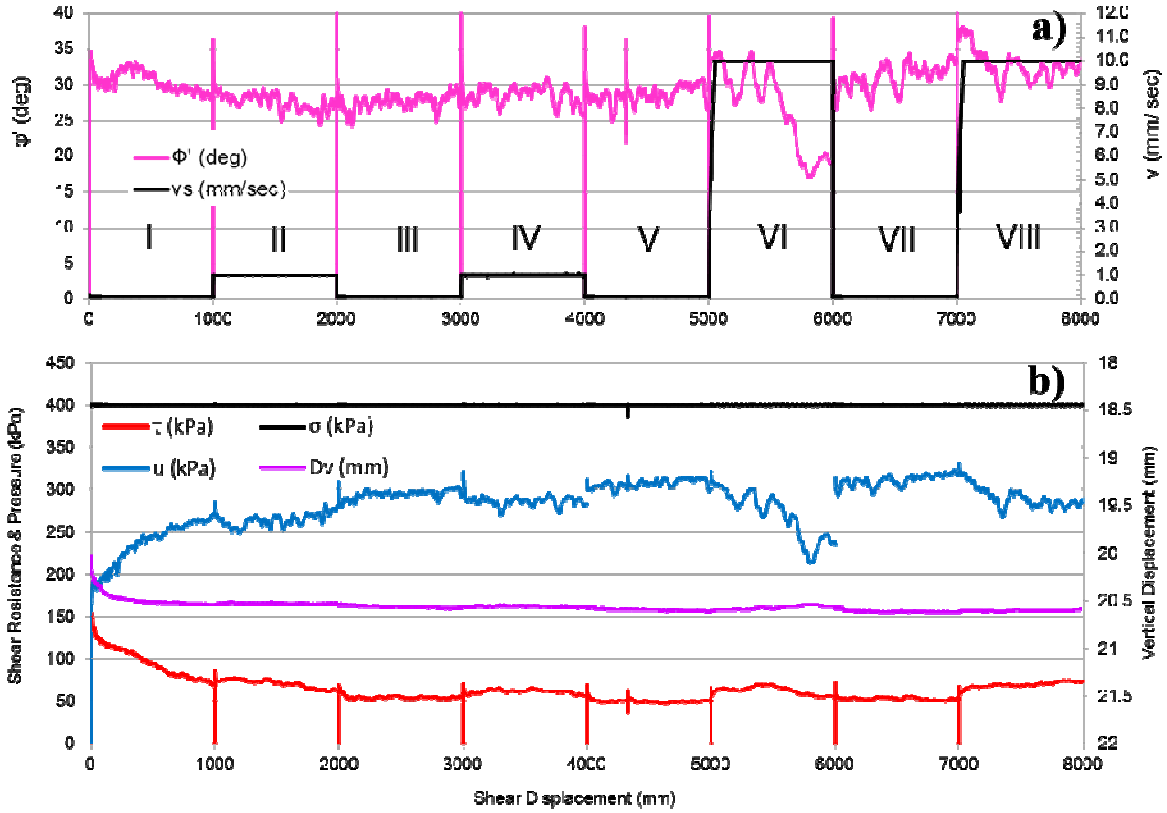

Fig. A.6.1 Cumulative shear displacement and a) Effective friction angle (Φ') and rate of displacement (v_s), b) Shear resistance (τ) , pore pressure (u) and vertical displacement (D_v)

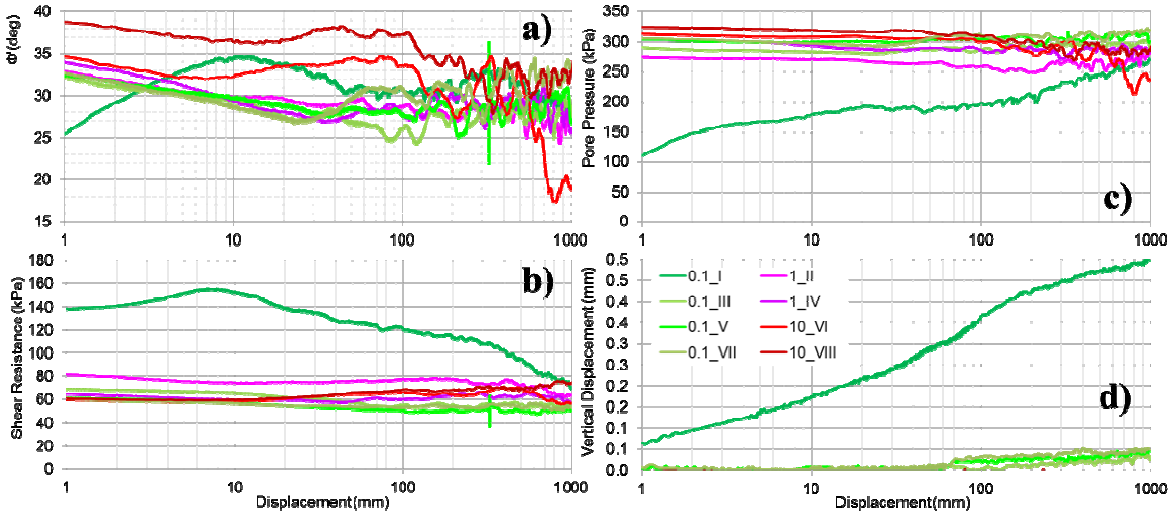

Fig. A.6.2 Shear displacement and a) Effective friction angle (Φ'), b) Shear resistance, c) Pore pressure and d) Vertical displacement.

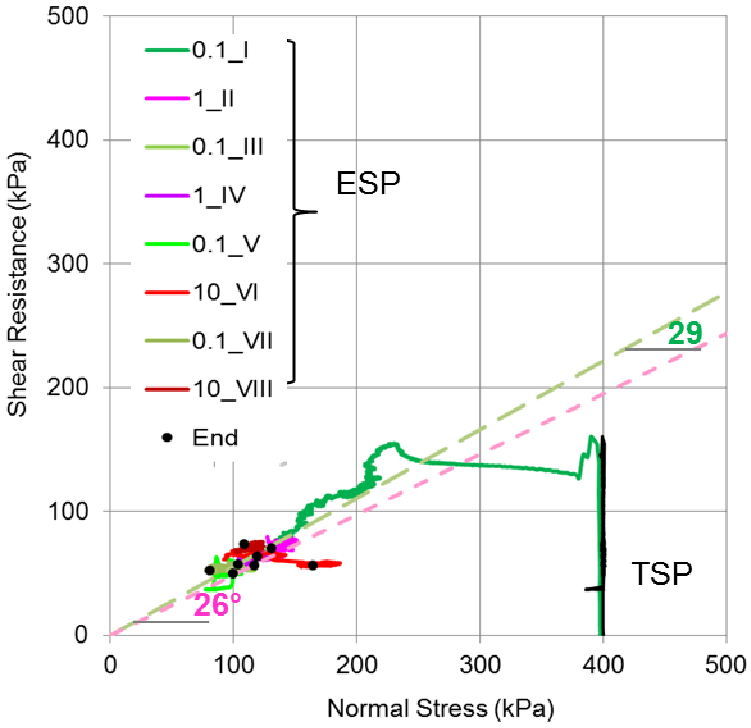

Fig. A.6.3 Stress path of all stages (I-VIII), TSP- total stress path, ESP- effective stress path.

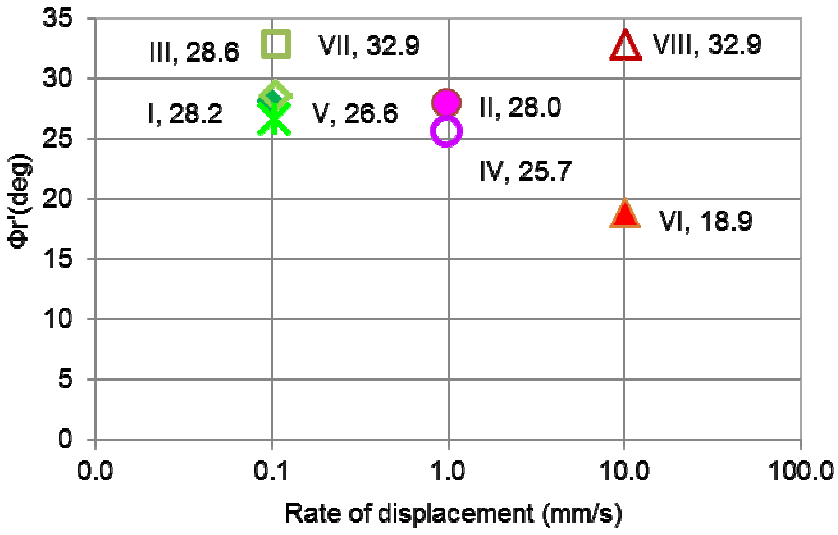

Fig. A.6.4 Rate of displacement and effective friction angle.

A.7 Test T 15-SB 20-Partialy drained shearing with consolidation (I-VIII; O-O)

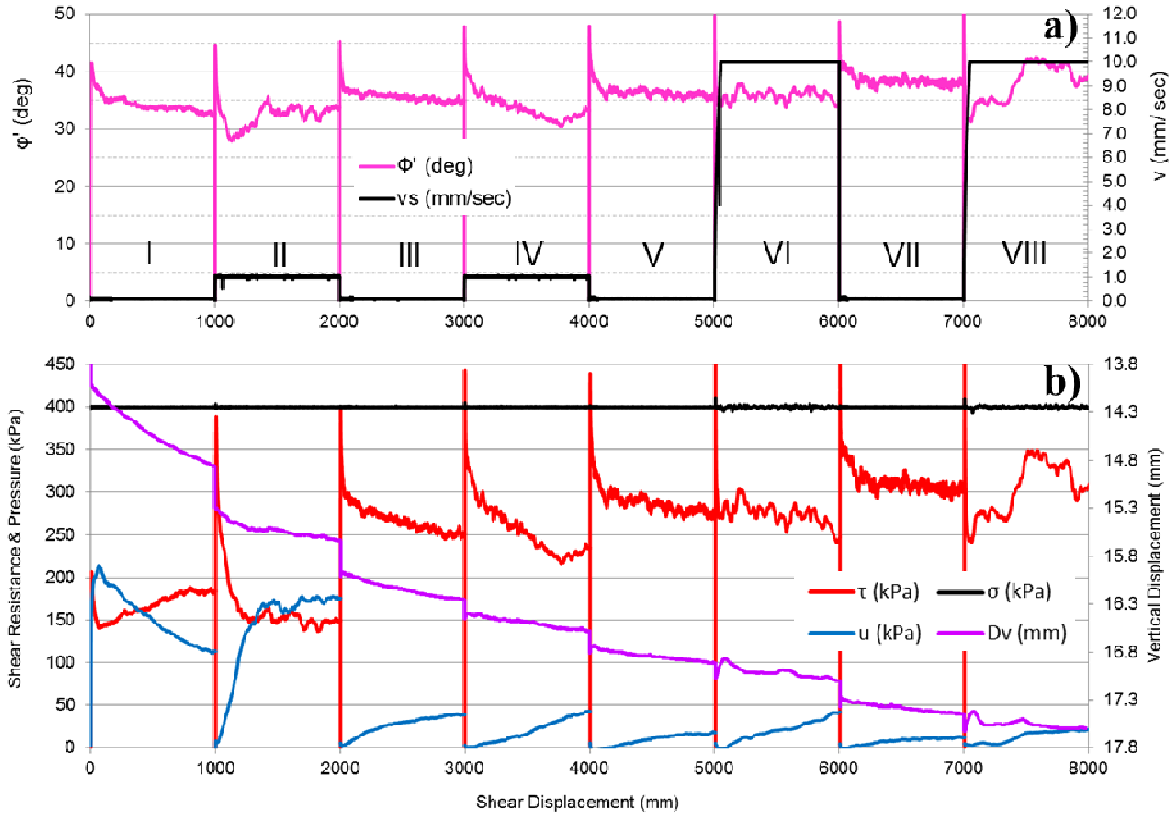

Fig. A.7.1 Cumulative shear displacement and a) Effective friction angle (Φ') and rate of displacement (v_s), b) Shear resistance (τ) , pore pressure (u) and vertical displacement (D_v)

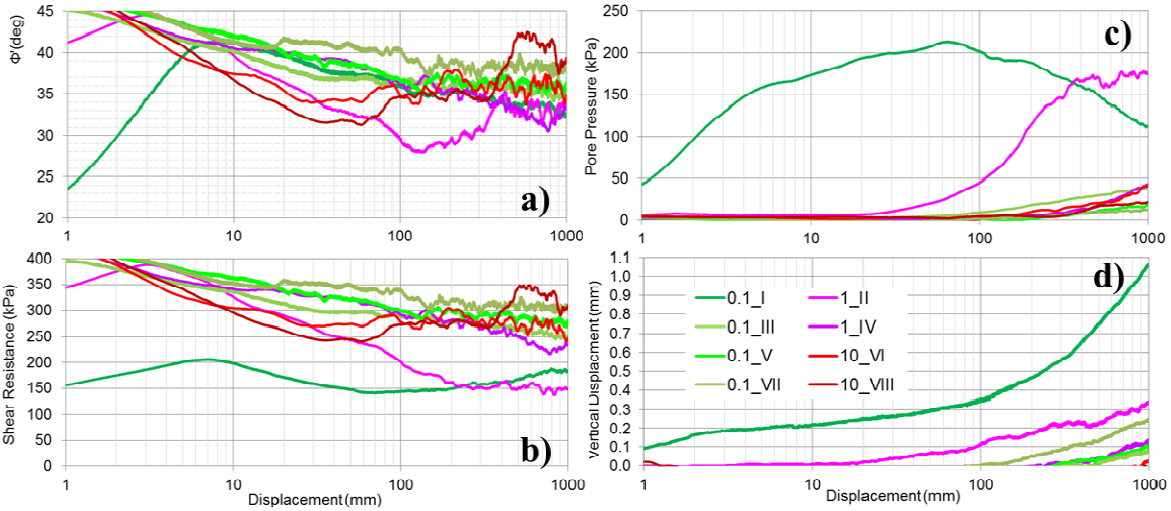

Fig. A.7.2 Shear displacement and a) Effective friction angle (Φ'), b) Shear resistance, c) Pore pressure and d) Vertical displacement.

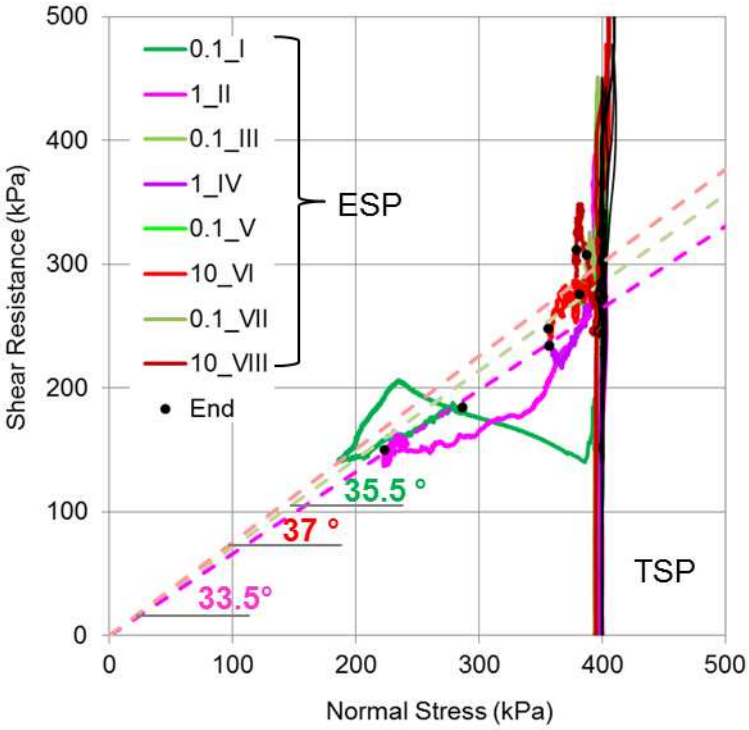

Fig. A.7.3 Stress path of all stages (I-VIII), TSP- total stress path, ESP- effective stress path.

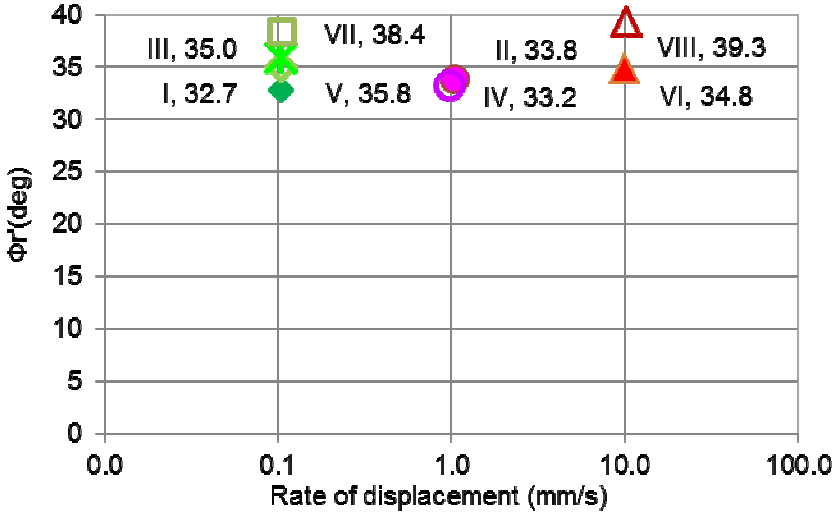

Fig. A.7.4 Rate of displacement and effective friction angle.

A.8 Test T 16-SB 20-Undrained shearing with consolidation (I-IV; C-O)

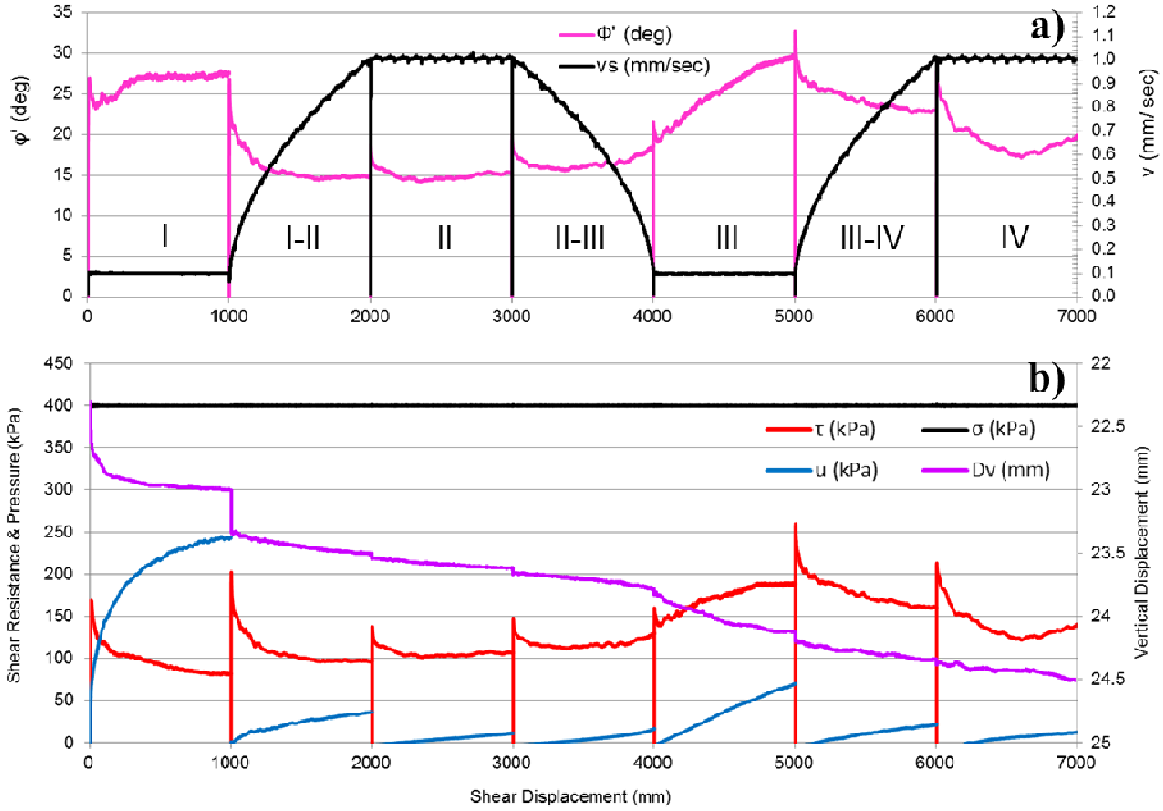

Cumulative shear displacement and a) Effective friction angle (Φ') and rate of displacement (v_s), b) Shear resistance (τ) , pore pressure (u) and vertical displacement (D_v)

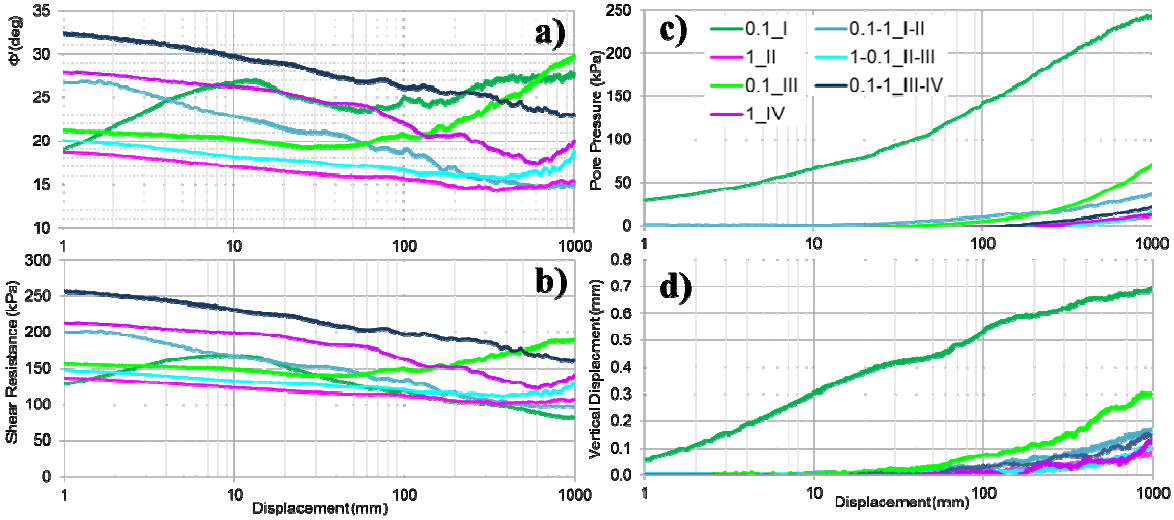

Fig. A.8.2 Shear displacement and a) Effective friction angle (Φ'), b) Shear resistance, c) Pore pressure and d) Vertical displacement.

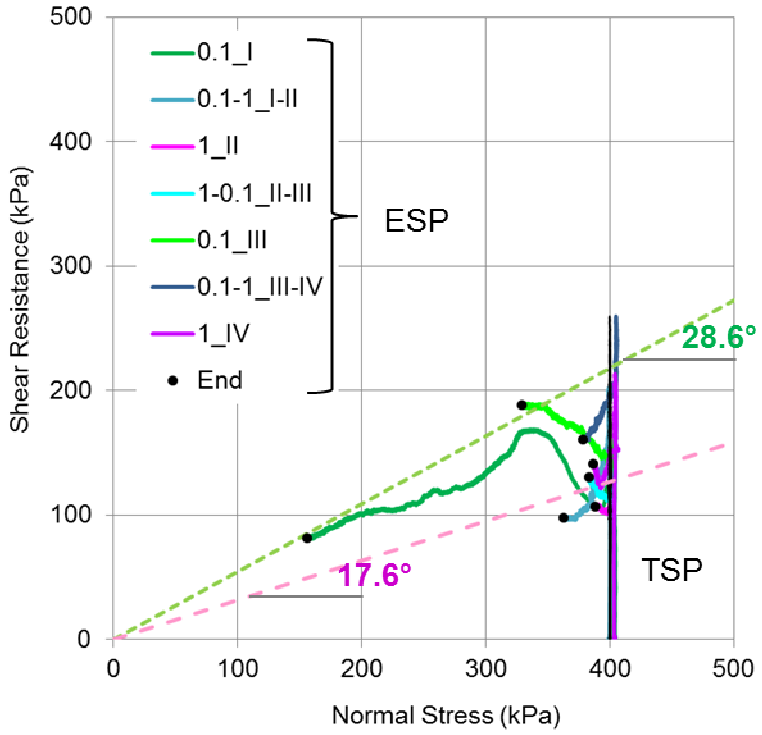

Fig. A.8.3 Stress path of all stages (I-VIII), TSP- total stress path, ESP- effective stress path.

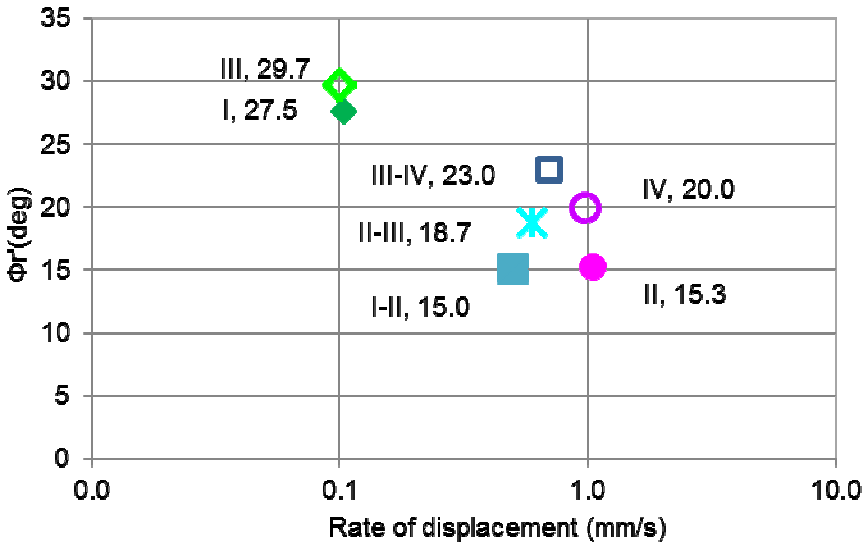

Fig. A.8.4 Rate of displacement and effective friction angle.

A.9 Test T 21-SB 30-Undrained shearing with consolidation (I-VIII; C-O)

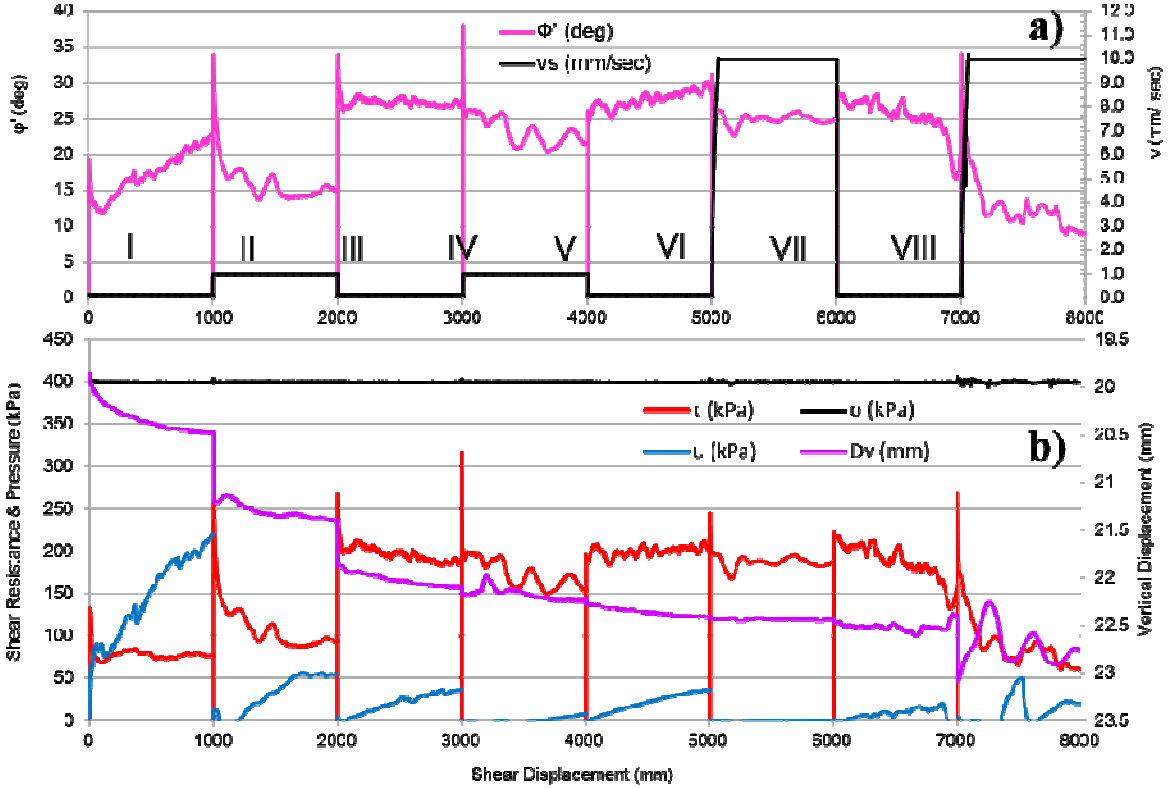

Fig. A.9.1 Cumulative shear displacement and a) Effective friction angle (Φ') and rate of displacement (v_s), b) Shear resistance (τ) , pore pressure (u) and vertical displacement (D_v)

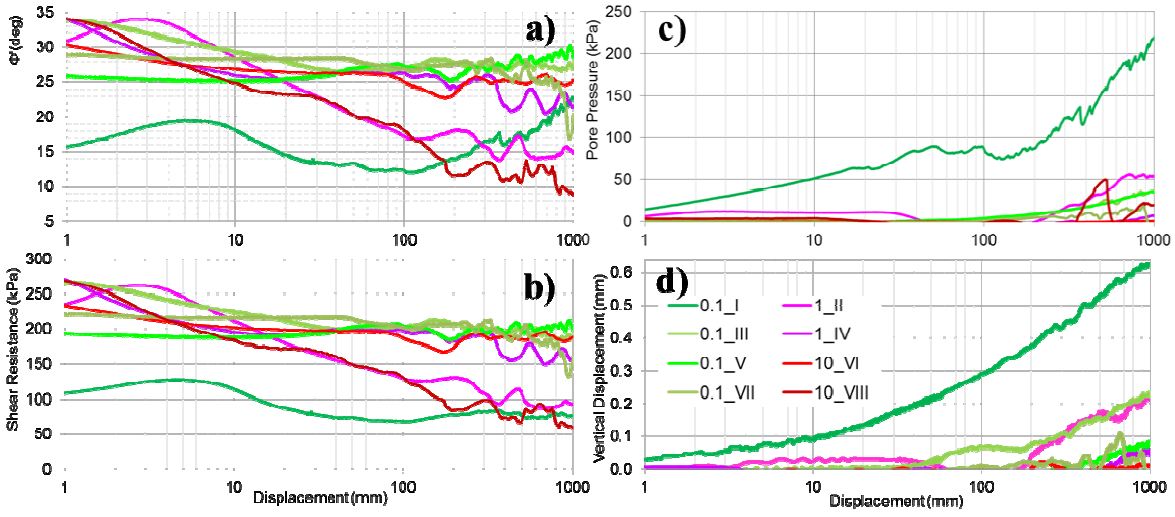

Fig. A.9.2 Shear displacement and a) Effective friction angle (Φ'), b) Shear resistance, c) Pore pressure and d) Vertical displacement.

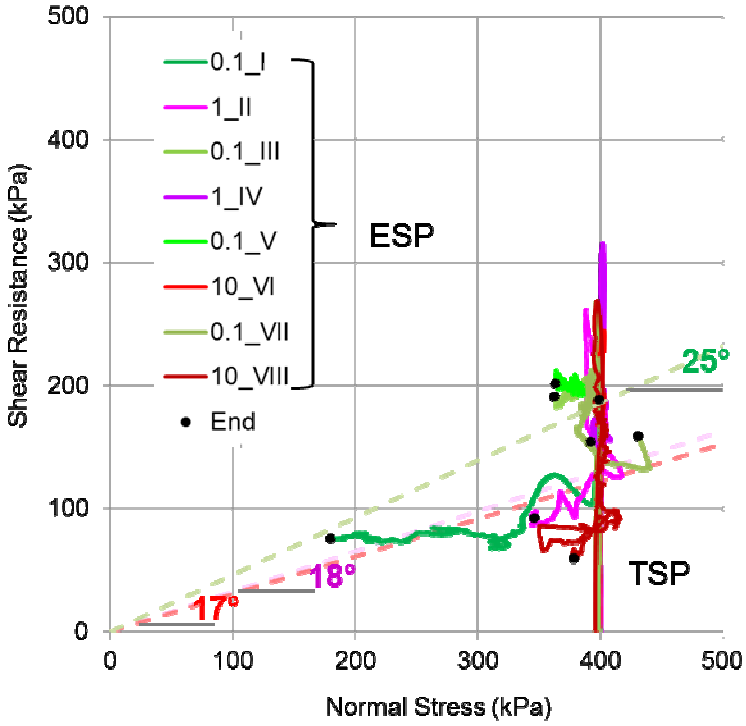

Fig. A.9.3 Stress path of all stages (I-VIII), TSP- total stress path, ESP- effective stress path.

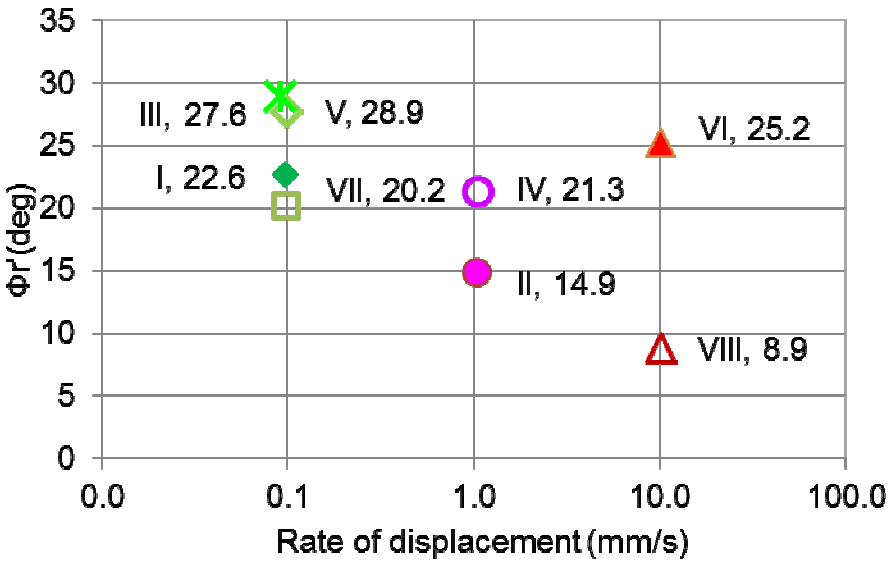

Fig. A.9.4 Rate of displacement and effective friction angle.

A.10 Test T 23-SB 30-Partialy drained shearing with consolidation (I-VIII; O-O)

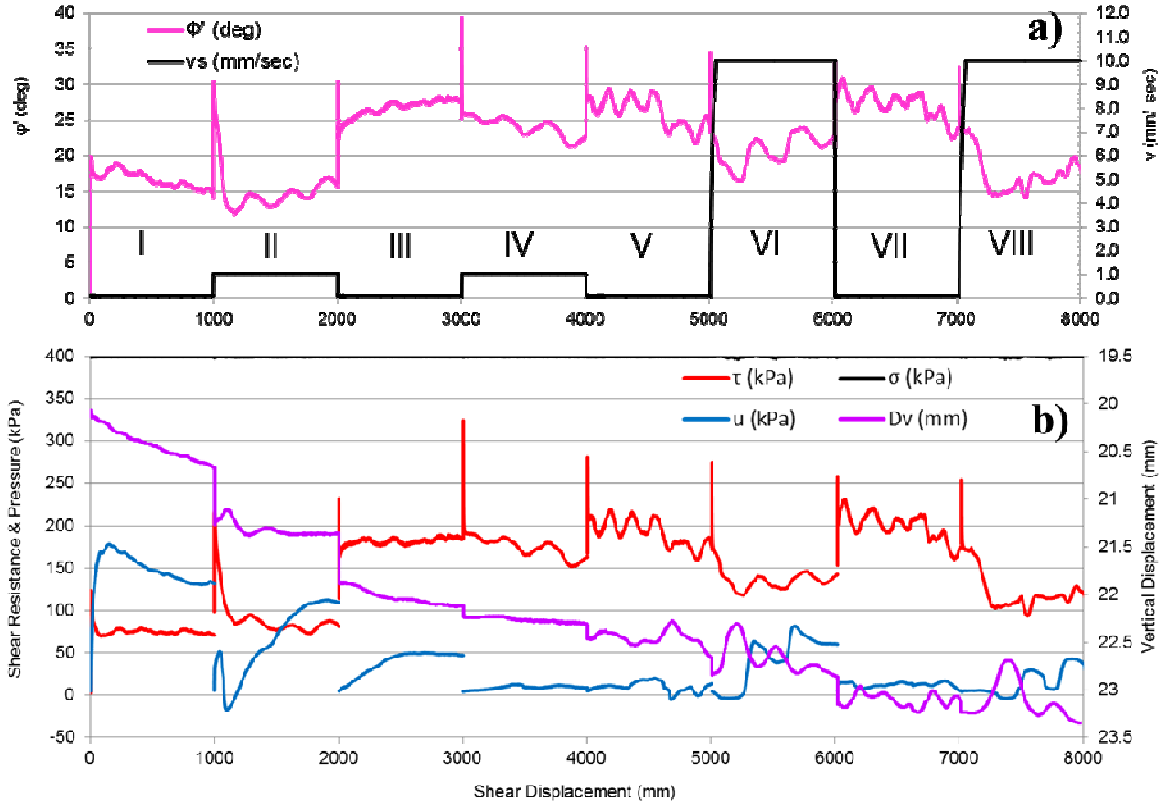

Fig. A.10.1 Cumulative shear displacement and a) Effective friction angle (Φ') and rate of displacement (v_s), b) Shear resistance (τ) , pore pressure (u) and vertical displacement (D_v).

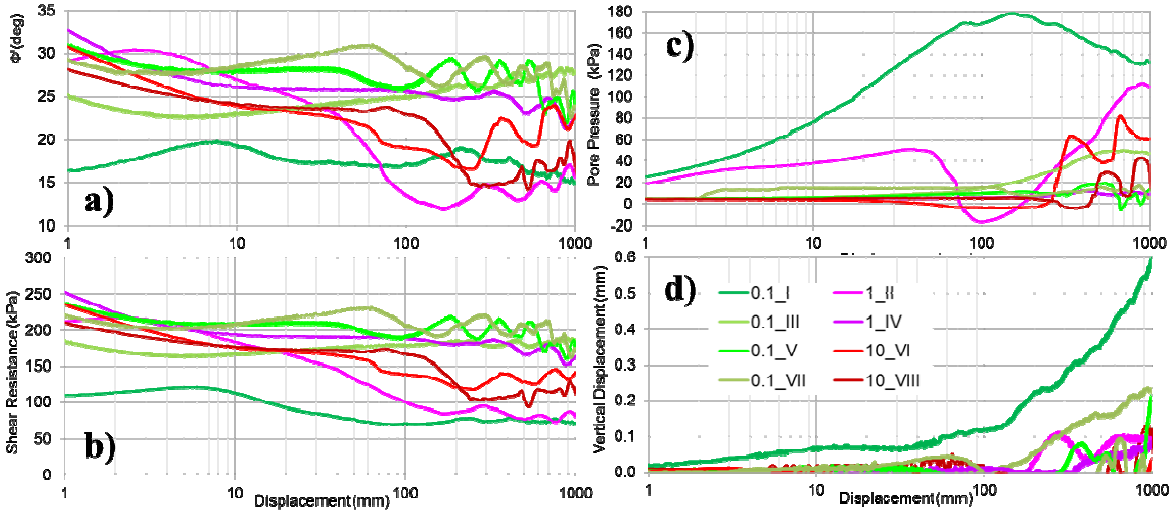

Fig. A.10.2 Shear displacement and a) Effective friction angle (Φ'), b) Shear resistance, c) Pore pressure and d) Vertical displacement.

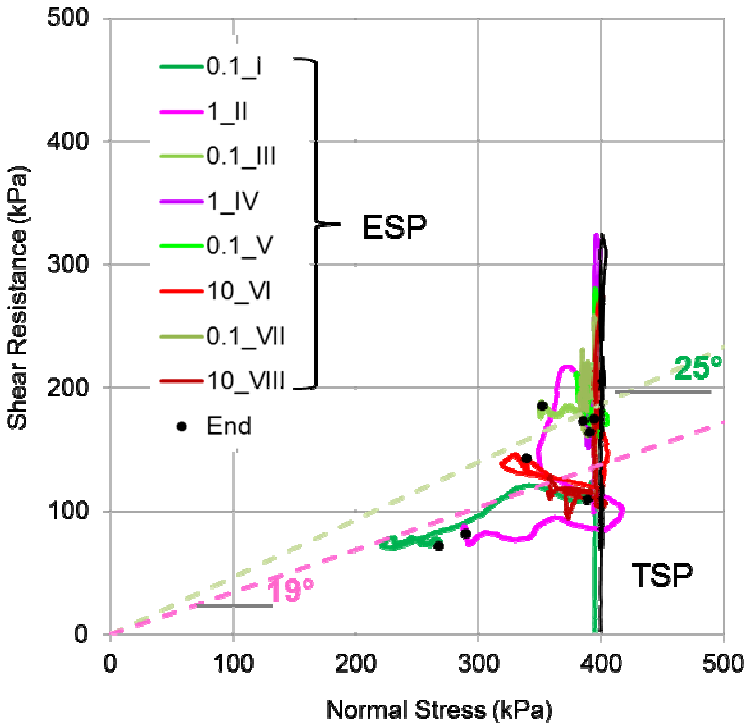

Fig. A.10.3 Stress path of all stages (I-VIII), TSP- total stress path, ESP- effective stress path.

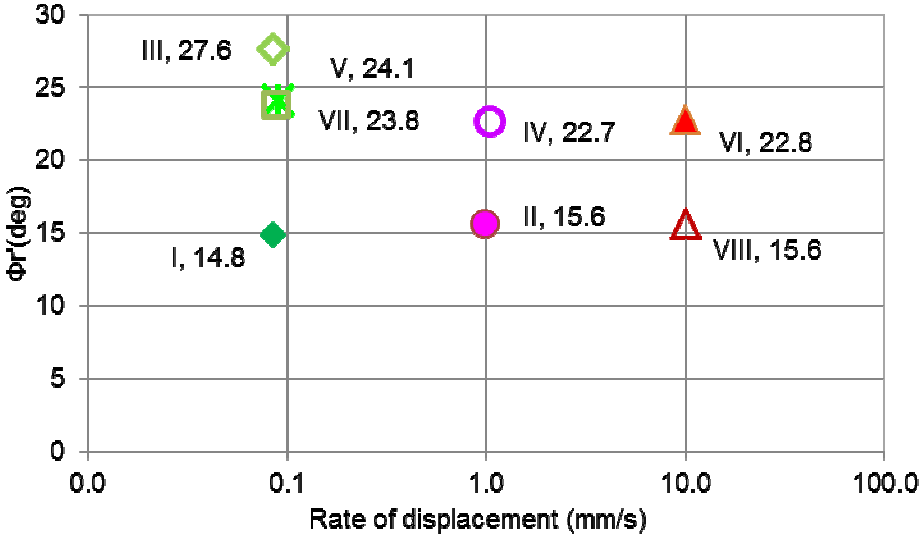

Fig. A.10.4 Rate of displacement and effective friction angle.

A.11 Test T 24-SB 30-Undrained shearing with consolidation (I-IV; C-O)

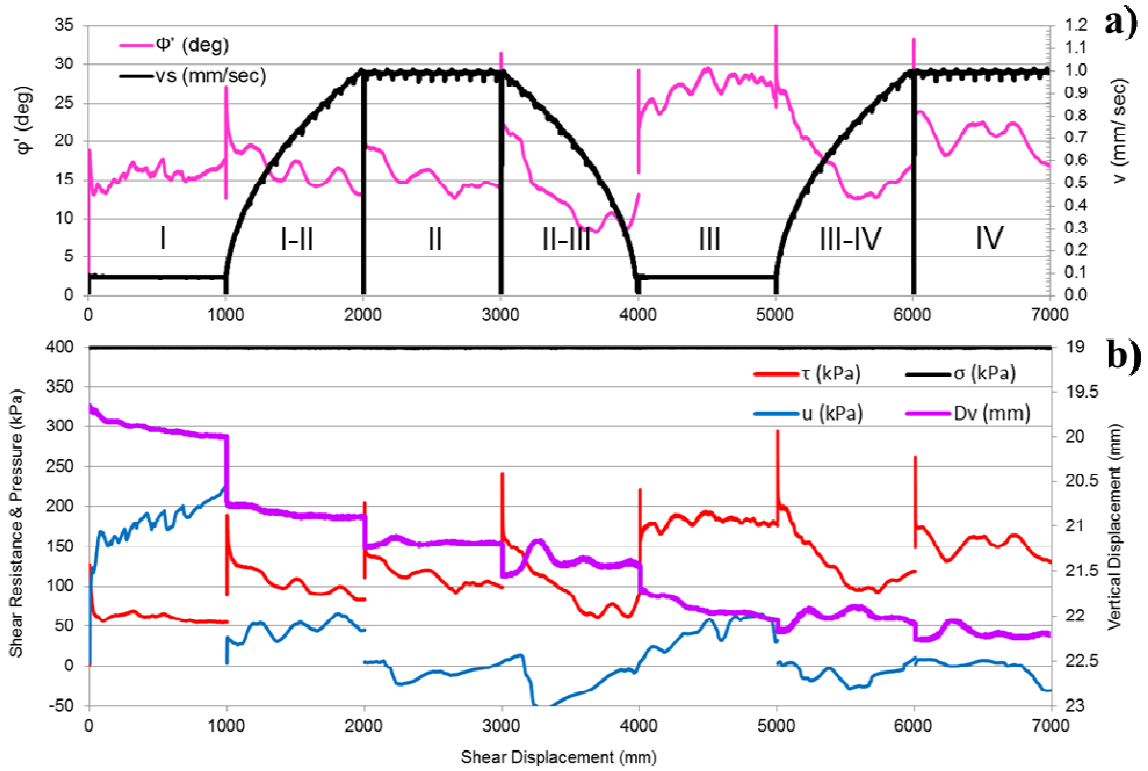

Fig. A.11.1 Cumulative shear displacement and a) Effective friction angle (Φ') and rate of displacement (v_s), b) Shear resistance (τ) , pore pressure (u) and vertical displacement (D_v).

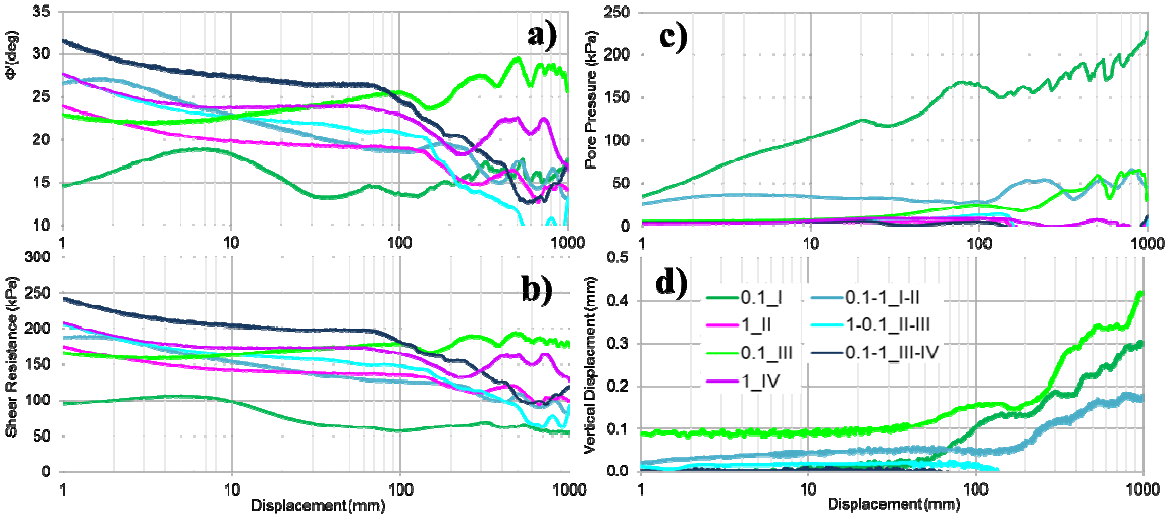

Fig. A.11.2 Shear displacement and a) Effective friction angle (Φ'), b) Shear resistance, c) Pore pressure and d) Vertical displacement.

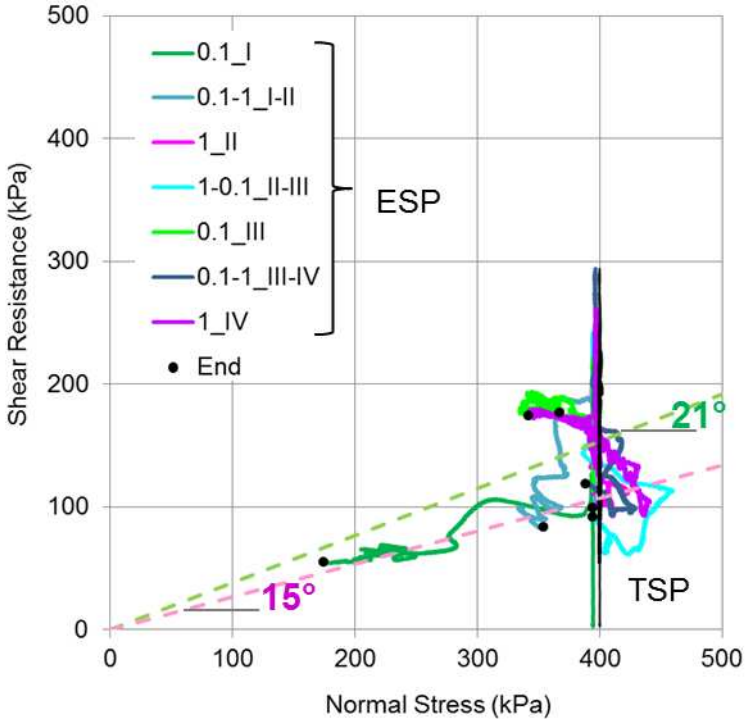

Fig. A.11.3 Stress path of all stages (I-VIII), TSP- total stress path, ESP- effective stress path.

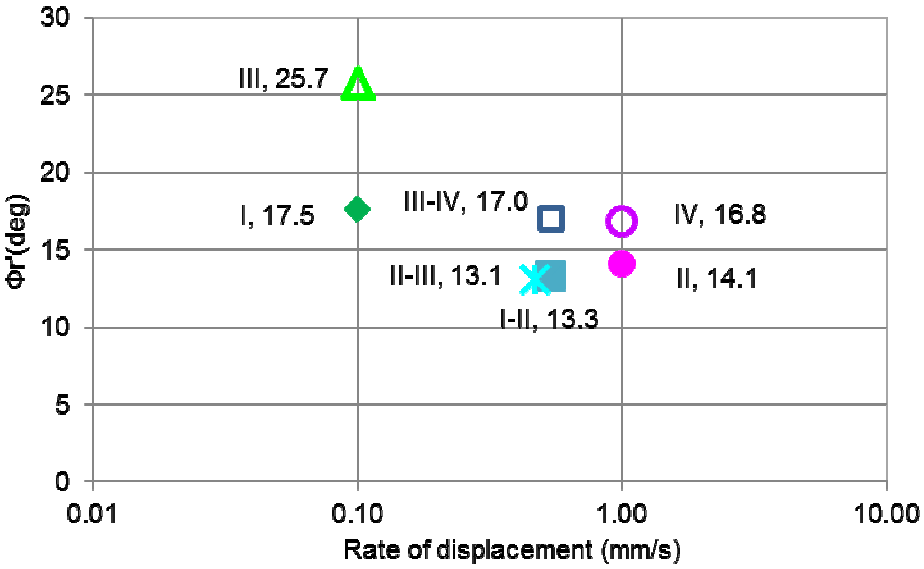

Fig. A.11.4 Rate of displacement and effective friction angle.